

https://dspace.org/

Synthesis and use of Silica materials as supports for the Fischer-Tropsch reaction

Mokoena, Emma Magdeline

2006-11-17T09:30:54Z
http://hdl.handle.net/10539/1848

Downloaded from a DSpace repository. https://dspace.org/

SYNTHESIS AND USE OF SILICA MATERIALS AS SUPPORTS FOR THE FISCHER-TROPSCH REACTION

Emma Magdeline Mokoena

A thesis submitted to the Faculty of Science, University of the Witwatersrand, Johannesburg, in fulfilment of the requirements for the degree of Doctor of Philosophy.

Johannesburg, 2005

Declaration

I declare that this thesis is my own, unaided work. It is being submitted for the degree of Doctor of Philosophy in the University of the Witwatersrand, Johannesburg. It has not been submitted before for any degree or examination in any other university.

_____ day of _____ 2005

Abstract

The objective of the study was to prepare novel silica materials and then use them as supports/binders for the Fisher-Tropsch (F-T) reaction. Hence the thesis is divided into two parts - (i) the synthesis of silica materials (ii) use of silica materials as supports.

PART I

The studies that were carried out in this thesis evaluated the effect of templates and synthesis conditions on the nano- and microstructure and properties of silica materials that are obtained by the sol-gel method.

The studies with DL-tartaric acid and citric acid as templates revealed that synthesis conditions (temperature, NH_4OH concentration, water/ethanol concentration, time before NH_4OH addition, static versus stirred conditions, stirring rate and solvent) all have an effect on the microstructure of the silica and influence the formation of particular silica morphologies.

DL-tartaric acid produced longer and more uniform tubes when compared to citric acid. Tubes that are formed by DL-tartaric acid are hollow and open ended; however the ones formed in citric acid are a mixture of filled and hollow but closed tubes. Hollow spheres are exclusively formed when citric acid is used under certain conditions while only filled spheres are formed when DL-tartaric

acid is used. The surface areas of the silicas formed from DL-tartaric acid are lower that the surface areas obtained for materials produced by citric acid. The nitrogen adsorption-desorption isotherms of silica materials obtained from both templates showed that the materials were mesoporous with some microporosity present in them.

Studies with mucic and tartronic acids as templates also showed that the template as well as the synthesis conditions (such as solvent, temperature and stirring) affect the resulting silica morphology. Mucic acid produced silica materials with high surface areas, mesopores and a morphology that reveals fragmented tubes. Tartronic acid produced hollow tube materials with low surface areas and a combination of micro- and mesopores. The yield of the tubes was higher at lower temperatures for both templates.

When sugars (e.g. glucose) were used only spherical particles were obtained and some sugars gave particle sizes that are smaller than the ones that are normally obtained by the sol-gel method.

PART II

Catalysts (Fe/Cu/K) supported on a range of silica materials with different morphologies (hollow nanotubes, hollow spheres, Stöber/closed spheres) were evaluated in the Fischer-Tropsch reaction (8 bar, 250 °C, 400 h^{-1} GHSV). The supported iron catalysts modified the physico-chemical properties and activity of

the catalysts but not the catalyst selectivity. A Ruhrchemie catalyst (known F-T catalyst standard) was also evaluated under the same reaction conditions as the new catalysts for comparison purposes.

The Ruhrchemie catalyst was found to be the most active catalyst followed by the catalyst supported on nanotubes, Stöber spheres and hollow spheres respectively. Catalysts containing 18% silica showed the best activity compared to the 9% and 27% silica catalysts.

The product distribution and WGS activity were largely influenced by the potassium that is present in the samples and not the support type.

Mössbauer spectroscopy showed that some active catalysts contained χ' – $Fe_{2.5}C$ and some superparamagnetic iron oxides or carbides while other catalysts also contained α – Fe and Fe_3O_4 in addition to χ' – $Fe_{2.5}C$ and some superparamagnetic iron oxides or carbides species. This finding supports the hypothesis that carbide formation is a requirement for active F-T catalysts. It also suggests that metallic iron is necessary for carbiding to occur, hence the need for a reduction pre-treatment.

To my husband Wilfred

and my daughter Boitumelo,

for your unconditional love and support

Acknowledgements

The work presented in this thesis would not have been possible without the assistance of a number of people and institutions. I would like to express my gratitude to the following:

Prof. N.J. Coville, my supervisor for his guidance and enthusiasm about catalysis and chemistry in general which he was also able to impress on me.

Prof. A.K. Datye, for allowing me to spend time with his research group at the University of New Mexico in the USA and whose interest and knowledge in the field of Fischer-Tropsch catalysis was invaluable.

B. Chassoulas, for designing and constructing the electronic circuitry and for helping me solve the equipment problems that invariably cropped up.

The members of the physics workshop and S. Ganon and B. Fairbrother (the glassblowers) for manufacturing the various pieces of equipment required.

My colleagues in the Wits catalysis group, for showing me how to use the characterisation equipment and for creating a conducive environment for doing research.

Prof. M. Witcomb, C. Lalkhan and A. Seema of the WITS Electron Microscope Unit and H Pham of UNM (University of New Mexico) for all their assistance with the microscopy work.

T. Motjope and L. Lodya of the Materials Characterisation group at Sasol Technology, for their assistance with Mössbauer spectroscopy.

Dr A. Debeila for helping me get started on the F-T reactor system.

K. Chiloane, the chemistry honours student, for performing some of the sol-gel work with mucic and tartronic acids.

L. Daniels, K. Banda, A. Pointeer, A. Morgan, E. Valoyi and D. Moloto of the WITS chemistry department for their assistance in various ways.

The University, Sasol, THRIP, NRF and the WITS catalysis group for their generous funding.

The Almighty God for granting me the strength to face each day and his daily blessings that befell me throughout the duration of the study.

Publications and Presentations arising from this Work

Poster Presentation:

TEM and SEM Studies of Silica Used in Supporting Iron Catalysts for the Fischer-Tropsch Reaction, CATSA, Wigwam Hotel, Rustenburg, 1999.

Oral Presentations:

1. *Use of Citric and DL-Tartaric Acids in the Synthesis of Silica Materials Obtained by the Sol-Gel Method*, CATSA/SACI: Conference on Catalysis and Inorganic Chemistry, Bakgatla Resort, Pilanesburg, 2001.
2. *Silica Nanotube Synthesis via DL-Tartaric Acid Templates*, 15th International Congress on Electron Microscopy, Durban, 2002.
3. *Silica with Various Morphologies Used as Supports for the Iron Fischer-Tropsch Catalyst*, CATSA, Protea Hotel President, Cape Town, 2002.
4. *Silica Tubes and Spheres as Supports for Fe Fischer-Tropsch Catalysts*, The 19th Meeting of the North American Catalysis Society, Philadelphia, USA, May 22 – 25, 2005. (Oral presentation by Neil J. Coville).

Publications

1. *A Systematic Study of the Use of DL-Tartaric Acid in the Synthesis of Silica Materials Obtained by the Sol-Gel Method,* E.M. Mokoena, A.K. Datye and N.J. Coville, *J. Sol-Gel Sci. Tech.*, **28**, 307 - 317, 2003.

2. *Synthesis and Study of Ammonium Oxalate Sol-gel Templated Silica Gels*, Keneiloe Khoabane, Emma M. Mokoena and Neil J. Coville, *Microporous and Mesoporous Materials*, **83**, 67 – 65, 2005.

Table of Contents

Declaration……i

Abstract……ii

Dedication……v

Acknowledgements……vi

Publications and Presentations arising from this Work……viii

Table of Contents……x

List of Tables……xvi

List of Figures……xix

List of Abbreviations and Symbols……xxv

PART I: Synthesis of Silica Materials by the Sol-Gel Method.....1

Chapter One:

The Synthesis of Inorganic Materials by Sol-Gel Processing: A Review……2

1.1 Introduction

1.1.1 Terminology……3

1.1.2 Principles of the Sol-Gel Process……5

1.1.3 History of the Sol-Gel Process……6

1.1.4 Advantages of the Sol-Gel Process……9

1.2 Sol-Gel Chemistry……..9

1.3 Role of Templates in the Sol-gel Synthesis……..13

1.4 Sol-Gel Synthesized Oxide Supports……..…15

1.4.1 Silica……..…..15

1.4.2 Alumina……...17

1.4.3 Other Sol-Gel Generated Simple Oxides……..18

1.5 Conclusions……20

1.5 References……....22

Chapter Two:

A Systematic Study of the Use of DL-Tartaric Acid in the Synthesis of Silica Materials Obtained by the Sol-Gel Method……...28

2.1 Introduction……28

2.2 Experimental……..31

2.2.1 Preparation……31

2.2.2 Characterization……35

2.3 Results……...36

2.4 Discussion……55

2.5 Conclusions……..59

2.6 References……...61

Chapter Three:

A Systematic Study of the Use of Citric Acid in the Synthesis of Silica

Materials Obtained by the Sol-Gel Method……..64

3.1 Introduction……64

3.2 Experimental…….66

3.2.1 Preparation……...66

3.2.2 Characterization……..72

3.3 Results and Discussion…….72

3.4 Conclusions…….92

3.5 References……..93

Chapter Four:

Templates Containing COOH and/or OH Groups for the Preparation of Silica Materials……..95

4.1 Introduction…….95

4.2 Experimental……..98

4.2.1 Preparation…….98

4.2.2 Characterisation…….98

4.3 Use of Mucic and Tartronic Acids as Templates……..99

4.3.1 Solvent Effects……...99

4.3.2 Temperature Effects……...103

4.3.3 Stirring vs Non-stirring Conditions……107

4.3.4 Surface Area and Pore Analysis……...110

4.3.5 Thermal analysis…….120

4.4 Use of Sugars as Templates……122

4.5 Conclusions……128

4.6 References……..129

PART II: The Application of Novel Silica Materials in the Fischer-Tropsch Synthesis……131

Chapter Five:

The Fischer-Tropsch Synthesis: An Overview……132

5.1 Introduction……132

5.2 The Fischer-Tropsch Synthesis……..133

5.3 Process Reactors……..136

5.4 Fischer-Tropsch Catalysts……...138

5.4.1 Iron……...139

5.4.2 Cobalt……..141

5.4.3 Ruthenium……..142

5.4.4 Nickel……..142

5.4.5 Other F-T Catalysts……..143

5.5 Promoter Effects……143

5.5.1 Potassium……..145

5.5.2 Copper……148

5.6 Support Effects……..150

5.7 Fischer-Tropsch Mechanism and Kinetics……....154

5.8 Aims of This Study……....159

5.9 References……161

Chapter Six:

Experimental Method……170

6.1 Introduction……170

6.2 Materials and Chemicals Used……171

6.2.1 Support……171

6.2.2 Metals……171

6.2.3 Gases……171

6.3 Catalyst Preparation……172

6.4 Reactor System……174

6.5 Fischer-Tropsch Synthesis……177

6.5.1 Product Analysis……177

6.5.2 Mass Balance Calculations……180

6.6 Catalyst Characterisation……184

6.6.1 BET Surface Area Measurement……184

6.6.2 Temperature Programmed Reduction (TPR)……184

6.6.3 Transmission Electron Microscopy……185

6.6.5 Mössbauer Spectoscopy……185

6.7 References……186

Chapter Seven:

Silica With Various Morphologies as a Binder/Support for iron Fischer-

Tropsch Catalysts…….....187

7.1 Introduction……...187

7.2 Experimental Procedure……190

7.2.1 Catalyst Synthesis……...190

7.2.2 Catalyst Characterization……..191

7.2.3 Catalyst Evaluation……192

7.3 Results and Discussion……192

7.3.1 BET Surface Area Analysis……..192

7.3.2 Temperature Programmed Reduction (TPR) Study…….196

7.3.3 Transmission Electron Microscopy (TEM) Study……..202

7.3.4 Reactor Study……209

7.3.5 Mössbauer Spectroscopy……217

7.4 Conclusions……221

7.5 References……222

Chapter Eight:

Conclusions……..…..226

Appendix……234

List of Tables

Table 1.1. Elements used to date in the sol-gel process. *p.8*

Table 1.2. Some of the alkoxides used in sol-gel synthesis. *p.12*

Table 2.1. Effect of temperature on the morphology of silica. *p.36*

Table 2.2. Effect of varying %NH_3 to water in NH_4OH. *p.40*

Table 2.3. Effect of H_2O/EtOH dilution. *p.42*

Table 2.4. Effect of varying time before the addition of NH_4OH. *p.45*

Table 2.5. Effect of adding NH_4OH under both static and stirring conditions (rapid addition). *p.47*

Table 2.6. Effect of diffusion on the amount of tubes that form. *p.48*

Table 2.7. Effect of solvent on structure and number of tubes formed. *p.49*

Table 2.8. Effect of template on surface area. *p.50*

Table 3.1. Effect of temperature on the morphology of silica. *p.73*

Table 3.2. Effect of varying % NH_3 to water in NH_4OH. *p.76*

Table 3.3. Effect of H_2O/EtOH dilution. *p.79*

Table 3.4. Effect of varying time before the addition of NH_4OH. *p.81*

Table 3.5. Effect of adding NH_4OH under both static and stirring conditions (rapid addition). *p.85*

Table 3.6. Effect of stirring rate on the amount of tubes that form. *p.85*

Table 3.7. Effect of solvent on structure and number of tubes formed. *p.87*

Table 4.1. Effect of solvent on the particle size and structure of silica at 25 °C. *p.100*

Table 4.2. Dielectric constants of solvents used. *p.100*

Table 4.3. Effect of solvent dilution (1.1% water, vol%) on the morphology of silica at 25 °C. *p.101*

Table 4.4. Effect of solvent on the morphology of silica at 25 °C. *p.103*

Table 4.5. Effect of temperature on the morphology of silica when using various solvents. *p.104*

Table 4.6. Effect of temperature on the structure and particle size of the silica when using different solvents. *p.106*

Table 4.7a. Effect of stirring on the structure and particle size of silica at 25 °C for mucic acid. *p.108*

Table 4.7b. Effect of stirring on the structure and particle size of silica at 25 °C for tartronic acid. *p.109*

Table 4.8. Summary of BET surface area results. *p.111*

Table 4.9. Tabular summary of results discussed in this section. *p.120*

Table 4.10. TGA data of the material obtained when using mucic acid as a template and diethyl ether as a solvent. *p.121*

Table 4.11. TGA data of the material obtained when using tartronic acid as a template and ethanol as a solvent. *p.121*

Table 4.12. Effect of different templates on the surface area and particle size. *p.123*

Table 5.1. Selectivity (carbon basis) of Sasol processes. *p.135*

Table 7.1. BET results of catalysts. *p.195*

Table 7.2. Summary of reactor study data. *p.215*

Table 7.3. Hyperfine interaction parameters of the Fe based catalysts. *p.220*

Table 8.1. Summary of types of silicas and properties that can be obtained by using different templates and synthesis conditions. *p.230*

List of Figures

Figure 2.1. Structures of D and L tartaric acids. *p.30*

Figure 2.2. TEM image of spherical silica particles obtained at 75 °C. *p.37*

Figure 2.3. SEM image of silica tubes formed at 0 °C. *p.37*

Figure 2.4. TEM image of a hollow silica tube obtained at 0 °C. *p.38*

Figure 2.5. SEM image of silica tubes obtained at room temperature showing that they are hollow with an inner square shape. *p.39*

Figure 2.6. The effect of % NH_3 to water in NH_4OH on the amount (▫) and average length (•) of tubes formed. *p.41*

Figure 2.7. Effect of % water to ethanol (vol %) used on the amount (▫) and average length (•) of tubes formed. *p.43*

Figure 2.8. TEM image of nanotubes and fragments obtained when water is used as a solvent (no ethanol present). *p.44*

Figure 2.9. Effect of time before the addition of NH_4OH on the amount (▫) and average length (•) of tubes formed. *p.46*

Figure 2.10. TEM image of silica fragments obtained after 12 hours. *p.46*

Figure 2.11. Effect of stirring rate on the number of tubes formed. *p 48*

Figure 2.12. N_2 adsorption-desorption isotherm of SiO_2 where DL-tartaric acid was used as a template (the sample was prepared at room temperature using 28% ammonia solution and non-stirring condition). *p.51*

Figure 2.13. BJH pore size distribution plot (adsorption mode). *p.52*

Figure 2.14. TGA curve of the uncalcined silica material (room temperature, 28% ammonia solution and non-stirring). *p.53*

Figure 2.15. Powder XRD pattern of silica nanotubes (room temperature, 28% ammonia solution and non-stirring). *p.54*

Figure 2.16. IR spectrum of a silica material (recorded in KBr) obtained at room temperature. *p.55*

Figure 3.1. Chemical structure of citric acid. *p.66*

Figure 3.2. Synthesis of citric acid templated silica materials by the sol-gel method. *p.71*

Figure 3.3. TEM image of hollow spheres obtained at 75 °C. *p.74*

Figure 3.4. TEM image of tubes obtained at 0 °C. *p.74*

Figure 3.5. The effect of % NH_3 to water in NH_4OH on the amount (▫) and average length (•) of tubes formed. *p.77*

Figure 3.6. TEM image of the mixture of hollow and filled spheres obtained when 16% NH_3 (aq) concentration is used. *p.78*

Figure 3.7. TEM image of spherical particles (filled) obtained when 5% of water is used. *p.80*

Figure 3.8. Effect of time before the addition of NH_4OH on the amount (∆) and average length (•) of tubes formed. *p.82*

Figure 3.9. TEM image of a hollow tube obtained after 6 hours. *p.83*

Figure 3.10. TEM image of silica fragments obtained after 12 hours. *p.84*

Figure 3.11. Effect of stirring rate on the number of tubes formed. *p.86*

Figure 3.12. N_2 adsorption-desorption isotherm of SiO_2 (ethanol/water, 0 °C). *p.88*

Figure 3.13. BJH pore size distribution plot (adsorption mode). *p.89*

Figure 3.14. TGA curve of silica obtained at 0 °C. *p.90*

Figure 4.1. Structures of all templates used. *p.97*

Figure 4.2. TEM image of SiO_2 obtained at 0 °C when ethanol is used as a solvent. *p.107*

Figure 4.3. Nitrogen adsorption-desorption isotherm of SiO_2 synthesised from mucic acid (diethyl ether, 25 °C). *p.112*

Figure 4.4. BJH pore size distribution for SiO_2 synthesised from mucic acid (diethyl ether, 25 °C), desorption mode. *p.113*

Figure 4.5. Nitrogen adsorption-desorption isotherm of SiO_2 synthesised from mucic acid (diethyl ether, 75 °C). *p.114*

Figure 4.6. BJH pore size distribution for SiO_2 synthesised from mucic acid (diethyl ether, 75 °C), desorption mode. *p.115*

Figure 4.7. Nitrogen adsorption-desorption isotherm of SiO_2 formed from tartronic acid (ethanol, 25 °C). *p.116*

Figure 4.8. BJH pore size distribution for SiO_2 synthesised from tartronic acid (ethanol, 25 °C). *p.117*

Figure 4.9. Nitrogen adsorption-desorption isotherm of SiO_2 formed from tartronic acid, ethanol, 75 °C). *p.118*

Figure 4.10. BJH pore size distribution plot for SiO_2 synthesised from tartronic acid (ethanol, 75 °C), adsorption mode. *p.119*

Figure 4.11. SEM image showing the spherical particles obtained when using glucose as a template. *p.124*

Figure 4.12. N_2 adsorption-desorption isotherm of SiO_2 that was obtained when glucose was used as a template. *p.126*

Figure 4.13. Powder XRD pattern of silica produced when sucrose was used as a template. *p.127*

Figure 4.14. IR spectrum of a silica material formed from sucrose (recorded in KBR). *p.128*

Figure 5.1. Various F-T reactors: (A) Multi-tubular ARGE fixed-bed, (B) Circulating fluidised synthol, (C) Fixed fluidised or slurry phase. *p.137*

Figure 5.2. Potassium effect on relative activity. *p.146*

Figure 5.3. Anderson-Schulz-Flory plot of the formation of hydrocarbons from CO hydrogenation, where W is the weight fraction of products having n carbon atoms. *p.157*

Figure 5.4. Schematic of the alkyl mechanism for the polymerisation of surface methylenes to surface alkyls. p.*157*

Figure 5.5. The alkenyl mechanism for the stepwise polymerisation of methylenes in the Fischer-Tropsch reaction. *p.159*

Figure 6.1. Experimental set-up used for the precipitation of the iron catalyst. *p.173*

Figure 6.2. The plug flow reactor system configuration. *p.174*

Figure 6.3. The plug flow reactor. *p.175*

Figure 6.4. A typical spectrum using a TCD and a Carbosieve IIS column. *p.179*

Figure 6.5. The hydrocarbon separation using a Porapak Q column. *p.179*

Figure 6.6. The separation obtained using BP1 Megabore capillary column. *p.180*

Figure 7.1. The proposed structure of a) 9% SiO_2, b) 18% SiO_2, c) 27% SiO_2 catalysts. *p.194*

Figure 7.2. TPR profiles of catalysts a) Ruhrchemies, b) Nanotubes, c) Hollow spheres, d) Stöber spheres. *p.200*

Figure 7.3. TPR profile of copper supported on silica. *p.201*

Figure 7.4. TEM images of the 18Ru catalyst. *p.204*

Figure 7.5. Low and high magnification TEM images of the 18Nano catalyst. *p.205*

Figure 7.6. TEM images of the 18Holo catalyst. *p.206*

Figure 7.7. TEM images of the 18Stob catalyst. *p.206*

Figure 7.8. TEM image of a 9Ruhr catalyst. *p.207*

Figure 7.9. TEM images of the 9Nano catalyst. *p.207*

Figure 7.10. a) TEM image of a 9Holo catalyst, b) TEM image showing some broken hollow spheres. *p.208*

Figure 7.11. Low and high magnification TEM images of the 9Stob catalyst. *p.208*

Figure 7.12. Effect of support type and content on catalyst activity and stability: a) 9% SiO_2, b) 18% SiO_2, c) 27% SiO_2. *p.212*

Figure 7.13. Selectivities of catalysts. *p. 216*

Figure 7.14. Olefin to paraffin ratios of catalysts. *p.216*

List of Abbreviations and Symbols

PART I

A_N	-	Nucleophilic addition
aq	-	Aqueous
BET	-	Brunaer, Emmett and Teller
°C	-	Degrees celcius
BJH	-	Barret, Joyner and Halenda
EtOH	-	Ethanol
Fig.	-	Figure
H_2O	-	Water
IR	-	Infrared
KV	-	Kilovolts
K	-	Kelvin
N	-	Coordination number
NH_4OH	-	Ammonium hydroxide
NH_3	-	Ammonia
nm	-	Nanometer
Pa	-	Pascals
S_N	-	Nucleophilic substitution
SEM	-	Scanning Electron Microscopy
SiO_2		Silica

TBOT	-	Tetrabutylorthotitanate
TEOS	-	Tetraethylorthosilicate
TEM	-	Transmission Electron Microscopy
TGA	-	Thermogravimetric Analysis
μm	-	Micrometer
Vol %	-	Volume percent
XRD	-	X-ray diffraction
Z	-	Oxidation state

PART II

α	-	Alpha
ASF	-	Anderson, Schulz and Flory
$A_{C2,cal}$	-	Area of the C2 hydrocarbon in the calibration gas
$A_{HC,i}$	-	Area of the ith hydrocarbon
Ar	-	Argon
Ar_{in}	-	Area of the argon peak in the feed
Ar_{out}	-	Area of the argon peak in the product
B_{HF}	-	Hyperfine magnetic field
BET	-	Brunaer, Emmett and Teller
CFB	-	Circulating Fluidised Bed
CH_2	-	Methylene
CO	-	Carbon monoxide

CO_2	-	Carbon dioxide
CO_{in}	-	Area of the CO peak in the feed
CO_{out}	-	Area of the CO peak in the product
Cu	-	Copper
X'-$Fe_{2.5}C$	-	Chi carbide
ε'-$Fe_{2.2}C$	-	Epsilon prime carbide
F_{in}	-	Gas flow rate into the reactor (ml/s)
F_{out}	-	Gas flow rate out of the reactor (ml/s)
Fe	-	Iron
FFB	-	Fixed Fluidised Bed
FID	-	Flame Ionisation Detector
Fig.	-	Figure
F-T	-	Fischer-Tropsch
FTS	-	Fischer-Tropsch synthesis
G.C	-	Gas chromatograph
GHSV	-	Gas hourly space velocity
h	-	Hour
H_2	-	Hydrogen
HTFT	-	High Temperature Fischer-Tropsch
IS	-	Isomeric shift
K	-	Potassium
KNO_3	-	Potassium nitrate
LTFT	-	Low Temperature Fischer-Tropsch

m_i	-	Mass of component i
M_i	-	Moles of type i hydrocarbons
ml	-	Mililiters
nm	-	Nanometer
PFR	-	Plug Flow Reactor
PSD	-	Pore size distribution
QS	-	Quadruple splitting
r_{CO}	-	Specific activity (mmol CO reacted /g /s)
r_p	-	Rate of chain propagation
r_t	-	Rate of chain termination
Rf_i	-	Response factor of the ith hydrocarbon
S	-	Mass fraction of component i
SAS	-	Sasol Advanced Synthol
SEM	-	Scanning Electron Microscopy
SiO_2	-	Silica
SSBR	-	Sasol Slurry Bed Reactor
TCD	-	Thermal Conductivity Detector
TEM	-	Transmission Electron Microscopy
TFBR	-	Tubular Fixed Bed Reactor
TPR	-	Temperature Programmed Reduction
µm	-	Micrometre
µS	-	microSiemen
UHP	-	Ultra High Purity

W_n	-	Weight fraction of product having n atoms
WGS	-	Water-gas-shift
$X_{C2,cal}$	-	Mole fraction of the C2 hydrocarbon in the calibration gas
$X_{HC,i}$	-	Mole fraction of the ith hydrocarbon

PART I

SYNTHESIS OF SILICA MATERIALS BY THE SOL-GEL METHOD

CHAPTER ONE

THE SYNTHESIS OF INORGANIC MATERIALS BY SOL-GEL PROCESSING: A REVIEW

1.1 Introduction

The creation of powerful new materials for innovative applications is one of the big scientific and technical challenges of our day. The sol-gel route, because it controls the variables involved in solid synthesis, can be considered as an extremely useful way of preparing these advanced materials. Therefore identifying and controlling the early stages of the sol-gel reaction process is vital to understanding many advanced material developments and applications.

This portion of the thesis provides a short review of the preparation of inorganic materials (from molecular precursors) using the sol-gel technique. Following a general introduction to the background of sol-gel chemistry, the synthesis and applications of sol-gel chemistry, the role of templates in sol-gel synthesis, and the synthesis of sol-gel oxide supports with potential use in catalysis is then described.

1.1.1 Terminology[1]

Prior to a discussion of the use of the sol-gel technique to synthesize inorganic materials, some terms used in the sol-gel literature are described below.

A *colloid* is defined as a suspension in which the dispersed phase is so small (~1 – 1000 nm) that gravitational forces are negligible and interactions are dominated by short-range forces, such as van der Waals attraction as well as surface charges. A *sol* is a colloidal suspension of solid particles in a liquid. A *gel* consists of continuous solid and fluid phases of colloidal dimensions. In the sol-gel process, the precursors for the preparation of a colloid consist of a metal or metalloid element surrounded by various *ligands* (appendages *not* including another metal or metalloid atom). For example, a common precursor used to synthesize aluminium oxide is an organic compound such as $Al(OC_4H_9)_3$. The latter is an example of an *alkoxide*, the class of precursors most widely used in sol-gel studies.

Metal alkoxides are members of the family of *metalorganic* compounds, which have an organic ligand attached to a metal or metalloid atom. The most thoroughly studied example is tetraethylorthosilicate (TEOS), $Si(OC_2H_5)_4$. *Organometallic* compounds are defined as having direct metal-carbon bonds, not metal-oxygen-carbon linkages as in metal alkoxides; thus alkoxides are not true organometallic compounds, although this usage is frequently found in the literature.

A *polymer* is an enormous molecule (also called a *macromolecule*) formed from hundreds of units called *monomers*. A monomer is capable of forming at least two bonds. An *oligomer* is a molecule of intermediate size – much larger than a monomer, but smaller than a polymer.

If a monomer can make more than two bonds, then there is no limit on the size of the 3-D molecule that can be formed from the monomer. If one molecule reaches macroscopic dimensions and extends throughout the solution, the substance formed is a gel. Thus, a gel is a substance that contains a continuous solid skeleton enclosing a continuous liquid phase, both of colloidal dimensions. The continuity of the structure gives elasticity to the gel. Continuity means that one could travel through the solid phase from one side of the sample to the other without having to enter the liquid; conversely, one could make the same trip entirely within the liquid phase. If the smallest dimension of the gel is greater than a few millimetres, the object formed is generally called a *monolith*.

The term *aging* is applied to the process of change in structure and properties after gelation. Drying by evaporation under normal conditions gives rise to capillary pressure that causes shrinkage of the gel network. The resulting dried gel, called a *xerogel*, is often reduced in volume by a factor of 5 to 10 compared to the original wet gel. If the wet gel is placed in an autoclave and dried under supercritical conditions, there is no interface between liquid and vapour, so there is no capillary pressure and relatively little shrinkage. This process is called *supercritical drying* and the product produced is called an

aerogel. The gels may indeed be mostly air, having volume fractions of solid as low as ~1 %. They are the lowest density materials known.

Xerogels and aerogels are useful in the preparation of dense ceramics, but they are also interesting in themselves because their high porosity and surface area make them useful as catalytic substrates, filters and so on. Most gels are amorphous (i.e. non-crystalline), even after drying, but many crystallize when heated at high temperatures or calcined. It is found that the dried gel contains many labile sites that offer opportunities for new chemical reactions.

1.1.2 Principles of the Sol-Gel Process

The sol-gel process involves the formation of a sol followed by the formation of a gel. The gel is then dried to remove the organic solvents and leave a porous network. The sol-gel approach to material synthesis is based on the preparation of hydrolysable molecular precursors, mostly metal or semi-metal alkoxides e.g. ($Si(OR)_4$) due to their high reactivity.

Hydrolysis and polycondensation reactions lead to the formation of oxo-polymers or metal oxides.[1] The mild conditions used in the sol-gel process allow the introduction of organic molecules inside an inorganic network.[2,3] These fundamental chemical processes are influenced by several parameters which, once they are understood for a particular chemical system, allow the control of the homogeneity (or controlled heterogeneity) of the nano- and micro- structure of the derived material.[4]

'Design' of sol-gel materials therefore is possible, in a simplified sense, by variation of the chemical composition of the molecular building blocks and by variation of the nano- and micro-structure. Both influence the properties of the final material to a very high degree.

In general, the sol-gel process offers significant control over specific surface area, porosity, pore volume and pore size distribution of the material.

1.1.3 History of the Sol Gel Process

The first metal alkoxide was prepared from $SiCl_4$ and ethanol by Ebelmen[5] (in 1845) who found that the compound gelled on exposure to the atmosphere. This metal alkoxide was called silicon tetraethoxide (also variously known as tetraethoxysilane, tetraethylorthosilicate or TEOS)

The discovery of the exceptional tendency of organosilicon compounds to form siloxane polymers containing organic side groups (silicones) caused an explosion of activity in the 1930's (almost a century later) that established a chemical and physical basis for understanding the processes of hydrolysis and condensation.[1] The process of supercritical drying to produce aerogels was invented by Kistler[6] in 1932 who was interested in demonstrating the existence of the solid skeleton of the gel, and in studying the structure. The rediscovery of aerogels took place in the 1960's. In 1968 Nicolaon and Teichner[7] proposed a new method for the preparation of silica aerogels by carrying out the sol-gel transition in the very solvent which was removed at supercritical conditions. This method allowed fast processing of the reactants

(a few hours), compared with the technique proposed by Kistler[6] (several weeks). This method was later extended to the preparation of other single- and multi-component inorganic oxides.[8] Hence, this method can be considered as one of the most important advances in sol-gel science.[9]

As far as xerogel powders are concerned, the vital breakthrough in the late 1960's was the demonstration that the process could be used to control the *shape* and *size* of solid particles; in particular, high-density spherical particles with narrow controlled size ranges could be achieved. One example of this was demonstrated by Stöber[10] and co-workers in 1968 when they synthesized monodispersed spherical particles with uniform sizes (0.05 – 2 μm) by the sol-gel method.

Silica gels are the oldest and most closely studied gels, but as Table 1.1 shows, there are now many systems that can be gelled from suitable sols, including almost half of the periodic table.

Table 1.1. Elements used to date in the sol-gel process[1]

Li	Y	Cr	B	N
Na	La	Fe	Al	P
K	Nd	Co	In	As
Cs	Th	Ni	C	Sb
Mg	U	Pd	Si	O
Ca	Ti	Au	Ge	S
Sr	Zr	Zn	Sn	F
Ba	Hf	Cd	Pb	

Hierarchial structures that incorporate inorganic-organic materials to form mesoscopic structures have been designed and synthesized in recent years. Morphological control as well as the handling and texture of mesoporous materials are extremely important for many applications. Mesoporous silicate materials with a variety of morphologies have been synthesized for many applications.[11-19]

Recently, there have been reports of mesoporous materials with various particle shapes such as fibers, spheres, ropes, discoids, toroids, hollow tubes, hollow spheres and dodecahedra.[19-28] The templates that have been used to date are surfactants, organogelators, hydroxy carboxylic acids, as well as porous or fibrous materials such as carbon nanotubes and membranes.

1.1.4 Advantages of the Sol-Gel Process

One of the main advantages of the sol-gel process is that it allows careful control of the size and morphology of clusters/particles in the sol or gel during the early processing stages, so that high quality end products (in the form of powders, films or coatings) can be developed to fulfil specific demands.[29,30] The mild reaction conditions allow the incorporation of organic moieties into inorganic networks. These organic-inorganic hybrid materials are particularly useful because components with different combinations of properties can be blended together.

The general properties of materials synthesized by the sol-gel method are high purity, better homogeneity, controlled porosity combined with the ability to form large surface area materials at low temperatures, possibility of preparing multi-component systems with broad ranges of compositions and good dispersion of minor components.[9]

1.2 Sol-Gel Chemistry

Considering the key role of sol-gel reactions in the preparation of organic-inorganic hybrid materials, it is difficult to understand their preparation without the basic knowledge of the sol-gel process.[31] Over the past four decades numerous studies have been carried out in the field of sol-gel chemistry, and great progress has been made in presenting a reaction mechanism consistent with the data.[1]

The three-step mechanism to describe the sol-gel process is as follows:[32]

Step 1: Hydrolysis of a metal or semi-metal alkoxide to form a hydroxylated product and the corresponding alcohol.

Hydrolysis:

$M(OR)_4 + xH_2O \rightarrow M(OH)_4 + xROH$ (1.1)

M = Si, Ti, Al, Zr, etc

R = Alkyl group

This mechanism is highly dependent on pH and can be catalysed under acidic or basic conditions.

Step 2: Condensation between an unhydrolyzed alkoxide group and a hydroxyl group or between two hydroxyls eliminates the solvent (water and alcohol) and forms a colloidal mixture called the sol.

Condensation:

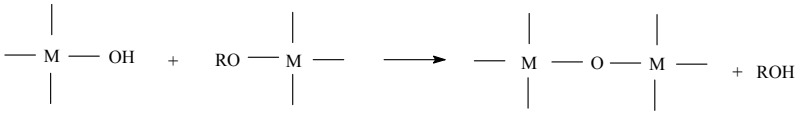

(2.1)

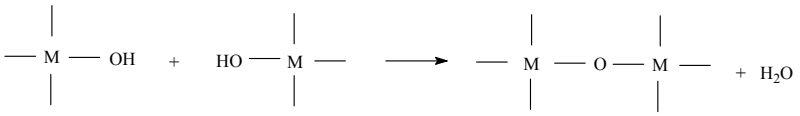

(2.2)

Step 3: Polycondensation between these colloidal sols as well as additional networking eventually results in the generation of a porous three-dimensional network.

Polycondensation:

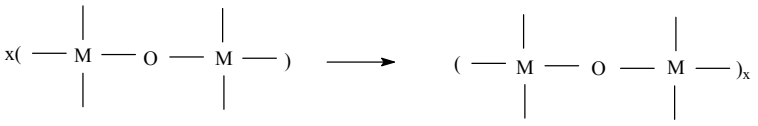

(3.1)

Both hydrolysis and condensation occur by nucleophilic substitution (S_N) mechanisms that involve three steps: nucleophilic addition (A_N), proton transfer within the transition state, and removal of the protonated species as either alcohol or water.

The sol-gel process generally starts with alcoholic or other low molecular weight organic solutions of monomeric metal or semi-metal alkoxide precursors $M(OR)_n$ and water. M represents a network-forming element such as Si, Al, Ti, B, etc. Table 1.2 shows some of the alkoxides that have been used in the sol-gel synthesis.

Table 1.2. Some of the alkoxides used in sol-gel synthesis[34]

Element	Alkoxide	Element	Alkoxide
Aluminium	$Al(O\text{-}isoC_3H_7)_3$	Phosphorus	$P(O\text{-}C_4H_9)_3$
	$Al(O\text{-}secC_4H_9)_3$	Silicon	$Si(O\text{-}CH_3)_4$
Barium	$Ba(O\text{-}C_3H_7)_2$		$Si(O\text{-}C_2H_5)_4$
Boron	$B(O\text{-}CH_3)_3$	Sodium	$Na(O\text{-}C_4H_9)$
Calcium	$Ca(O\text{-}C_2H_5)_2$	Titanium	$Ti(O\text{-}C_2H_5)_4$
			$Ti(O\text{-}C_4H_9)_4$
			$Ti(O\text{-}C_5H_7)_4$
Germanium	$Ge(O\text{-}C_2H_5)_4$	Yttrium	$Y(O\text{-}C_2H_5)_3$
Iron	$Fe(O\text{-}C_3H_7)_3$	Zirconium	$Zr(O\text{-}isoC_3H_7)4$
Niobium	$Nb(O\text{-}C_2H_5)_4$		$Zr(O\text{-}C_4H_9)_4$

Generally, both the hydrolysis and condensation reactions occur simultaneously once the hydrolysis reaction has been initiated. The thermodynamics of these reactions are governed by the strength of the entering nucleophile, the electrophilicity of the metal, and the partial charge and stability of the leaving group.

As can be seen in eqs. 1.1, 2.1 and 2.2, both hydrolysis and condensation steps generate low molecular weight by-products such as alcohol and water. The small molecules must be removed from the system, and such removal would lead in the limit, to a tetrahedral SiO_2 network if the species M were silicon. The removal of these by-products also contributes to the high shrinkage that occurs during the classical sol-gel process.[33]

For non-silicate metal alkoxides e.g. aluminium alkoxide, generally no catalyst is needed for the hydrolysis and condensation reactions. The reactions are very rapid. In the case of silicon based metal alkoxides, the hydrolysis and condensation reactions typically proceed with either an acid or base as catalyst. Therefore, the structure and or morphology of the resulting network strongly depends on the nature of the catalyst and the pH of the reaction.[31]

1.3 Role of templates in the sol-gel synthesis

Since the sol-gel method has emerged as a versatile way of obtaining new types of materials with controlled microstructures which can be 'tailored' chemically under low temperatures. Many synthetic routes and strategies have been developed to yield a wide diversity of materials with various frameworks, chemical compositions and pore structures. So far, most of these materials were synthesized by combining template technology with the sol-gel method.

The template technology uses template agents such as organic molecules (e.g. surfactants, organogelators, and hydroxycarboxylic acids, etc), inorganic or organometallic molecules, polymers or solid particles, to intercross or arrange with the material's major components by the way of co-operation or self-assembly to form a new organic-inorganic system. Porous nano-structured materials are then achieved by the elimination of templates by calcination or extraction.[35,36]

Since Kresge et al[37] of Mobil Corporation developed a class of mesoporous materials of the M41S family with narrow pore size distributions by utilizing ionic surfactants as structure-directing agents, more explorations and studies have been done on the many aspects of template technology such as synthesis process, synthesis mechanism,[38] template agent's roles and the resulting material structures and properties.[39,40] Hence the templated sol-gel method appears to be a new way of tailoring porous structures.

In the surfactant templating route to mesoporous materials, pore diameters can be controlled by changing the alkyl chain length of the surfactant,[41-43] or by adding auxiliary hydrocarbons,[41,44] or by adjusting the initial pH of the synthesis mixture.[45] Whereas in the non-surfactant templating route the material's pore diameters can be controlled by varying the template concentration. (But the control ability of pore diameter by template content is limited, in that the template molecules will crystallize from the gel at high template content[46])

The template-directed sol-gel method cannot just be used to control the pore diameter of the materials but it can also be used to give wide-ranging materials with various external shapes and internal structures. For example, in the case where surfactants are used to prepare mesoporous materials such as MCM41, surfactant assemblies act as templates for hexagonally packed mesopores. As for synthesis of tubular materials, various organic and inorganic templates have been used associated with the sol-gel synthesis. For example, hollow tubes of amorphous silica have been prepared by using the

external surface of self-assembled phospholipids fibers,[47] organic gel filaments,[48] viroid cylinders,[49] anodic alumina nano array,[50] and cylindrical assemblies of surfactant.[51] All the templates for the silica tube described, are however specialized molecules or arrays that are costly. Thus the studies that were carried out by Nakamura and Matsui[23] to prepare silica tubes by using simple organic acids such as D,L-tartaric acid seem to be a more attractive option to use when preparing tubular materials.

1.4 Sol-Gel Synthesized Oxide Supports

Performance in many catalytic systems is not only known to be influenced by the inherent catalytic activity of the active phase, but also by the textural and physico-chemical properties of the support. The inherent preparative advantages offered by the sol-gel method have prompted its use for synthesizing many oxidic catalytic supports notably silica and alumina.

1.4.1 Silica

High purity silica is used in a variety of industrial applications. It is used as a catalytic support, a filler, in fused silica wares, in optical glasses and as a waveguide.[34] Silica gels are also used as thermal and accoustic insulators. One of the methods of obtaining pure silica is by the controlled hydrolysis of silicon alkoxides.[52-55]

The discovery of the exceptional tendency of organosilicon compounds to form siloxane polymers containing organic side groups (silicones) caused an explosion of activity in the 1930's that established a chemical and physical

basis for understanding the processes of hydrolysis and condensation[1]. The +4 oxidation state of silicon (z = 4) is the only important oxidation state in the chemistry of silicon in naturally occurring systems[55] and the coordination number of silicon, (N), is most often 4. Compared to aluminium and the transition metals, silicon is generally less electropositive.[56] This renders silicon comparatively less susceptible to nucleophilic attack.[1] Si-C bonds are thus hydrolytically stable and allow an easy anchoring of functional organic groups.[4] Also, since N = z, coordination expansion does not spontaneously occur in silicon alkoxides on reacting with nucleophilic reagents.[1] These factors make the kinetics of hydrolysis and condensation considerably slower than that observed for alumina or transition metal alkoxide systems.[1]

Consequently, hydrolysis and condensation reactions in silicon-based alkoxide systems are usually facilitated by acid or base catalysis. For common silicon alkoxides, the hydrolysis rate is high under an acidic environment relative to that of condensation. Acid catalysis, therefore, promotes the development of more linear or polymer-like molecules in the initial stages of the reaction. On the other hand, base catalysis results in a higher condensation rate.[31] Thus this environment tends to produce more of a dense-cluster growth leading to silica with dense, colloidal particulate structures.[1, 33, 57,58]

Silica can be used as a metal catalyst support (e.g. in the Fischer-Tropsch reaction) and several research groups continue to express interest in the preparation of amorphous silica prepared by the sol-gel method.[59-61] Silica is

also active in some oxidation reactions such as methanol oxidation,[62] methane to formaldehyde oxidation[63] and ammoxidation.[64] The main advantages of sol-gel prepared silica are compositional homogeneity and low processing temperatures. Normally the alkoxide is dissolved in alcohol and hydrolyzed by the addition of water under acidic, neutral or basic conditions, yielding SiO_2 as the final product.

1.4.2 Alumina[65]

Alumina is widely used in various industries as a support, catalyst and sorbent. Its role as a support in catalysis is enhanced since it can be obtained with a wide range of surface area values. In particular, an alumina-based oxide support with high surface area (at 1000 ºC), is used in automobile exhaust gas purification catalysts.[66] Combustion catalysts used at high temperature require an even more thermo-stable support. Many experiments have been performed to improve the thermo-stability of alumina-based supports. The addition of barium oxide or lanthanum oxide has proven to be extremely effective in improving the thermo-stability of the support. Silica-doped aluminas have also been reported to show high surface area.[67] Very often, however, these additives change not only the thermo-stabilities but also other properties associated with the original support.

Developing a synthesis procedure for high surface area alumina with no additive is certainly an approach to the production of a more effective catalyst.[67] Aluminas prepared from various aluminium salts are generally contaminated with residual ions such as alkaline cations or acid residues.

Aluminium alkoxide has been used as an uncontaminated starting material to obtain pure alumina of high surface area because the alkoxide is easily purified by distillation. Conventionally, alumina synthesis by hydrolysis of the alkoxide has been carried out in solvents such as water, common alcohols or hydrocarbons such as benzene. Since Yoldas[33] developed the sol-gel technique, preparation conditions for the formation of monolithic alumina gel have been extensively studied by regulating reaction conditions such as temperature, concentration, pH, solvent, drying method etc.[1]

1.4.3 Other Sol-Gel Generated Simple Oxides

Most literature references to the applications of the sol-gel method for catalyst preparation have been reported for silica or alumina-based catalytic systems. Occasionally though, the synthesis of other simple oxidic catalysts by the sol-gel route have been reported. Some examples are listed below.

Lopez *et al.*[68] discussed the importance of preparing MgO samples with different degrees of surface hydroxylation in order to obtain a better understanding of the behaviour (activity, selectivity and deactivation) of metal catalysts dispersed on these supports. For that purpose, they prepared MgO starting from magnesium ethoxide using a series of different catalysing agents and polycondensation reactions. The control of pH and the thermal treatment allowed preparation of magnesia with controlled levels of surface –OH groups.

Nishiwaki *et al.*[69] prepared TiO_2 (anatase) from titanium isopropoxide in propyl alcohol. Solids were obtained by slowly pouring a $Ti(OC_3H_7)_3$ solution into

distilled water with vigorous stirring. These materials were dried and calcined at 420 ºC in air. Depending on the concentrations of the solutions, the particle sizes could be varied from 4 to 40 nm. The study revealed that the smaller the particle size, the greater the surface area of the sample. The effect was explained on the grounds of charge imbalance at surface species, Ti(1)-O-Ti(2), where Ti(1) and Ti(2) represent Ti atoms in different environments. The smaller the particle size, the higher the number of titanium atoms with low coordination numbers that were present at the surface.

Carturan *et al*.[70] proposed a sol-gel method to prepare catalysts by coating glass microspheres with inorganic oxides obtained from alkoxide solutions. Glass spheres (0.04 - 0.08 mm of diameter) were wetted with alcoholic solutions of several selected alkoxides including $Zr(OPr)_4$ and $Fe(OEt)_3$. The damp material was exposed to moisture to hydrolyse the alkoxide and then dried by slow solvent evaporation followed by heating at 400 ºC. The final product maintained the spherical geometry of the initial carrier and, when using dilute alkoxide solutions, the single glass pearls did not collapse to aggregates. The specific surface area was between 200 and 300 m^2/g. In this way, a cheap support, glass, can be used to disperse active oxide catalysts. The method is also interesting from the point of view of the design of catalytic reactors, leading to catalysts with good mechanical properties and avoiding diffusion problems which can appear when dealing with bulk gel materials.

Mixed-metal alkoxide systems are also of great interest because of their potential chemical and physical properties.[31] For example the petroleum

industry uses metallo-silicates as catalysts for cracking processes, for the alkylation of benzene with propylene and ethylene, and adsorbents. These alkoxide systems can be prepared by the sol-gel process. Kolesnikov et al.[71] synthesized various metallo-silicates such as aluminium silicate and zirconium silicate and these materials were tested for cumene conversion. Increase in catalytic activity, by up to a factor of 2, were recorded.

Mixed oxides of the type SiO_2-$AlPO_4$, SiO_2-Al_2O_3-$AlPO_4$ and SiO_2-Al_2O_3 were obtained by Wijzen *et al.*[72] via hydrolysis of tetraethylorthosilicate (TEOS) in the presence of aqueous solutions of aluminium salts and/or phosphoric acid. The solids were characterised and showed high values of both their BET surface area and pore volume and a good thermal re-crystallisation stability. Similarly, titania-silica sonogels (gels prepared by ultrasonic mixing) of very high surface area (800 m^2/g) have been prepared by Bernal and co-workers[73] using TEOS and tetrabutyl orthotitanate (TBOT).

1.5 Conclusions

The sol-gel method is a fascinating new method for the generation of new materials. This is because the main advantage of the sol-gel process is that it allows careful control of the size and morphology of clusters/particles in the sol or gel during the early process stage, so that high quality end products (in the form of powders, films or coatings) can be developed to fulfil specific demands. The template-directed sol-gel method makes the sol-gel method even more versatile because wide-ranging materials with various external shapes and internal structures can be synthesized. The inherent preparative

advantages offered by the sol-gel method have prompted its use for synthesizing many oxidic catalytic supports notably silica and alumina.

1.5 References

1. C.J Brinker and G. Scherer, Sol-Gel Science: *The Physics and Chemistry of Sol-Gel Processing*, (Academic Press, London, 1990).
2. C. Sanchez, F. Robot and B. Lebeau, *J. Mater. Chem*., **9**, 35, (1999).
3. G.L. Wilkes, B. Orler and H.H. Huang, *Polym. Prep*., **26**, 300, (1985); (b) G-S. Sur and J.E. Mark, *Eur. Polym. J*, **21**, 1051, (1985); (c) H. Schmidt, A. Kaiser, H. Patzelt and H. Sholze, *J. Phys*., **43**, 275, (1982).
4. U. Schubert, *J. Chem. Soc., Dalton Trans*, 3343, (1996).
5. M. Ebelmen, *Ann. Chim. Phys*., **15**, 319, (1845).
6. S.S. Kistler, *J. Phys. Chem*., **36**, 52, (1932).
7. G.A. Nicolaon and S.J. Teichner, *Bull. Soc. Chim. France*, 1906, (1968).
8. S.J. Teichner, G.A. Nicolaon, M.A. Vicarini and G.E.E. Gardes, *Adv. Coll. Sci.*, **5**, 245, (1976).
9. M.A. Cauqui and J.M. Rodríquez-Izquierdo, *J. Non-Cryst. Solids*, **147,148**, 725, (1992).
10. W. Stober, A. Fink and E. Bohn, *J. Coll. Int. Sci*., **26**, 62, (1968).
11. P.T. Tanev, Y. Liang and T.J.Pinnavaia, *J. Am. Chem. Soc*., **119**, 8616, (1997).
12. P.T. Tanev and T.J. Pinnavaia, *Science*, **271**, 1267, (1996).
13. S.H. Tolbert, T.E. Schäffer, J. Feng, P.K. Hansma and G.D. Stucky, *Chem. Mater.,* **9**, 1962, (1997).
14. Q. Huo, D. Zhao, J. Feng, K. Weston, S.K. Buratto, G.D. Stucky, S. Schächt and F. Schüth, *Adv. Mater.*, **9**, 974, (1997).

15. P. Yang, T. Deng, D. Zhao, P. Feng, D.J. Pine, B.F. Chmelka, G.M. Whitesides and G.D. Stucky, *Science*, **282**, 2244, (1998).
16. S.S. Kim, W. Zhang and T.J. Pinnavaia, *Science*, 1998, **282**, 1302, (1998).
17. Q. Huo, J. Feng, F. Schüth and G.D. Stucky, *Chem. Mater*., **9**, 14, (1997).
18. S.M. Yang, H. Yang, N. Coombs, I. Sokolov, C.T. Kresge and G.A. Ozin, *Adv. Mater*., **11**, 52, (1999).
19. P.J. Bruinsma, A.Y. Kim, J. Liu and S. Baskaran, *Chem. Mater*., **9**, 2507, (1997).
20. S.S. Park, C.H. Lee, J.H. Cheon and D.H. Park, *J. Mater. Chem*., **11**, Advance Article, (2001).
21. (a) M. Trau, N. Yao, E. Kim, Y. Xia, G.M. Whitesides and I.A. Aksay, *Nature*, **390**, 674, (1997). (b) H. Yang, N. Coombs and G.A. Ozin, *Adv. Mater*., **9**, 811, (1997).
22. S. Oliver, A. Kuperman, N. Coombs, A. Lough and G.A. Ozin, *Nature*, 1995, **378**, 47, (1995).
23. H. Nakamura and Y. Matsui, *J. Am. Chem. Soc*., **117**, 2651, (1995); (b) H. Nakamura and Y. Matsui, *Adv. Mater*., **7**, 871, (1995).
24. L. Wang, S. Tomura, F. Ohashi, M. Maeda, M. Suzuki and K. Inukai, *J. Mater. Chem.*, **11**, 1465, (2001).
25. Y. Zhang, Y. Bando, K. Wada and K. Kurashima, *J. Mater. Sci. Lett*., **18**, 1911, (1999).
26. L. Sudheendra and A.R. Raju, *Bull. Mater. Sci*., **22**, 1025, (1999).

27. F. Miyaji, S.A. Davis, J.P.H. Charmant and S. Mann, *Chem. Mater*., **11**, 3021, (1999).
28. C.E. Fowler, D. Khushalani and S. Mann, *J. Mater. Chem.,* **11**, 1968, (2001).
29. M.Z. Hu, J.T. Zielke, C.H. Byers, J.S. Lin and M.T. Harris, *J. Mater. Sci. Lett*., **35**, 1957, (2000).
30. L.L. Hench and J.K. West, *Chem. Rev*., **90**, 33, (1990).
31. J. Wen and G.L. Wilkes, *Chem. Mater*., 1996, **8**, 1667.
32. C.M. Ingersol and F.V. Bright, *Chemtech*, 1997, January, 26.
33. B.E. Yoldas, *J. Mater. Sci*., 1986, **21**, 1086.
34. R.H. Hoppener, and H.K. Bowen., *Adv. Ceram. Mat*., 1988, **3(6)**, 595.
35. A. Ayral, C. Balzer, T. Dabadie, et al., *Catal. Today*, **25**, 219, (1995).
36. N.K. Raman and C.J. Brinker, *J. Membr. Sci*., **105**, 273, (1995).
37. C.T. Kresge, M.E. Leonowicz, W.J. Roth, J.C Vartuli and J.S. Beck, *Nature*, **359**, 710, (1992).
38. G. Bellussi, C. Perego, A. Carati, et al., *Stud. Surf. Sci. Catal*., **A84**, 85, (1994).
39. J.C. Vartuli, K.D. Schmitt, C.T. Kresge, et al., *Chem. Mater*., **6(12)**, 2317, (1994).
40. B.Z. Sophie and L.O. Mario, *Catal. Rev. Sci. Eng*., **40(3)**, 329, (1998).
41. J.S. Beck, J.C Vartuli, W.J. Roth, M.E. Leonowicz, C.T. Kresge, K.D. Schmitt, C.T.W. Chu, D.H. Olson, E.W. Sheppard, S.B. McCullen, J.B. Higgins and J.L. Schlenker, *J. Am. Chem. Soc*., **114**, 10834, (1992).
42. S. Namba, A. Machizuki and M. Kito, *Chem. Lett*., 569, (1998).
43. P.T. Tanev and T.J. Pinnavaia, *Science*, **267**, 865, (1995).

44. D. Zhao, Q. Huo, J. Feng B.F. Chemelka and G.D. Stucky, *J. Am. Chem. Soc*., **120**, 6024, (1998).

45. A. Wang and T. Kabe, *Chem. Commun*., 2067, (1999).

46. Y. Wei, D. Jin, T. Ding, W.H. Shih, X. Liu, S.Z.D. Cheng and Q. Fu, *Adv. Mater*., **3**, 313, (1998).

47. S. Baral and S. Schoen, *Chem. Mater*., **5**, 145, (1992).

48. Y. Ono, K. Nakashima, M. Sano, Y. Kanckiyo, K. Inoue, J. Iiojo and S. Shinkai, *Chem. Commun*., 1477, (1989).

49. W. Shenton, T. Douglas, M. Young, G. Stubbs and S. Mann, *Adv. Mater*., **11**, 253, (1999).

50. M. Zhang, Y. Bando and K. Wada, *J. Mater., Res*., **15**, 387, (2000).

51. M. Harada and M. Adachi, *Adv. Mater*., **12**, 839, (2000).

52. E.J. Brinker, K.D. Keeffer, D.W. Schaefer, and C.S. Ashley, *J Non. Cryst. Solids*, 1982, **48**, 47.

53. N. Toghe, G.S. Moore and J.D. Mackenzie*, J. Non.Cryst*. Solids, 1984, **63**, 95.

54. M.A Butler, P.F. James and J.D Jackson, *J. Mater. Sci*., 1996, **31**, 1675.

55. S.R. Kumar, P.K. Pillai and K.G.K. Warrier, *Polyhedron*, 1998, **17(10)**, 1699.

56. J. Livage, M. Henry and C. Sanchez, *Sol-Gel Chemistry of Transtion Metal Oxides, Progress in solid state chemistry* (Plenum Press, 1989).

57. K.D. Keefer, *Mater. Res. Soc. Symp. Proc*., 1984, **32**, 15.

58. D.W. Schaefer, J.P. Wilcoxon, K.D. Keefer, B.C. Bunker, R.K. Pearson, I.M. Thomas and D.E. Miller, *AIP Conf. Proc*., 1987, **154**, 63.

59. C. Sanchez and J. Livage, *New J. Chem*., 1990, **14**, 513.

60. D. Ulrich, *J. Non-Cryst. Solids*, 1988, **100(1-30)**, 174.

61. P.A. Haas, *Chem. Engr. Prog*. 1989, April.

62. L. Cairati and F. Trifirò. *J. Catal*., 1983, **80**, 25.

63. G.N. Kastanas, G.A. Tsigdinos and J. Schwank, *Appl. Catal*., 1988, **44**, 83.

64. J.N. Amor, *J. Catal*., 1981, **20**, 72.

65. V.I. Okafor, *Synthesis, Characterisation and Evaluation of a Diverse Range of Heterogeneous Catalysts*, PhD Thesis, University of the Witwatersrand, Johannesburg, 1998.

66. W.S. Briggs, in: *Alumina Chemicals: Science and Technology Handbook*, ed. L.D. Hart, (The American Ceramic Society, Westerville, Ohio, 1990).

67. B. Bequin, E. Garbowski and M. Primet, *J. Catal*., 1991, **127**, 595.

68. T. López, I. García-Cruz and R. Gómez, *J. Catal*., 1991, **127**, 75.

69. K. Nishiwaki, N. Kakuta and A. Ueno, *J. Catal*. 1989, **118**, 498.

70. G. Carturan, G. Francchin, V. Gottardi and G. Navazio, *J. Non-Cryst. Solids*, 1984, **63**, 274.

71. I.M. Kolesnikov, A.V. Yuablonky, S.I. Kolesnikov, A. Busenna and M.Y. Kiljanov, *Preparation of Catalysts VI*, eds. G. Poncelet, J. Martens, B. Delmon, P.A. Jacobs and P. Grange, (Elsevier, Amsterdam, 1995).

72. F. Wijzen, A. Rulmont and B. Koch, *Preparation of Catalysts VI*, eds. G. Poncelet, J. Martens, B. Delmon, P.A. Jacobs and P. Grange, (Elsevier, Amsterdam, 1995).

73. S. Bernal, J.J. Calvino, M.A. Cauqui, J.M. Rodríguez-Izquierdo and H. Vidal, *Preparation of Catalysts VI*, eds. G. Poncelet, J. Martens, B. Delmon, P.A. Jacobs and P. Grange, (Elsevier, Amsterdam, 1995).

CHAPTER TWO

A SYSTEMATIC STUDY OF THE USE OF DL-TARTARIC ACID IN THE SYNTHESIS OF SILICA MATERIALS OBTAINED BY THE SOL-GEL METHOD[1]

2.1 Introduction

The synthesis of novel porous materials has recently attracted much attention because of the potential applications of these materials in catalysis, separation science, and nanotechnology.[2] The sol-gel process has so far been one of the most attractive ways of synthesizing these porous materials because of the mild synthesis conditions required.[3]

Silica oxide nanotube materials are normally prepared by sol-gel processing in the presence of a template. The kinds of templates that have been used so far include porous or fibrous materials e.g. carbon nanotubes,[4-6] nanoporous membranes,[7-9] and organic molecules.[10-18]

---

[1]Published in *Journal of Sol-Gel Science and Technology*, **28**, 307-317, 2003

* Since this work was published a related paper by Miyaji *et al*[20] has appeared on the use of DL-tartaric acid as a template.

Porous or fibrous materials are used in the "direct" template method, where they act as guides to the formation of nanotubes. In contrast organic molecules also can act to bring about self-assembly between inorganic precursors and organic templates and offer an alternative method in the formation of inorganic nanotube materials. A detailed mechanism for the formation of silica nanotubes in the presence of laurylamine hydrochloride as template provides a useful model for envisaging the growth processes involved in tube formation[19] (see Appendix 1). So far organic templates that have been used for silica nanotube formation are long chain surfactants,[10-11] organogelators[12-14] and organic hydroxycarboxylic acids.[15-18]

Nakamura and Matsui reported on the synthesis of silica materials with different morphologies (tubes, spheres) using tartaric acid[15] and citric acid[16] as templates. The reactions were performed in an ethanol/water/tetraethylorthosilicate (TEOS)/NH_4OH reaction system under static conditions. The authors obtained hollow silica nanotubes when using DL-tartaric acid and worm-like structures when using citric acid. Recently Wang *et al.*[17] reported that citric acid could also be used to prepare silica nanotubes. Wang *et al.* found that rapid addition of aqueous ammonia under static conditions gave only uniform micrometer sized rods while slow addition of aqueous ammonia under stirring conditions gave nanotubes. Hence it appears that synthetic conditions play a key role in influencing the formation of particular forms of silica. However, a detailed evaluation of the synthetic parameters required to control the silica morphologies was not given. The

preparation of single silica nanotubes is still a major challenge as compared to the synthesis of porous materials with integrated structures.

DL-Tartaric acid is a 50:50 mixture of the two chiral enantiomers of tartaric acid. Such a mixture is called a racemic mixture or racemate, and it is denoted either by the symbol (±) or by the prefix DL to indicate a mixture of dextrorotatory and levorotatory forms. The structures of the D and L forms of tartaric acid are shown in Figure 2.1.

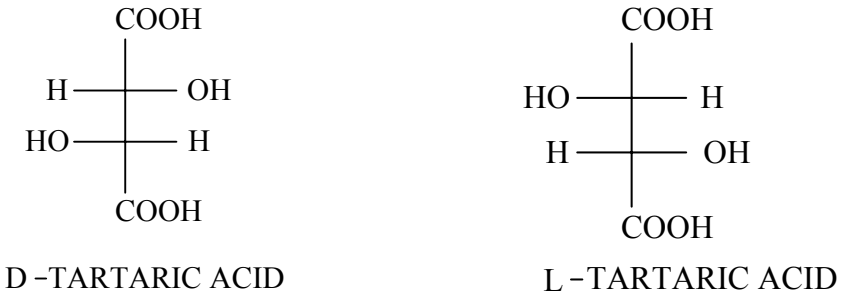

Figure 2.1. Structures of D and L tartaric acids.

In this study we have used DL-tartaric acid as a template to prepare silica materials. In particular we have prepared the silica materials using a range of reaction conditions in order to maximize the formation of nanotubes and at the same time study in detail parameters that play an important role in determining the microstructure of the silica formed in the synthesis.

2.2 Experimental

2.2.1 Preparation

Ethanol (Saarchem, 99.9%), water, tetraethylorthosilicate (TEOS), (Aldrich, 98%), DL-tartaric acid (Sigma, 98%), and ammonium hydroxide (Fluka, 98%) were used as chemical sources. The synthesis procedure followed a standard approach. The parameters that were varied during the silica synthesis were a) temperature, b) NH_4OH concentration, c) water/ethanol concentration, d) time before NH_4OH addition, e) static versus stirred conditions, f) stirring rate and g) solvent. Both the yield and product morphology were determined after each reaction.

a) Synthesis procedure when varying temperature

The synthesis when varying temperature was as follows:

- 0.26 g of template (DL-tartaric acid) was dissolved in 0.6 ml of water and then 50 ml of ethanol was added.
- The mixture was then heated to 75 ºC or cooled to 0 ºC or left at room temperature (depending on the synthesis temperature to be used).
- 7.3 g TEOS was then added to the mixture at either 0 ºC, 25ºC or 75ºC.
- The solution was left to stand at the synthesis temperature for 30 minutes to form a sol.
- Finally 20 ml of NH_4OH (28% aqueous solution) that was at room temperature was added to a sol that was at synthesis temperature to form a gel.

- After 15 – 20 minutes at the reaction temperature the reaction was observed to be complete.
- The gel was then aged at room temperature for 2 hours, and then dried in an oven at 110 ºC.
- The products were calcined under static air at 600 ºC for 4 hours.

b) Synthesis procedure when varying the concentration of NH_4OH

(The synthesis was carried out at room temperature and all the other parameters were kept constant except the concentration of NH_4OH)

- 0.26 g of DL-tartaric acid was dissolved in 0.6 ml of water and then 50 ml of ethanol was added.
- 7.3 g TEOS was then added to the mixture.
- The solution was left to stand for 30 minutes to form a sol.
- Finally 20 ml of NH_4OH (7%, 16%, 25%, 28% or 33% aqueous solution) was added to the sol to form a gel.
- After 15 – 20 minutes the reaction was observed to be complete.
- The gel was then aged at room temperature for 2 hours and then dried in an oven at 110 ºC.
- The products were calcined under static air at 600 ºC for 4 hours.

c) Synthesis procedure when varying water/ethanol concentration

(The synthesis was carried out at room temperature and all the other parameters were kept constant except the water/ethanol concentration)

- 0.26 g of DL-tartaric acid was dissolved in 0.6 – 5 ml of water and then 50 ml of ethanol was added.

- 7.3 g TEOS was then added to the mixture.
- The solution was left to stand for 30 minutes to form a sol.
- Finally 20 ml of NH_4OH (28% aqueous solution) was added to the sol to form a gel.
- After 15 – 20 minutes the reaction was observed to be complete.
- The gel was then aged at room temperature for 2 hours and then dried in an oven at 110 ºC.
- The products were calcined under static air at 600 ºC for 4 hours.

d) Synthesis procedure when varying time before NH_4OH addition

(The synthesis was carried out at room temperature and all the other parameters were kept constant except time taken before NH_4OH addition)

- 0.26 g DL-tartaric acid was dissolved in 0.6 ml of water and then 50 ml of ethanol was added.
- 7.3 g TEOS was then added to the mixture.
- The solution was left to stand for 15 minutes to 24 hours to form a sol.
- Finally 20 ml of NH_4OH (28% aqueous solution) was added to the sol to form the gel.
- After 15 – 20 minutes the reaction was observed to be complete.
- The gel was then aged at room temperature for 2 hours and then dried in an oven at 110 ºC.
- The products were calcined under static air at 600 ºC for 4 hours.

e) Synthesis procedure for static versus stirred conditions

(The synthesis was carried out at room temperature)

- 0.26 g of DL-tartaric acid was dissolved in 0.6 ml of water and then 50 ml of ethanol was added. The mixture was stirred with a magnetic stirrer and a stirring rate of about 300 rpm.
- 7.3 g TEOS was then added to the stirred mixture.
- The solution was left to stand for 30 minutes while stirring to form a sol.
- Finally 20 ml of NH_4OH (28% aqueous solution) was added to the sol to form a gel.
- After 15 – 20 minutes the reaction was observed to be complete.
- The stirring was stopped and the gel was aged at room temperature for 2 hours and then dried in an oven at 110 ºC.
- The products were calcined under static air at 600 ºC for 4 hours.

For the non-stirring condition the synthesis procedure was the same except that the stirrer was not used.

f) Synthesis procedure when varying the stirring rate

The synthesis procedure when varying the stirring rate was the same as above. All the other parameters were kept constant, but the stirring rate was varied between 100 and 1200 rpm.

g) Synthesis procedure when varying the solvent

The procedure was the same as used for the non-stirring condition but here the solvent was changed. The solvents used were ethanol, water, mixture of ethanol and water, methanol and iso-propanol.

2.2.2 Characterization

Transmission electron microscopy (TEM) images were observed with JEOL-100S and JEOL-2010 electron microscopes. A JEOL JSM 840 scanning electron microscope (SEM) was utilised to obtain scanning electron micrographs of the samples. Samples for TEM analysis were prepared by sonicating about 1 mg material into 1 ml ethanol for at least 4 minutes. A few drops of the suspension were added to a Cu grid coated with a carbon film. After approximately one minute, excess liquid was removed by touching one edge of the grid to a Whatman filter paper. Samples for SEM analysis were coated with a gold-palladium coating. BET surface areas and BJH pore size distributions were determined by nitrogen physisorption at 77 K using a Micromeritics ASAP 2010 instrument. (Degassing of the samples to 0.1 Pa at 393 K preceded every measurement. Specific adsorption pore volumes were calculated by the Barret-Joyner-Halenda (BJH) method[21] that is assumed to cover the cumulative adsorption pore volume of pores in the range 1.7 to 300 nm in diameter. Assessment of micropore volume was made from t-plot constructions using the Harkins-Jura correlation.[22]) Thermogravimetric analysis was performed on a Perkin Elmer, Thermogravimetic Analyser Pyris 1 (TGA) with a heating rate of 10º per minute. X-ray powder diffraction measurements were carried out on a Philips PW1820 instrument with a graphite monochromator using CuKα radiation generated at 40 KV and 20 mA.

2.3 Results

Table 2.1 shows the effect of varying temperature on the structure of the silica. The table shows that synthesis at 0 ºC gives a higher yield of tubes compared to reactions performed at higher temperature. At 75 ºC only spherical particles are obtained (Fig. 2.2) while long hollow tubes (100 – 250 table µm) were obtained at 0 ºC (Figs. 2.3, 2.4 and 2.5). The spheres formed at 75 ºC are much smaller than the ones formed at room temperature and 0 ºC. The tubes formed at 25 ºC are also hollow with an inner square shape. A white arrow in Figure 2.5 points at an inner square shape.

Table 2.1. Effect of temperature on the morphology of silica

Temperature [ºC]	Particle size [µm][a]	Structure[b]
0	L: 100 – 250	Tubes (95%) + Spheres (5%)
	D: 0.2 – 0.6	
	S: 0.1 – 0.3	
25	L: 15 – 120	Tubes (75%) + Spheres (25%)
	D: 0.3 – 0.5	
	S: 0.4 – 0.6	
75	S: 0.01 – 0.02	Spheres

[a]L = length of tube, D = outer diameter of tube, S = diameter of sphere

[b]% in brackets gives an estimate of the amount of material formed as determined by TEM

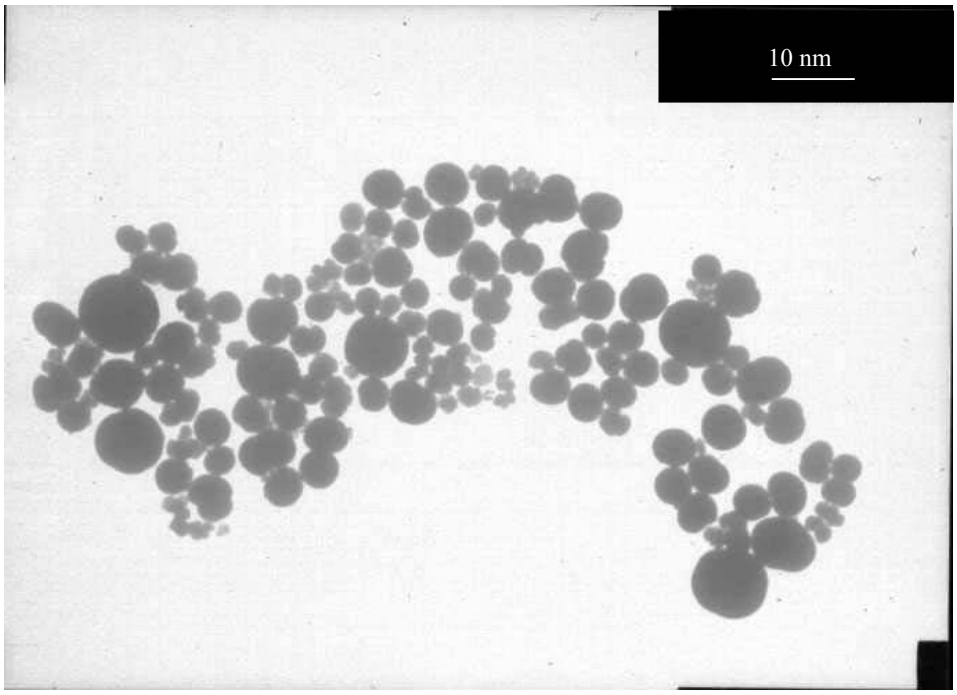

Figure 2.2. TEM image of spherical silica particles obtained at 75 °C.

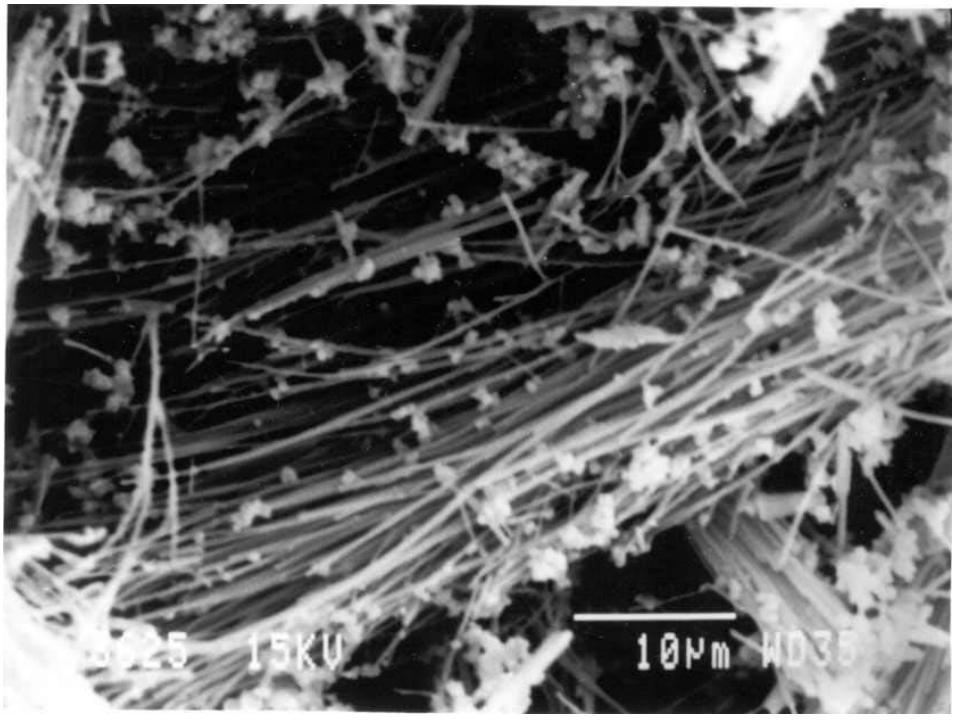

Figure 2.3. SEM image of silica tubes formed at 0 ˚C.

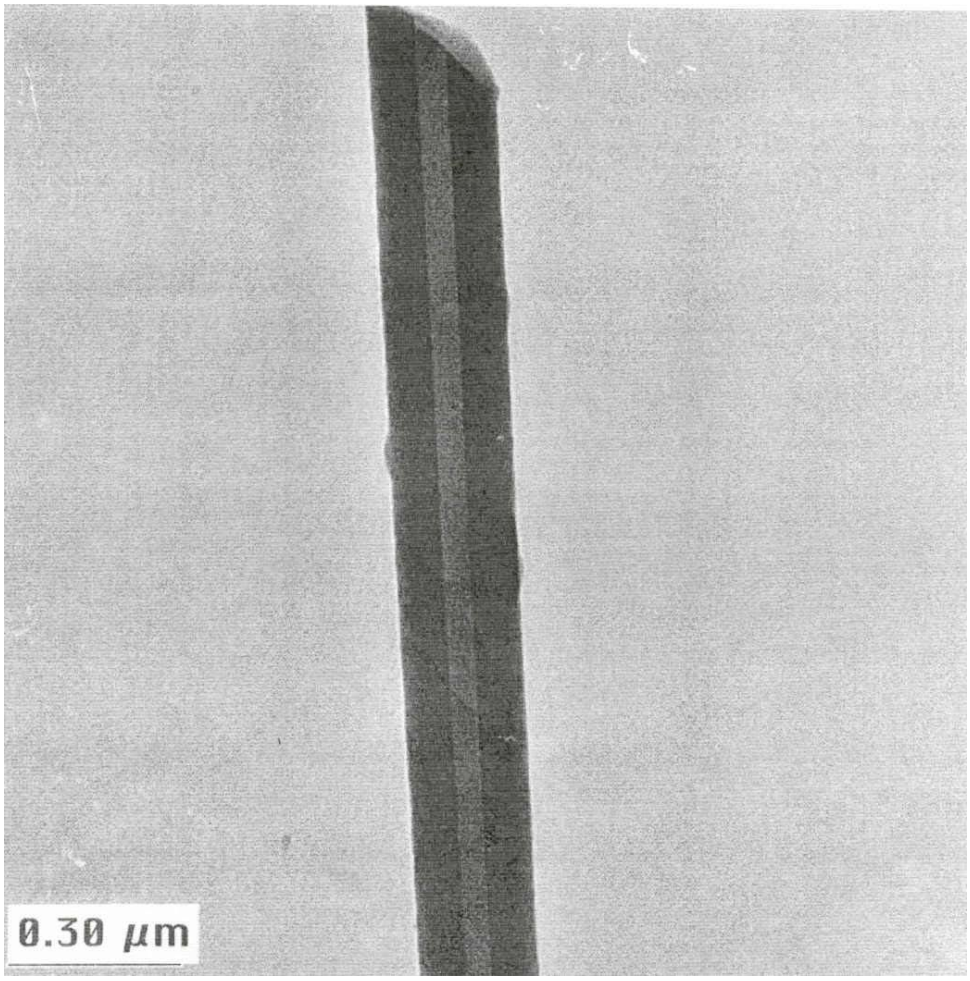

Figure 2.4. TEM image of a hollow silica tube obtained at 0 ˚C.

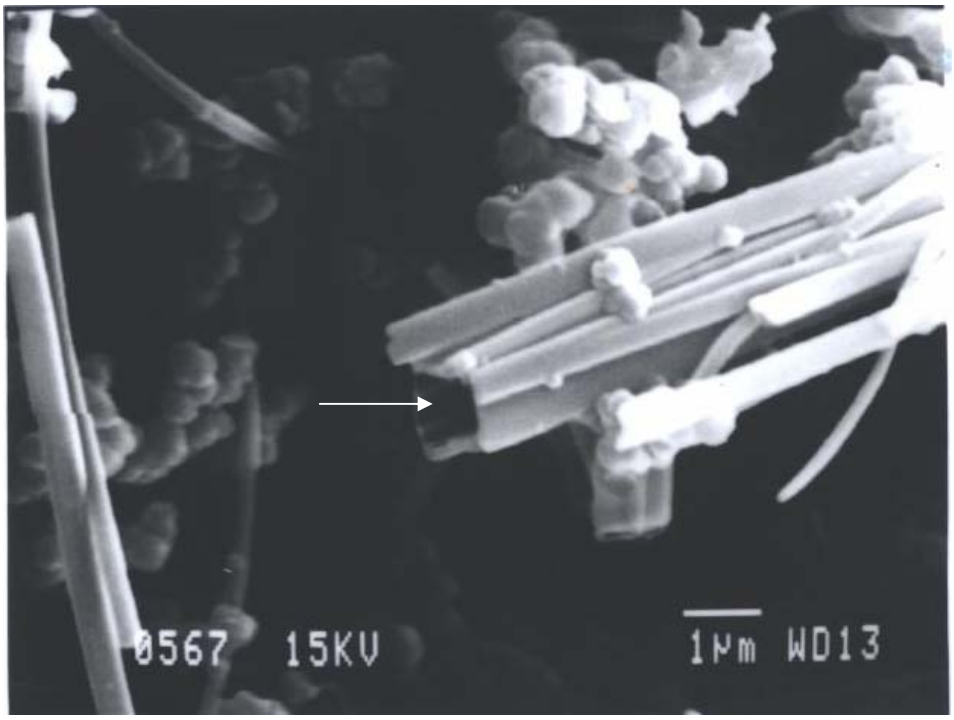

Figure 2.5. SEM image of silica tubes obtained at room temperature showing that they are hollow with an inner square shape (see arrow).

Table 2.2 and Figure 2.6 show that the yield and length of the silica tubes increase as the percentage of NH_3 to water in NH_4OH is increased. The widths of the tubes and spheres are about the same (~ 0.4 μm) when 28% aqueous ammonia solution is used. Table 2.2 shows that tube formation is detected when the NH_3 (aq) concentration >16%. When NH_4OH is not added to the reaction, the tubes that form are shorter than the ones obtained when NH_3 (aq) exceeds 25% and take a very long time to form.

Table 2.2. Effect of varying % NH_3 to water in NH_4OH

% NH_3 to water in NH_4OH	Particle size [μm][a]	Structure[b]
0	L: 7 - 10	Tubes (15%) + fragments
	D: 1 – 1.4	
7	S: 0.33 – 0.67	Spheres
16	L: 1 – 4	Tubes (20%) + spheres
	D: 0.1 – 0.2	(80%)
	S: 0.4 – 0.6	
25	L: 5 – 70	Tubes (40%) + spheres
	D: 0.067 – 0.33	(60%)
	S: 0.33 – 0.6	
28	L: 15 – 120	Tubes (75%) + spheres
	D: 0.3 – 0.5	(25%)
	S: 0.4 – 0.6	
33	L: 6.67 – 80	Tubes (80%) + spheres
	D: 0.2 – 0.5	(20%)
	S: 1.67 – 1.82	

[a]L = length of tube, D = outer diameter of tube, S = diameter of sphere

[b]% in brackets gives an estimate of the amount of material formed as determined by TEM

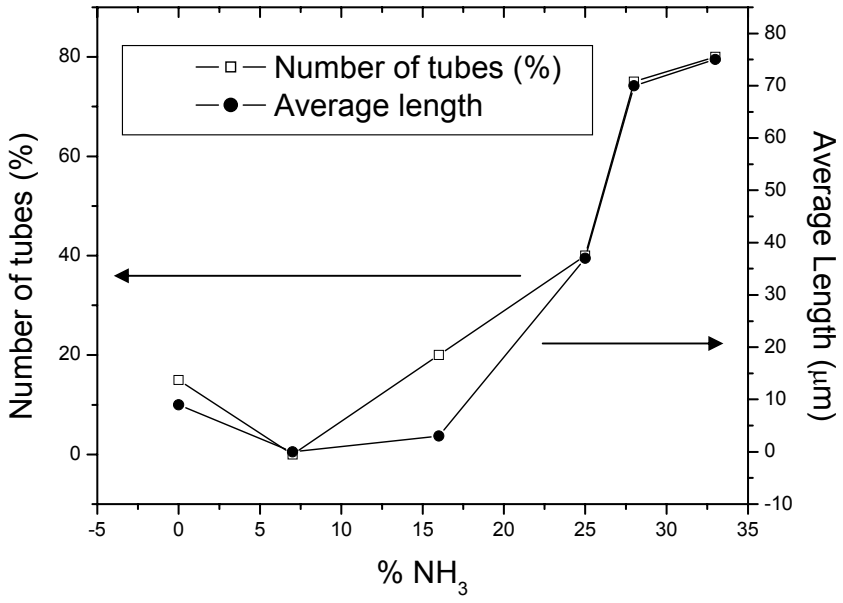

Figure 2.6. The effect of % NH_3 to water in NH_4OH on the amount (▫) and average length (●) of tubes formed.

Table 2.3 and Figure 2.7 show that the formation of the tubes is sensitive to the amount of water present during the reaction. Tubes form only when the percentage of water is < 5 % (vol %). Spherical particles become smaller as more water is used. When the concentration of water is 1.1% the tubes formed are the longest. The TEM images show that when water is the only solvent used the structure of the silica consists of nanotubes and silica fragments instead of nanotubes and spherical particles (Fig. 2.8). When ethanol is the only solvent used about 60% of silica is found in tubular form.

Table 2.3. Effect of H_2O/EtOH dilution

% H_2O (vol %)	Particle size [µm][a]	Structure[b]
0	L: 50 – 100 D: 0.40 - 0.60 S: 0.35 – 0.40	Tubes (60%) + spheres (40%)
1.1	L: 15 – 120 D: 0.3 – 0.5 S: 0.4 – 0.6	Tubes (75%) + spheres (25%)
3	L: 50 – 90 D: 0.25 – 0.30 S: 0.33 – 0.35	Tubes (60%) + spheres (40%)
5	L: 2.5 – 25 D: 0.05 – 0.07 S: 0.25 – 0.5	Tubes (50%) + spheres (50%)
10	S: 0.2 – 0.6	Spheres
100	L: 50 – 70 D: 1 – 1.25	Fragments + tubes (15%)

[a]L = length of tube, D = outer diameter of tube, S = diameter of sphere

[b]% in brackets gives an estimate of the amount of material formed as determined by TEM

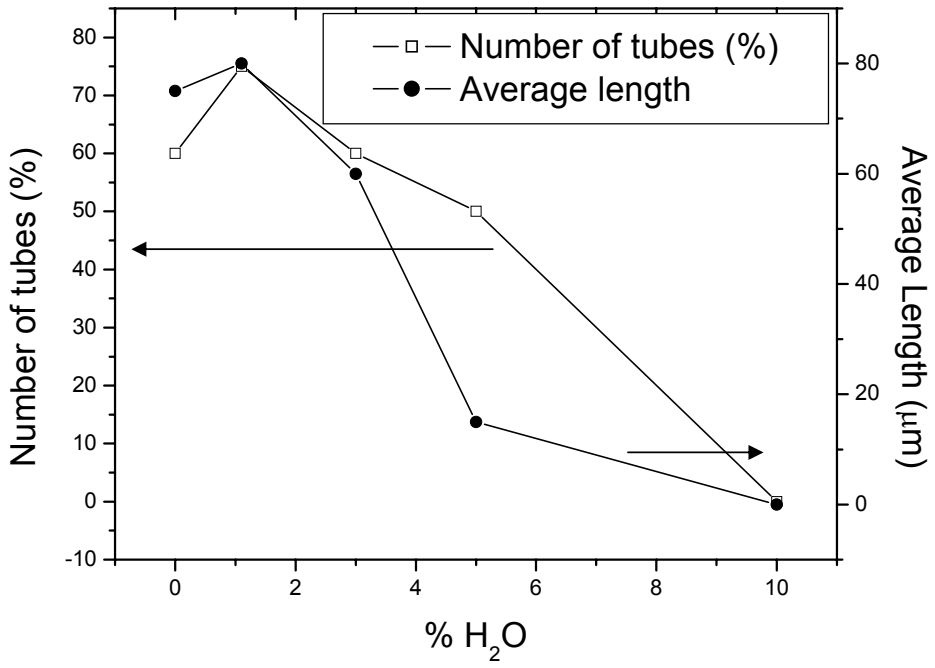

Figure 2.7. Effect of % water to ethanol (vol %) used on the amount (▫) and average length (●) of tubes formed.

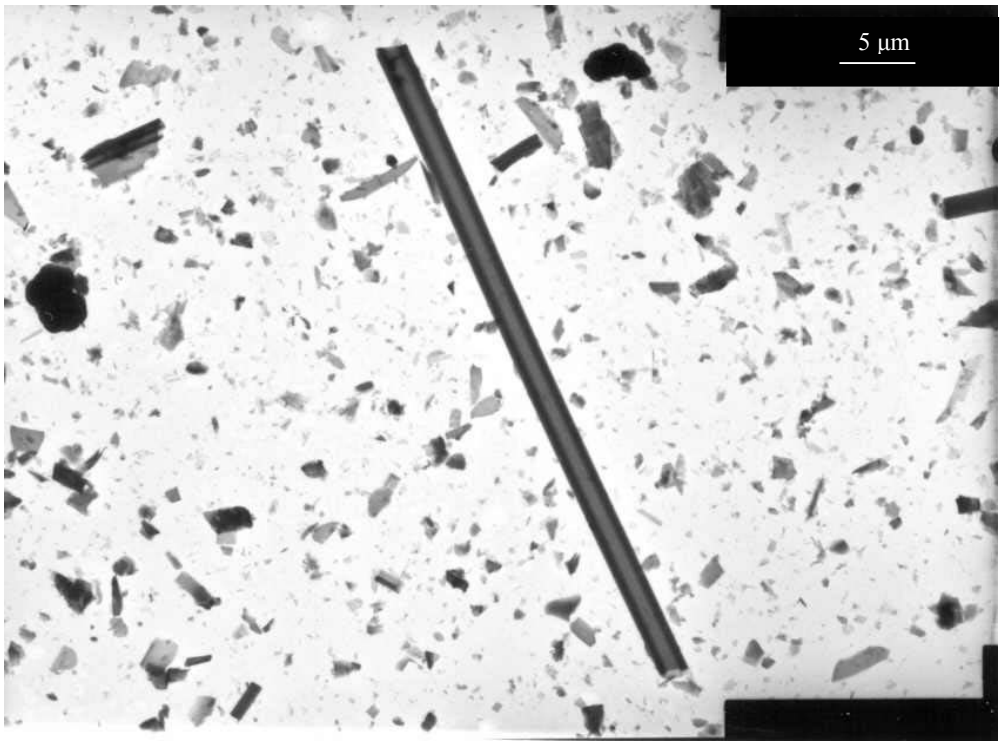

Figure 2.8. TEM image of nanotubes and fragments obtained when water is used as a solvent (no ethanol present).

Table 2.4 and Figure 2.9 show that the time taken before adding ammonium hydroxide to gel the solution has an effect on the yield and length of the tubes formed. The yield of tubes decreases as more time is taken before adding ammonium hydroxide but the length of tubes increases as the time is increased. After 12 hours silica fragments start to form instead of tubes (Fig. 2.10).

Table 2.4. Effect of varying time before the addition of NH_4OH

Time [hrs]	Particle size [μm][a]	Structure[b]
0.25	L: 20 – 100	Tubes (85%) + spheres (15%)
	D: 0.2 – 0.6	
	S: 0.4 – 0.5	
0.5	L: 15 – 120	Tubes (80%) + spheres (20%)
	D: 0.3 – 0.5	
	S: 0.4 – 0.6	
1.5	L: 30 – 200	Tubes (70%) + spheres (30%)
	D: 0.33 – 0.67	
	S: 0.33 – 0.45	
6	L: 30 - 220	Tubes (10%) + Fragments
	D: 0.5 – 0.8	
	S: 0.2 – 0.5	
12	-	Fragments
24	-	Fragments

[a]L = length of tube, D = outer diameter of tube, S = diameter of sphere

[b]% in brackets gives an estimate of the amount of material formed as determined by TEM

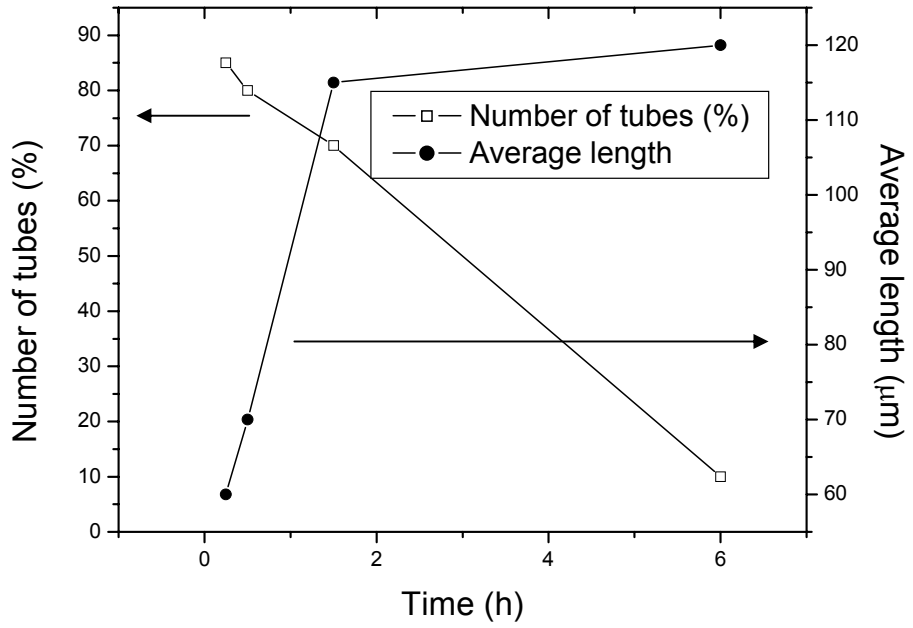

Figure 2.9. Effect of time before the addition of NH_4OH on the amount (▫) and average length (●) of tubes formed.

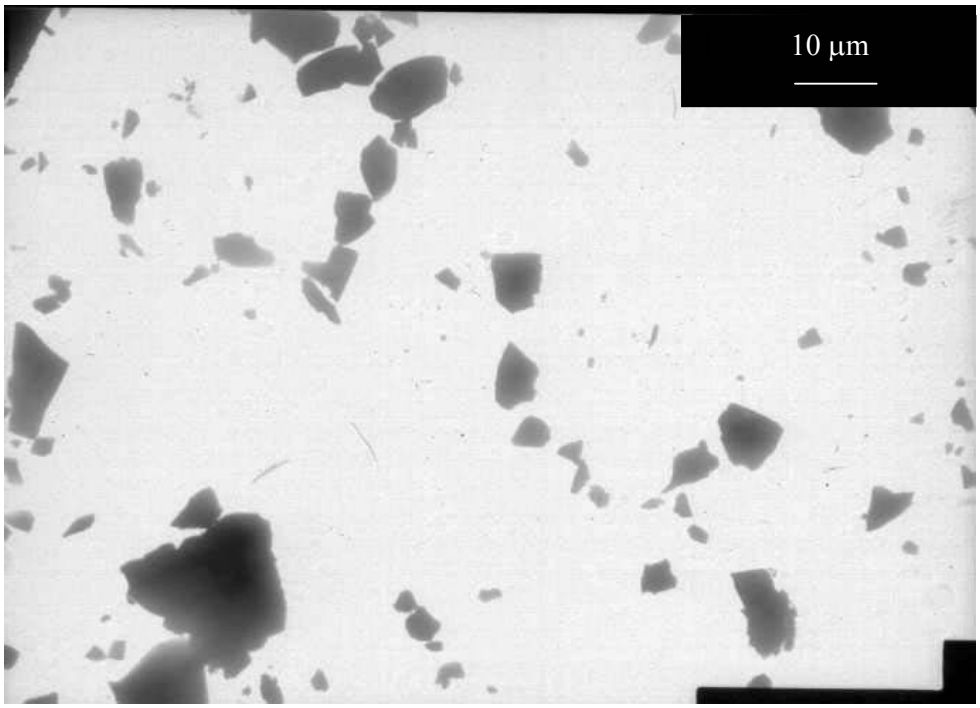

Figure 2.10. TEM image of silica fragments obtained after 12 hours.

Table 2.5 shows that stirring influences the formation and amount of tubes formed. More tubes are formed under stirred conditions and the tubes are also longer than the ones formed under non-stirred conditions. Table 2.6 and Figure 2.11 show that the yield of tubes increases as the stirring rate increases and the yield is at a maximum at 300 rpm and thereafter the yield decreases until no tubes are formed at all with stirring rates of 1200 rpm.

Table 2.5. Effect of adding NH_4OH under both static and stirring conditions (rapid addition)

	Non-stirring		**Stirring**	
Sample	Particle size[a] [μm]	Structure[b]	Particle size[a] [μm]	Structure[b]
15 min	L: 7 – 60 D: 0.5 – 0.7	Tubes (85%)	L: 16 – 95 D: 0.25 – 0.5	Tubes (96%)

[a]L = length of tube, D = outer diameter of tube, S = diameter of sphere

[b]% in brackets gives an estimate of the amount of material formed as determined by TEM

Table 2.6. Effect of diffusion on the amount of tubes that form

Stirring rate	Tubes formed (%)
0	80
100	85
300	95
600	40
1000	5
1200	0

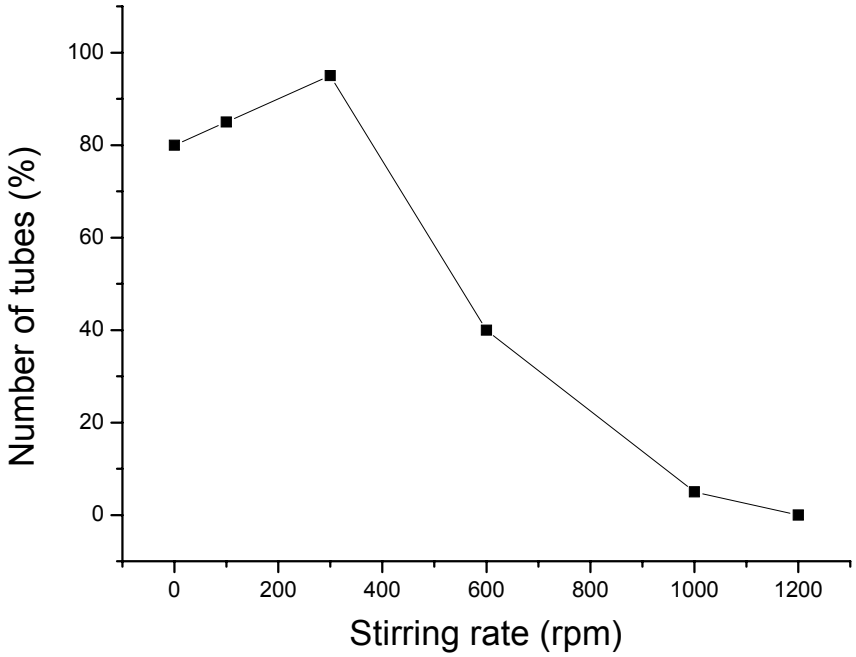

Figure 2.11. Effect of stirring rate on the number of tubes formed.

The solvent also plays a role in the formation of nanotubes and this is shown in Table 2.7. A high yield of tubes (75%) is obtained when ethanol/water (1.1%) solvent is used. When ethanol is used 60% of the silica material is in tubular form whereas when water is used the silica structure consists of mainly fragments and a small amount of tubes (15%). Spherical particles are obtained when methanol and iso-propanol are used.

Table 2.7. Effect of solvent on structure and number of tubes formed

Solvent	Particle size (μm)[a]	Structure[b]
Ethanol	L: 50 - 100 D: 0.4 – 0.6 S: 0.35 – 0.40	Tubes (60%) + spheres (40%)
H_2O/EtOH	L: 15 - 120 D: 0.3 – 0.5 S: 0.4 – 0.5	Tubes (75%) + spheres (25%)
Water	L: 50 – 70 D: 1 – 1.25	Fragments + tubes (15%)
Methanol	S: 0.3 – 0.5	Spheres
Iso-propanol	S: 0.2 – 0.4	Spheres

[a]L = length of tube, D = outer diameter of tube, S = diameter of sphere

[b]% in brackets gives an estimate of the amount of material formed as determined by TEM

Table 2.8 shows that the template used during the synthesis influences the BET surface areas of the silica. Only spherical particles are formed when D and L tartaric acids are separately used. DL-tartaric acid gave both spheres and nanotubes depending on the synthesis conditions. The surface areas for the silica that was formed from the D or L tartaric acids are lower than the one obtained from DL-tartaric acid.

Table 2.8: Effect of template on surface area

Template	BET SA (m^2/g) Calcination at 600 °C
DL-Tartaric acid	24.8
D-Tartaric acid	10.9
L-Tartaric acid	13.5

The nitrogen adsorption-desorption isotherm of SiO_2 synthesised from DL-tartaric acid (room temperature, 28% ammonia and non-stirring) shows a Type IV isotherm with a H3 type-like hysteresis loop, indicating the existence of narrow slit-like pores (tubular mesoporosity and microporosity) in the material (Figure 2.12). However; the desorption appears below the adsorption curve. This unusual phenomenon is attributed to the low surface area of the tartaric acid sample that leads to problems in accurately measuring voids. This type of problem has also been reported previously e.g. for microporous materials such as zeolites[23] or for samples with large average pore sizes (~ 132 nm). This proposal of micropores contributing to the unusual behaviour is

supported by the t-plot diagram which shows that the microporous volume contributes over 50% to the total pore volume. The BJH pore size distribution reveals pores that range from 1.7 – 3.1 nm in diameter (Figure 2.13).

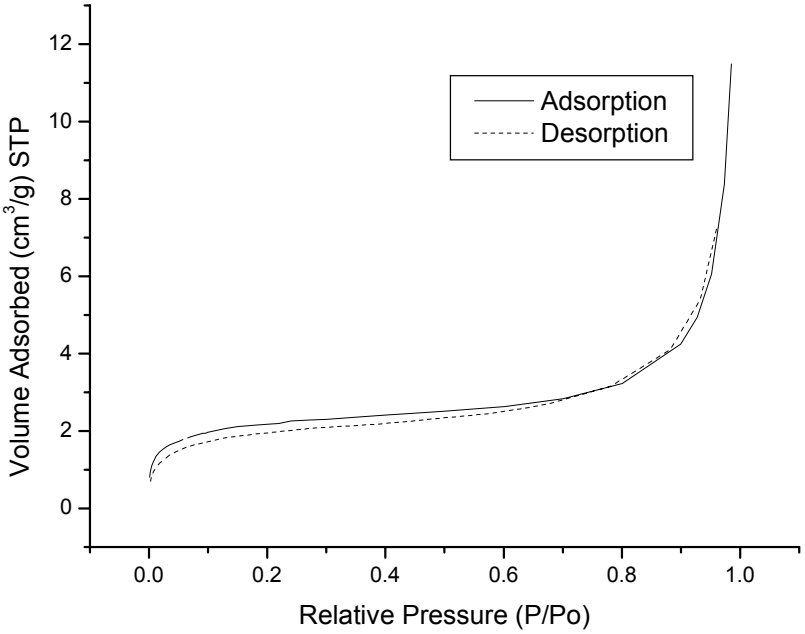

Figure 2.12. N_2 adsorption-desorption isotherm of SiO_2 where DL-tartaric acid was used as a template (the sample was prepared at room temperature using 28% ammonia solution and non-stirring condition).

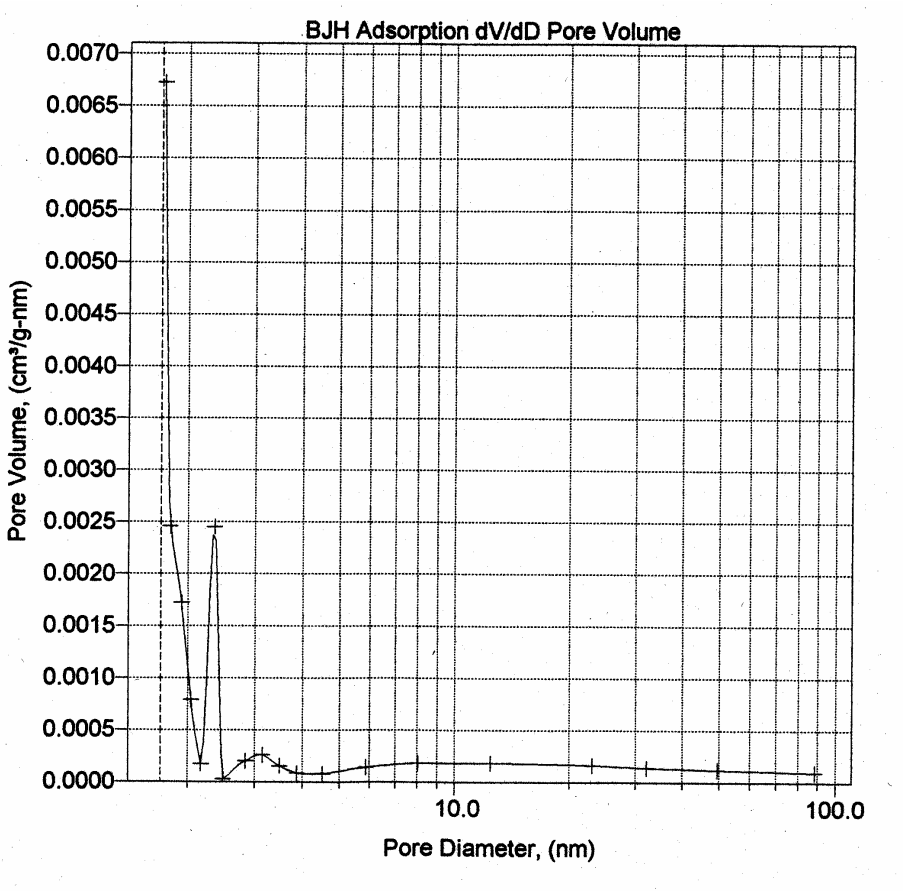

Figure 2.13. BJH pore size distribution plot (adsorption mode).

The TGA curve for the silica sample shows that the silica materials produced are moderately stable. Figure 2.14 shows that at 121 °C about 12% of the weight is lost, mainly due to the loss of the moisture in the sample. A further 10% in mass is lost at 255 °C and this is due to the loss of the template in the sample. Finally at 900 ºC ~ 22% of the weight is lost.

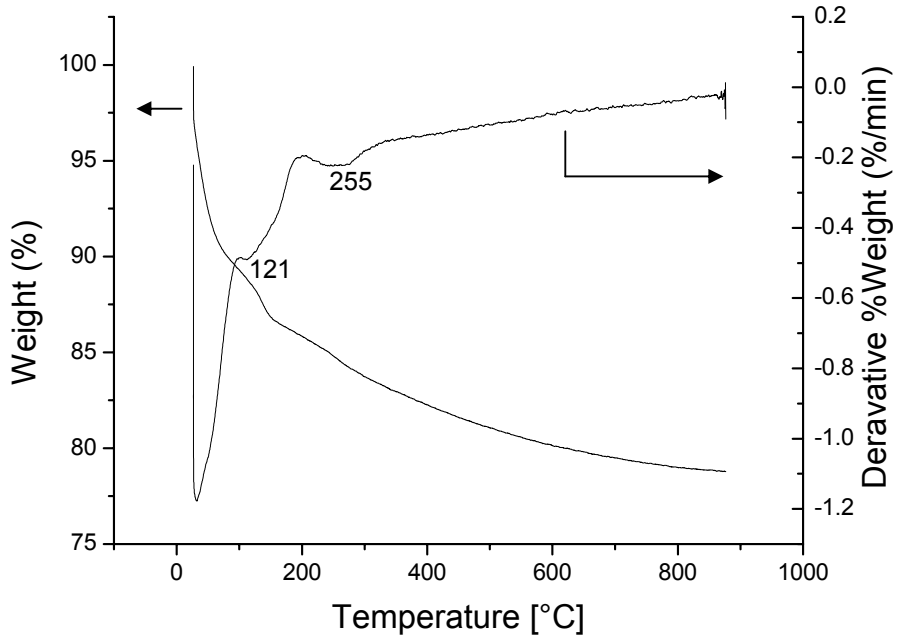

Figure 2.14. TGA curve of the uncalcined silica material (room temperature, 28% ammonia solution and non-stirring).

Powder XRD diffraction patterns for all the silica materials obtained show that only one broad peak appears at about 23 – 24º, indicating that the silica framework is amorphous (see Fig. 2.15).

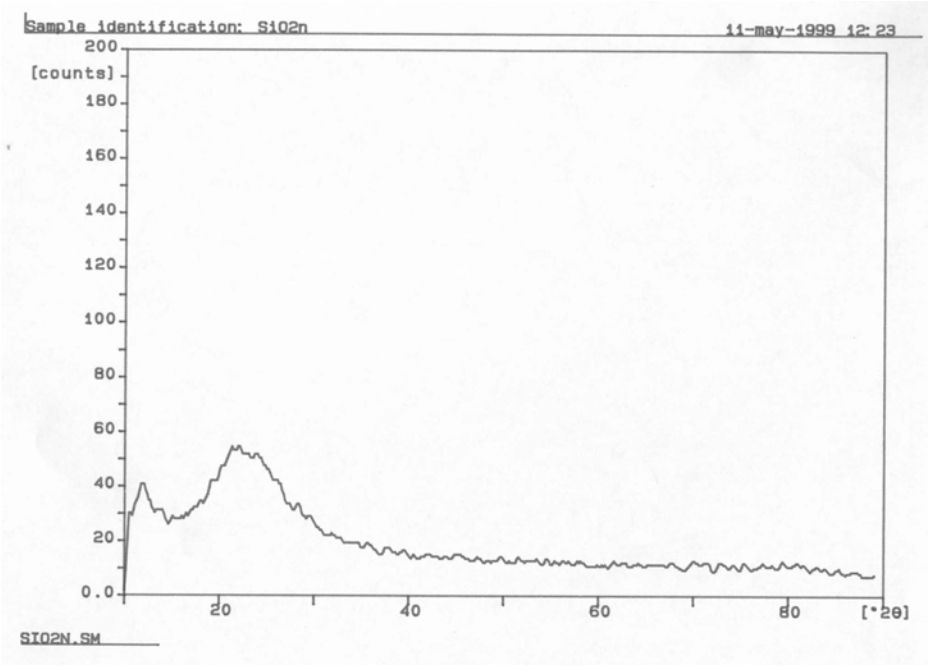

Figure 2.15. Powder XRD pattern of silica nanotubes (room temperature, 28% ammonia solution and non-stirring).

The IR spectra of the silica materials was recorded (see Figure 2.16). A broad band around 3396 cm^{-1} is caused by the O-H stretching vibration mode of the adsorbed water molecules, whose bending vibration mode is responsible for the band recorded at 1631 cm^{-1}. The intense peak at 1100 cm^{-1} is due to the Si-O-R stretching vibration (υ1) of ethoxy groups directly bonded to silicon while the peaks at 804 and 415 cm^{-1} are caused by the SiOH bending bands υ2 and υ3 modes respectively. These absorption bands of the calcined silica material (Fig. 2.16) are typical for silica derived from TEOS as reported in the literature.[24,25]

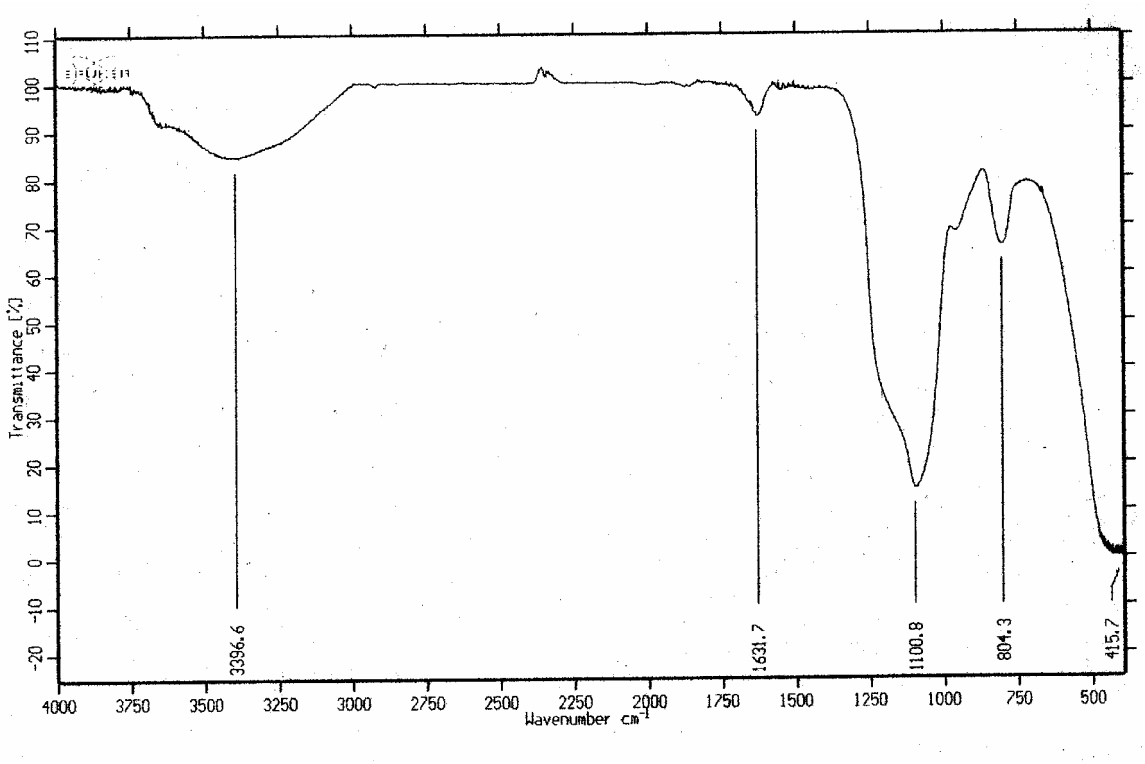

Figure 2.16. IR spectrum of a silica material (recorded in KBr) obtained at room temperature.

2.4 Discussion

Silica tubes with a range of morphologies have been synthesised in the last decade. Generally, factors that influence the formation of silica materials with various shapes and sizes have not been described in detail in the literature. It has been proposed that the well-defined shapes observed can be initiated by topological defects in seed molecules[26-27] and that the shape and that the length of mesoporous silica products depends strongly on the silica supply and on the self-assembly of the silica at the template/silica source interface[28].

Our studies with DL-tartaric acid as template reveal that synthesis conditions (temperature, NH_4OH concentration, water/ethanol concentration, time before

NH_4OH addition, static versus stirred conditions, stirring rate and solvent) all have an effect on the microstructure of the silica and influence the formation of particular silica morphologies. Indeed, the effects observed are those expected from diffusion and kinetic/thermodynamic considerations.

Temperature. It is observed that at high temperature small spheres (70 ^{0}C, average diameter ~ 5 nm) are synthesised while at lower temperature larger spheres are formed (room temperature, ~ 0.5 μm). Further, at low temperature tubes are predominantly formed while at high temperature spheres are exclusively formed (Figures 2.2, 2.3, 2.4 and Table 2.1). The lengths of the tubes also decrease with temperature while the diameters increase. Similar observations were made by Mann and co-workers,[30] an observation that they described as due to 'incipient crystallisation' of the template. However, the proposal by Matsui[15,16] that hydrogen bonding leads to the bulk template formation will also explain the observation.

At 0 ^{o}C less mobility of template and TEOS is expected. Consequently diffusion of TEOS to DL-tartaric acid micellar/crystal structures will be slow. Under these conditions the molecular template (tartaric acid) aggregates to form a rod like 'bulk' crystals. At 75 ˚C more rapid mobility of reagents/template is expected and under these conditions a smaller 'spherical bulk template' is formed. The micelles/crystals are expected to grow less perfectly and the silica would gel more rapidly at the higher temperature.

Ammonia concentration. Addition of a larger base concentration results in more and longer tubes (Table 2.2, Figure 2.6). This indicates the influence of

the base on the 'bulk template' formation. This is similarly reflected by the addition of water to the reactant solution. As water is added to the solution, the pH decreases (ammonia is diluted) and the quantity and length of the tubes decreases (Table 2.3). Combined with this effect is the influence of the solvent on tube/sphere formation. Use of different solvents reveals that tubes are formed in very few instances (Table 2.7).

NH_4OH addition: ageing effects. When the time prior to ammonium hydroxide addition is increased, the synthesis of the silica has more time to self assemble around the template prior to gelation. The outcome of this is the formation of longer, more uniform tubes with wider walls. Interestingly, if *extended* times are used before base addition (> 6 hours) the silica that has formed appears to be fragmented i.e. the silica produced appears to have broken down or to have re-dissolved. This occurs presumably because the silica framework that initially forms before NH_4OH is added has not completely hydrolysed or condensed (i.e. has not completely formed Si-O-Si bonds). The underlying silica structure is hence 'chemically' active. This result reveals the importance of obtaining appropriate condensation reactions in forming the silica structure.

Stirring rate. The effect of stirring could have two outcomes; break-up of the assembled crystal/template or increase of TEOS diffusion to the template. The data in table 2.5 reveal that the latter effect dominates. However, beyond a stirring rate of 400 rpm, tube formation decreases (Figure 2.11). The interplay

between these two effects is thus subtle and will have to be determined for every system.

Other templates. It was reported that only the DL form of tartaric acid was active in the synthesis of silica tubes.[15] Numerous attempts were made to use the D and L forms of tartaric acid with a wide range of reaction conditions but all attempts only produced amorphous materials. This implies that the 'bulk' template structure is an intrinsic property of the molecular template (relates to inter molecular H- bonding etc.) and that the conditions employed do not permit the structure to form in the ethanol/water solutions used. That the 'bulk' template for the different tartaric acid isomers is different is also revealed by the surface area measurements of the spherical silica's produced by the different tartaric acids. The surface areas for the silica formed from the D or L tartaric acids are lower than the areas obtained from DL-tartaric acid.

Silica characterisation. Removal of the template yields a hollow tube with an inner square shape, a typical example is shown in Figure 2.4 (outer diameter = 0.2 μm; inner diameter = 0.05 μm). It is worth noting that pore volume measurements indicate that a typical silica tube containing material shows Type IV adsorption isotherm characteristics with a H3 type-like hysteresis loop. This indicates the existence of narrow slit-like pores (tubular mesoporosity and microporosity) in the material (Figure 2.12) and a material showing mesopores and micropores. The BJH pore size distribution reveals pores that range from 1.7 – 3.1 nm (Figure 2.13). The peak at 1.7 nm is due to the micropores that are present in the silica and the peaks at 2.5 and 3.1 nm

are due to the mesopores that occur within the silica nanotube walls and the tube cavities respectively. The powder XRD data reveals that the silicas produced are amorphous (Figure 2.15). The IR spectra of the calcined silica materials (Fig. 2.16) is typical for silica derived from TEOS as reported in the literature.[24,25]

Mechanism of formation. Our study reveals that the morphology of the final silica materials depends on both the template molecule and on the silica supply and the self-assembly of the silica and/or template. This latter effect is influenced by the synthesis conditions in a predictable way.

In line with studies by others[29] our data are consistent with the following

i) Formation of rod-like micelles or 'crystallised' template molecules by a slow aggregation process. At higher temperatures rod-like structures do not form,

ii) interaction of the template with the TEOS,

iii) condensation/hydrolysis of the TEOS. Partial hydrolysis appears to yield a 'poorly' gelated material that breaks down readily in the presence of base.

Our data do not establish whether a coil like growth of the silica occurs in the reaction[29] (refer to Appendix 2 for coil-like growth).

2.5 Conclusions

This study has shown that the template together with the synthesis conditions influence the formation of particular silica morphologies. Of all the synthesis conditions investigated, temperature, stirring, reaction time and solvent have

the largest effect on the structure. These factors have a direct bearing on template formation. The formation of tubes is more enhanced at lower temperatures than elevated ones and this can be due to the fact that at a lower temperature molecules (reagents, template) diffuse more slowly and thus have enough time to self-assemble.

Pore size measurements indicate the existence of mesopores and some micropores in the formed silica materials. The powder XRD data reveals that the silicas produced are amorphous. The IR spectra of the calcined silica materials are typical for silica derived from TEOS as reported in the literature. TGA data shows that the silica materials obtained are thermally stable.

2.6 References

1. E.M. Mokoena, A.K. Datye and N.J. Coville, *J. Sol-Gel Sci. and Tech.,* **28**, 307 - 317, (2003).
2. Special Issue of *Chem. Mater*., **9**, 2247 – 2670, (1997).
3. C.J. Brinker, G.W. Scherer, Sol-Gel Science: *The Physics and Chemistry of Sol-Gel processing,* (Academic Press, London, 1990), p. 870.
4. P.M. Ajayan, O. Stephan, P. Redlich and C. Colliex, *Nature*, **375**, 564, (1995).
5. C.N.R. Rao, B.C. Satishkumar and A. Govindaraj, *Chem. Commun*., 1581, (1997).
6. B.C. Satishkumar, A. Govindaraj, E.M. Vogl, L. Bassumalick and C.N.R. Rao, *J. Mater. Res*., **12**, 604, (1997).
7. G.L. Hwang and K.C. Hwang, *J. Mater. Res*., **12**, 604, (1997).
8. B.B. Lakshmi, P.K. Dorhout and C.R Martin, *Chem. Mater.*, **9**, 857, (1997).
9. (a) M. Zhang, Y. Bando, K. Wada and K. Kurashima, *J. Mater. Sci. Lett*., **18**, 1911, (1999); (b) M. Zhang, Y. Bando and K. Wada, *J. Mater. Res*., **15**, 387, (2000).
10. M. Adachi, T. Harada and M. Harada, *Langmuir*, **15**, 7097, (1999).
11. H. Muhr, F. Krumeich, U.P. Schonholzer, F. Bieri, M. Niederberger, L. J. Gauchler and R. Nesper, *Adv. Mater*., **12**, 231, (2000).
12. Y. Ono, K. Nakashima, M. Sano, Y. Kanekiyo, K. Inoue, J. Hojo and S. Shinkai, *Chem. Commun*., 1477, (1998).

13. S. Kobayashi, K. Janabusa, N. Hamasaki, M.Kimura and H. Shirai, *Chem. Mater.*, **12**, 1523, (2000).
14. G.M. Clavier, J.L. Pozzo, H. Bouas-Laurent, C. Roux and C. Sanchez, *J. Mater. Chem.*, **10**, 1725, (2000).
15. H. Nakamura and Y. Matsui, *J. Am. Chem. Soc.*, **117,** 2651, (1995).
16. H. Nakamura and Y. Matsui, *Adv. Mater.*, **7**, 871, (1995).
17. L. Wang, S. Tomura, F. Ohashi, M. Maeda, M. Suzuki and K. Inukai, *J. Mater. Chem.*, **11**, 1465, (2001).
18. L. Sudheendra and A.R. Raju, *Bull. Mater. Sci.*, **22**, 1025, (1999).
19. M. Adachi, T. Harada, and M. Harada, *Langmuir*, **16**, 2376, (2000).
20. F. Miyaji, Y. Watanabe and Y. Suyama, *Materials Research Bulletin*, **38**, 1669, (2003).
21. E.P. Barret, L.G. Joyner and P.P. Halenda, *J. Am. Chem. Soc.*, **73**, 373, (1951).
22. W.D. Harkins and G. Jura, *J. Chem. Phys.*, **11**, 431, (1943).
23. E.G. Derouane, *The Magazine of Catalysis, CATTECH*, **6(1)**, 11-13, (2002).
24. D.L. Wood and E.M. Rabinovich, *Appl. Spectrosc.*, **43**, 263, (1989).
25. H. Izutsu, F. Mizukami, Y. Kiyozuma and K. Maeda, *J. Mater. Chem.*, **7(8)**, 1519 – 1525, (1997).
26. H. Yang, G.A Ozin and C.T Kresge, *Adv. Mater.*, **10**, 883, (1998).
27. I. Sokolov, H. Yang, G.A. Ozin and C.T. Kresge, *Adv. Mater.*, **11**, 636, (1999).
28. S.M. Yang, H. Yang, N. Coombs, I. Sokolov, C.T. Kresge and G.A. Ozin, *Adv. Mater.*, **11**, 52, (1999).

29. F. Kleitz, F. Marlow, G.D. Stucky and F. Schüth, *Chem. Mater*., **13**, 3587, (2001).

30. F. Miyaji, S.A. Davis, J.P.H. Charmant, and S. Mann, Chem. Mater., **11**, 3021, (1999).

CHAPTER THREE

A SYSTEMATIC STUDY OF THE USE OF CITRIC ACID IN THE SYNTHESIS OF SILICA MATERIALS OBTAINED BY THE SOL-GEL METHOD*

3.1 Introduction

The template-directed sol-gel synthesis of organized inorganic matter offers a new and wide-ranging approach to the making of useful materials with controlled architecture and porosity across a range of length scales.[1] Organic templates with extended long-range structures, such as block copolymer lyotropic mesophases,[2,3] colloidal crystals,[4,5] and bacterial superstructures[6] have been used to prepare monolithic forms of porous silica. In contrast, the direct synthesis of discrete inorganic architectures necessitates the use of dispersed organic supramolecular structures with commensurate dimensionality; for example, hollow fibers of amorphous silica have been prepared by template-directed processes using the external surface of self-assembled phospholipid fibers,[7] viroid cylinders,[8] or organic-gel filaments.[9]

---

* To be submitted for publication

The use of such specialized molecules, however, has the potential drawback that the costs associated with the scale-up are likely to be highly prohibitive.

Thus, the report by Nakamura and Matsui[10] on the formation of silica tubes from ethanol/water/NH_4OH/tetraethylorthosilicate (TEOS) mixtures that contained small amounts of a simple organic acid (for example, racemic *dl*-tartaric acid), is particularly interesting. Recently Wang *et al.*[11] reported that citric acid (another simple organic acid) could also be used to prepare silica nanotubes. Wang *et al.* found that rapid addition of aqueous ammonia under static conditions gave only uniform micrometer sized rods while slow addition of aqueous ammonia under stirring conditions gave nanotubes. Hence it appears that synthetic conditions play a key role in influencing the formation of particular forms of silica. However, a detailed evaluation of the synthetic parameters required to control the silica morphologies was not given. The preparation of single silica nanotubes is still a major challenge as compared to the synthesis of porous materials with integrated structures.

In this study we have used citric acid as a template to prepare silica materials. The chemical structure of citric acid is shown in Figure 3.1. In particular we have prepared the silica materials using a range of reaction conditions in order to maximize the formation of nanotubes and at the same time study in detail parameters that play an important role in determining the microstructure of other forms of silica generated in the synthesis. A comparison between the use of tartaric and citric acids has been made.

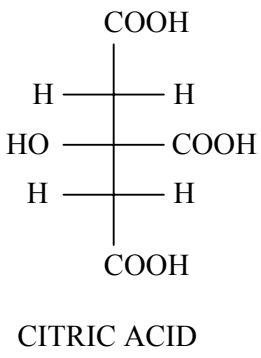

CITRIC ACID

Figure 3.1. Chemical structure of citric acid.

3.2 Experimental

3.2.1 Preparation

Ethanol (Saarchem, 99.9%), water, tetraethylorthosilicate (TEOS); (Aldrich, 98%), citric (Sigma, 98%), and ammonium hydroxide (Fluka, 98%) were used as chemical sources. The synthesis procedure followed was the same as the one used for DL-tartaric acid. The parameters that were varied during the silica synthesis were a) temperature, b) NH_4OH concentration, c) water/ethanol concentration, d) time before NH_4OH addition, e) static versus stirred conditions, f) stirring rate and g) solvent. Both the yield and product morphology were determined after each reaction.

a) Synthesis procedure when varying temperature

The synthesis condition used when varying temperature was as follows:

- 0.26 g of template (citric acid) was dissolved in 0.6 ml of water and then 50 ml of ethanol was added.
- The mixture was then heated to 75 ºC or cooled to 0 ºC or left at room temperature (depending on the synthesis temperature to be used).

- 7.3 g TEOS was then added to the mixture at either 0 ºC, 25ºC or 75ºC.
- The solution was left to stand at the synthesis temperature for 30 minutes to form a sol.
- Finally 20 ml of NH_4OH (28% aqueous solution) that was at room temperature was added to the sol that was at synthesis temperature to form a gel.
- After 15 – 20 minutes at the reaction temperature the reaction was observed to be complete.
- The gel was then aged at room temperature for 2 hours, and then dried in an oven at 110 ºC.
- The products were calcined under static air at 600 ºC for 4 hours.

b) Synthesis procedure when varying the concentration of NH_4OH

(The synthesis was carried out at room temperature and all the other parameters were kept constant except the concentration of NH_4OH)

- 0.26 g of citric acid was dissolved in 0.6 ml of water and then 50 ml of ethanol was added.
- 7.3 g TEOS was then added to the mixture.
- The solution was left to stand for 30 minutes to form a sol.
- Finally 20 ml of NH_4OH (7%, 16%, 25%, 28% or 33% aqueous solution) was added to the sol to form a gel.
- After 15 – 20 minutes the reaction was observed to be complete.
- The gel was then aged at room temperature for 2 hours and then dried in an oven at 110 ºC.

- The products were calcined under static air at 600 ºC for 4 hours.

c) Synthesis procedure when varying water/ethanol concentration

(The synthesis was carried out at room temperature and all the other parameters were kept constant except the water/ethanol concentration)

- 0.26 g of citric acid was dissolved in 0.6 – 5 ml of water and then 50 ml of ethanol was added.
- 7.3 g TEOS was then added to the mixture.
- The solution was left to stand for 30 minutes to form a sol.
- Finally 20 ml of NH_4OH (28% aqueous solution) was added to the sol to form a gel.
- After 15 – 20 minutes the reaction was observed to be complete.
- The gel was then aged at room temperature for 2 hours and then dried in an oven at 110 ºC.
- The products were calcined under static air at 600 ºC for 4 hours.

d) Synthesis procedure when varying time before NH_4OH addition

(The synthesis was carried out at room temperature and all the other parameters were kept constant except time taken before NH_4OH addition)

- 0.26 g citric acid was dissolved in 0.6 ml of water and then 50 ml of ethanol was added.
- 7.3 g TEOS was then added to the mixture.
- The solution was left to stand for 15 minutes to 24 hours to form a sol.
- Finally 20 ml of NH_4OH (28% aqueous solution) was added to the sol to form a gel.
- After 15 – 20 minutes the reaction was observed to be complete.

- The gel was then aged at room temperature for 2 hours and then dried in the oven at 110 ºC.
- The products were calcined under static air at 600 ºC for 4 hours.

e) Synthesis procedure for static versus stirred conditions

(The synthesis was carried out at room temperature)

- 0.26 g of citric acid was dissolved in 0.6 ml of water and then 50 ml of ethanol was added. The mixture was stirred with a magnetic stirrer and a stirring rate of about 300 rpm.
- 7.3 g TEOS was then added to the stirred mixture.
- The solution was left to stand for 30 minutes while stirring to form a sol.
- Finally 20 ml of NH_4OH (28% aqueous solution) was added to the sol to form a gel.
- After 15 – 20 minutes the reaction was observed to be complete.
- The stirring was stopped and the gel was aged at room temperature for 2 hours and then dried in the oven at 110 ºC.
- The products were calcined under static air at 600 ºC for 4 hours.

For the non-stirring condition the synthesis procedure was the same except that the stirrer was not used.

f) Synthesis procedure when varying the stirring rate

The synthesis procedure when varying the stirring rate was the same as that described above. All the other parameters were kept constant, but the stirring rate was varied between 100 and 300 rpm.

g) Synthesis procedure when varying the solvent

The procedure was the same as used for the non-stirred reaction but here the solvent was changed. The solvents used were ethanol, water, mixture of ethanol and water, methanol and iso-propanol.

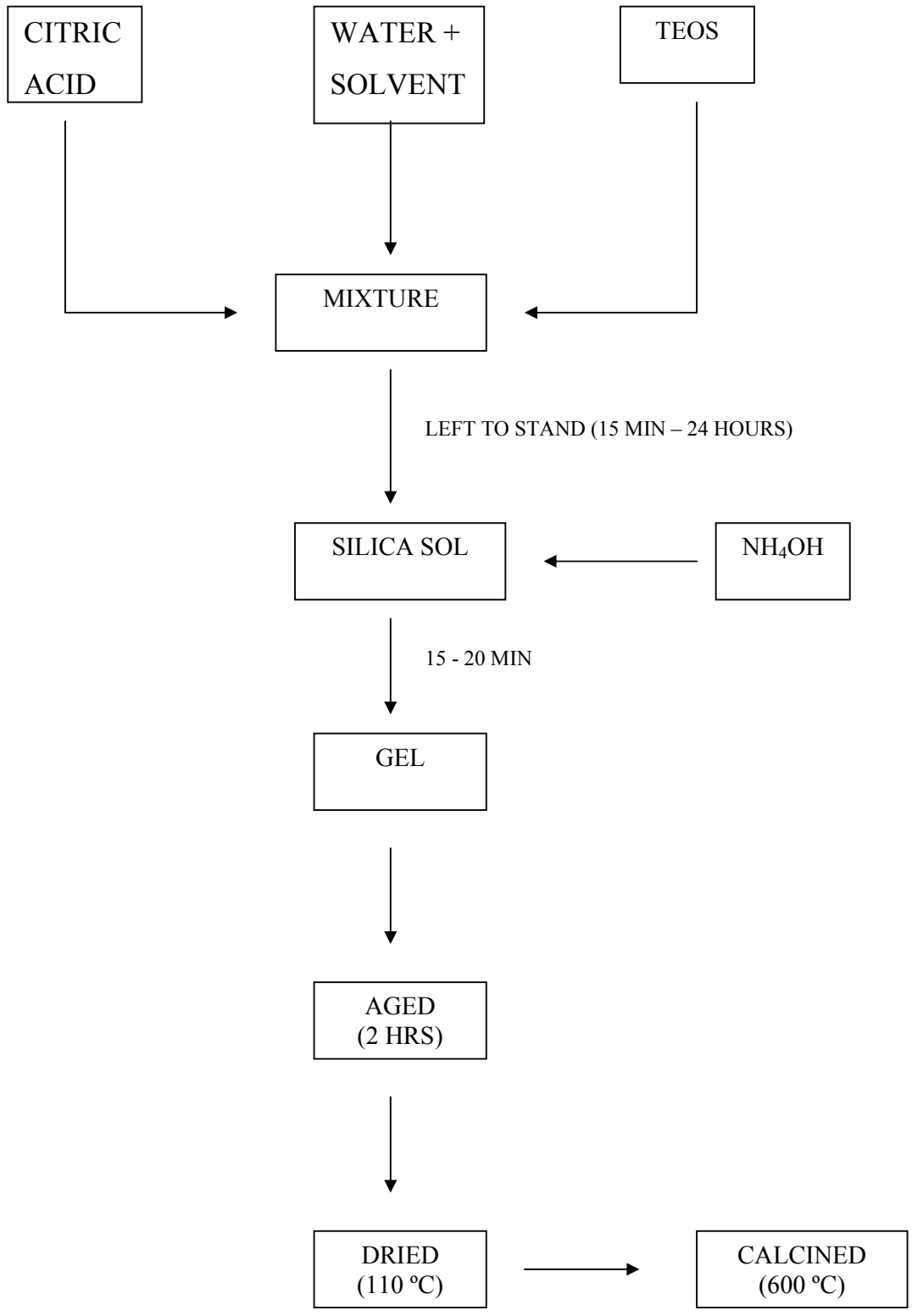

Figure 3.2. Synthesis of citric acid templated silica materials by the sol-gel method.

3.2.2 Characterization

Transmission electron microscopy (TEM) images were observed with JEOL-100S and JEOL-2010 electron microscopes. A JEOL JSM 840 scanning electron microscope (SEM) was utilised to obtain scanning electron micrographs of the samples. Samples for TEM analysis were prepared by sonicating about 1 mg material into 1 ml ethanol for at least 4 minutes. A few drops of the suspension were added to a Cu grid coated with a carbon film. After approximately one minute, excess liquid was removed by touching one edge of the grid to a Whatman filter paper. Samples for SEM analysis were coated with a gold palladium coating. BET surface areas and BJH pore size distributions were determined by nitrogen physisorption at 77 K using a Micromeritics ASAP 2010 instrument. (Degassing of the samples to 0.1 Pa at 393 K preceded every measurement. Specific adsorption pore volumes were calculated by the Barret-Joyner-Halenda (BJH) method[12] that is assumed to cover the cumulative adsorption pore volume of pores in the range 1.7 to 300 nm in diameter. Assessment of micropore volume was made from t-plot constructions using the Harkins-Jura correlation[13]). Thermogravimetric analysis was performed on a Perkin Elmer, Thermogravimetic Analyser Pyris 1 (TGA) with a heating rate of 10º per minute.

3.3 Results and Discussion

Table 3.1 shows that the effect of varying temperature on the structure of the silica. The table shows that synthesis at 0 ºC gives a higher yield of nanotubes compared to reactions performed at higher temperatures. At 75 ºC only hollow spherical particles are obtained (Figure 3.3). The spheres formed

at 75 ºC are hollow and the ones formed at room temperature and 0°C are filled. The formation of tubes (Figure 3.4) is more enhanced at lower temperatures than elevated ones. At lower temperatures less mobility of template and TEOS is expected and consequently diffusion of TEOS to citric acid micellar structures will be slow. This appears to be beneficial to tube formation. Under these conditions the molecular template (citric acid) aggregates to form a rod like 'bulk' template. At 75 °C more rapid mobility of reagents/template is expected and under these conditions a smaller 'spherical bulk template' is formed. The micelles/crystals are expected to grow less perfectly and the silica would gel more rapidly at the higher temperature.

Table 3.1. Effect of temperature on the morphology of silica

Temperature [ºC]	Particle size [µm][a]	Structure[b]
0	L: 0.75 – 2.5	Tubes (97%) + filled spheres
	D: 0.016 – 0 025	(3%)
	S: 0.010 – 0.015	
25	L: 1.67 – 2.67	Tubes (75%) + filled spheres
	D: 0.33 – 0.45	(25%)
	S: 0.30 – 0.50	
75	S: 0.166 – 0.20	Hollow spheres

[a]L = length of tube, D = outer diameter of tube, S = diameter of sphere

[b]% in brackets gives an estimate of the amount of material formed as determined by TEM

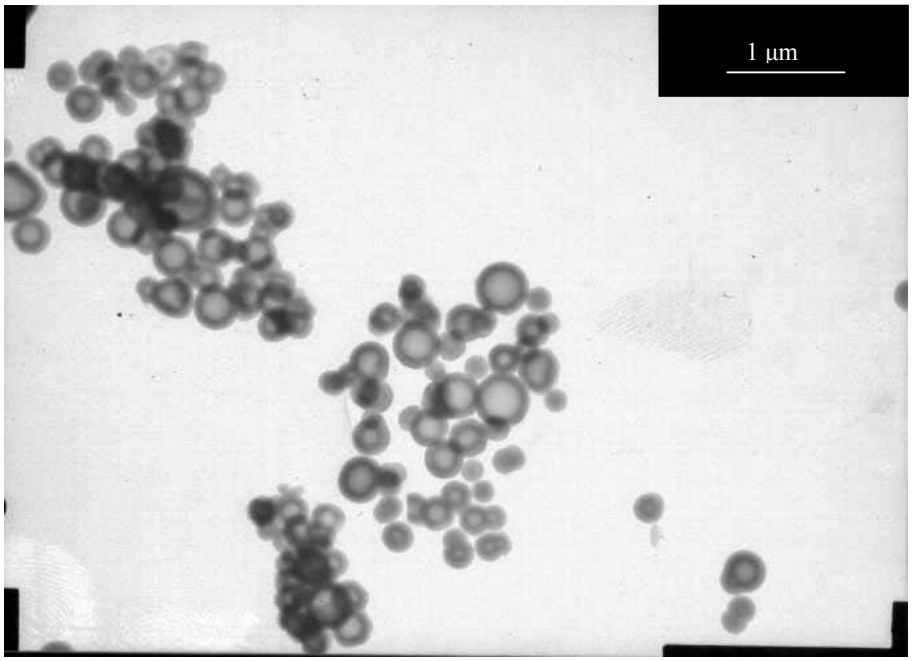

Figure 3.3. TEM image of hollow spheres obtained at 75 °C.

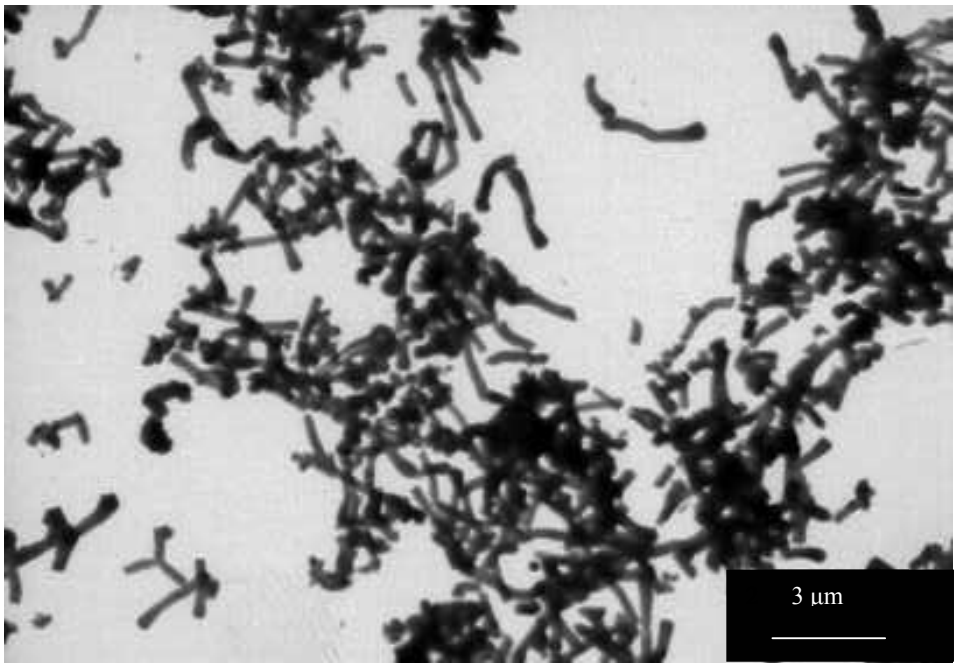

Figure 3.4. TEM image of tubes obtained at 0 °C.

Table 3.2 and Figure 3.5 show that the yield and length of the nanotubes increase as the percentage of ammonia is increased. This indicates the influence of the base on 'bulk template' formation. The average widths of the tubes and spheres are about the same (~ 0.4 μm) when 28 and 33% aqueous ammonia solutions are used. Table 3.2 shows that tube formation is detected when the NH_3 (aq) concentration > 25%. When NH_4OH is not added to the reaction, the tubes that form are longer and take a very long time to form, so NH_4OH acts to enhance the synthesis of nanotubes. Both hollow and filled spheres are obtained at 16% NH_3 (aq) concentration (Figure 3.6).

Table 3.2. Effect of varying % NH_3 to water in NN_4OH

% NH_3 to water in NH_4OH	Particle size [μm][a]	Structure
0	L: 9 – 11 D: 0.4 – 0.6 S: 0.5 – 0.6	Tubes (10%) + filled spheres (90%)
7	S: 0.5 – 0.7	Filled spheres
16	S: 0.5 – 0.7	Spheres (filled + hollow)
25	L: 3.25 – 4.0 D: 0.75 – 0.80 S: 0.25 – 0.33	Tubes (30%) + filled spheres (70%)
28	L: 1.67 – 5 D: 0.33 – 0.45 S: 0.33 – 0.44	Tubes (70%) + filled spheres (30%)
33	L: 2 - 7 D: 0.33 – 0.5 S: 0.33 – 0.67	Tubes (75%)+ filled spheres (25%)

[a]L = length of tube, D = outer diameter of tube, S = diameter of sphere

[b]% in brackets gives an estimate of the amount of material formed as determined by TEM

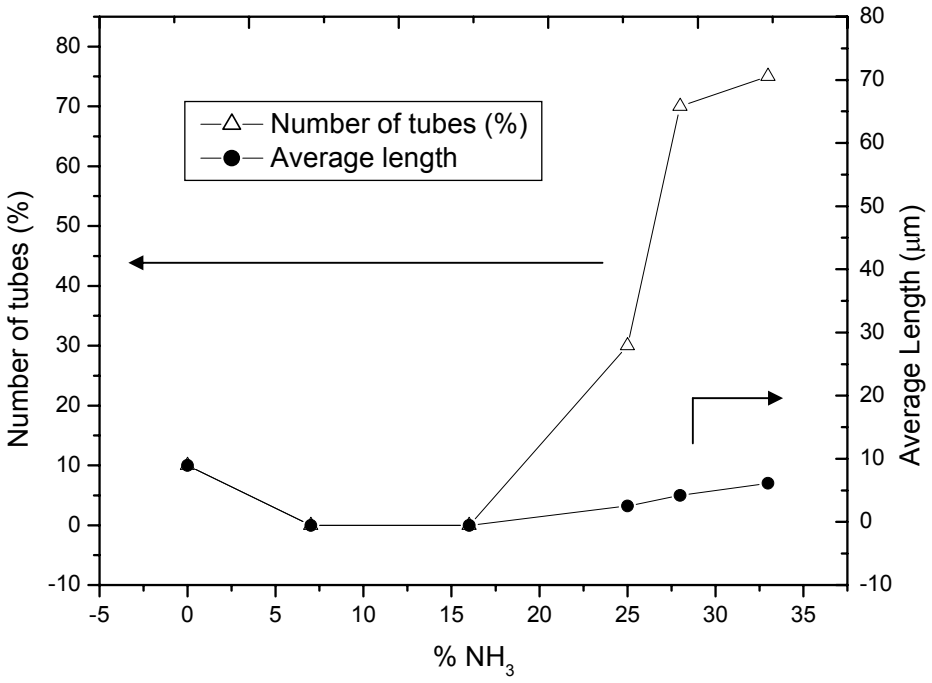

Figure 3.5. The effect of % NH_3 to water in NH_4OH on the amount (▫) and average length (●) of tubes formed.

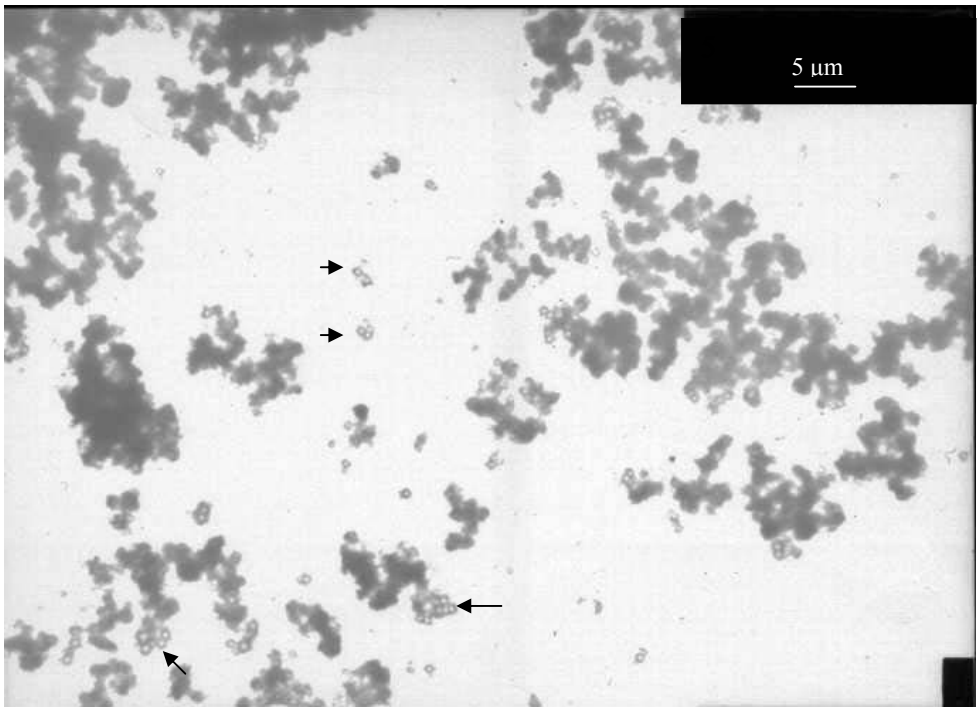

Figure 3.6. TEM image of the mixture of hollow and filled spheres obtained when 16% NH_3 (aq) concentration is used (black arrows show hollow spheres).

Table 3.3 shows that the formation of nanotubes seems to be sensitive to the amount of water present during the reaction. Nanotubes only form when the percentage of water is 1.1% or less. When ethanol is the only solvent used about 70% of silica is found in tubular form. Spherical particles (Figure 3.7) become smaller as more water is used. This indicates the influence of water on the reactant solution and 'bulk template' formation as ammonia gets diluted.

Table 3.3. Effect of H_2O/EtOH dilution

% H_2O (vol %)	Particle size [μm][a]	Structure[b]
0	L: 0.6 – 11 D: 0.4 – 0.6 S: 0.33 – 0.40	Tubes (70%) + filled spheres (30%)
1.1	L: 0.75 – 8.5 D: 0.5 – 0.6 S: 0.3 – 0.45	Tubes (97%) + filled spheres (3%)
3	S: 0.25 – 0.40	Filled spheres
5	S: 0.25 – 0.40	Filled spheres
10	S: 0.13 - 0.25	Filled spheres
100	S: 0.06 – 0.08	Filled spheres

[a]L = length of tube, D = outer diameter of tube, S = diameter of sphere

[b]% in brackets gives an estimate of the amount of material formed as determined by TEM

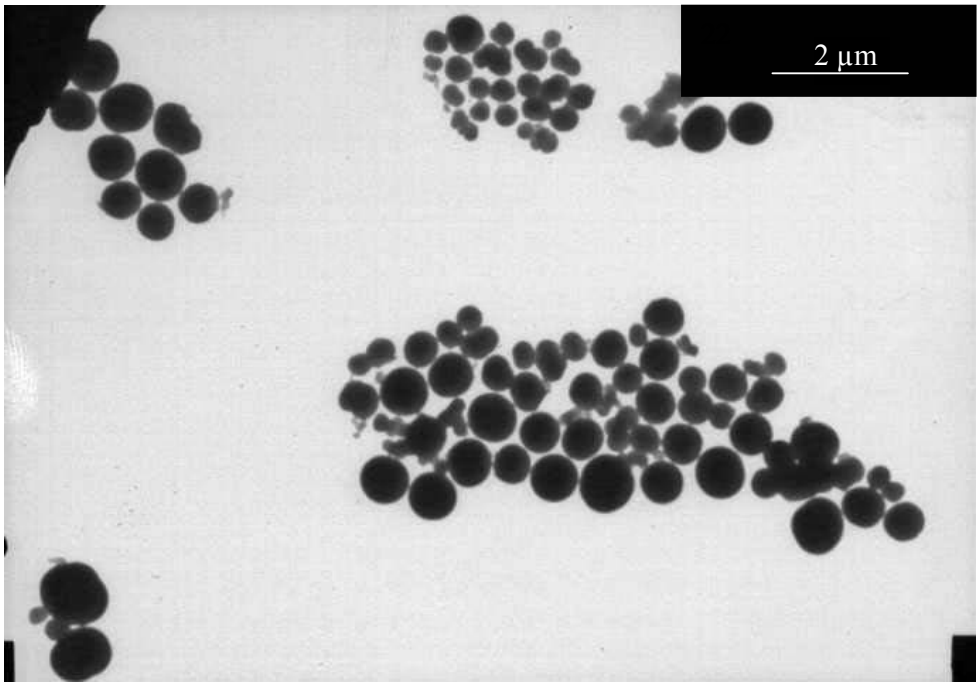

Figure 3.7. TEM image of spherical particles (filled) obtained when 5% of water is used.

Table 3.4 and Figure 3.8 show that the time taken before adding ammonium hydroxide to gel the solution has an effect on the yield and length of the tubes formed. The yield of tubes decreases as more time is taken before adding ammonium hydroxide but the length of tubes increases as the time is increased. This is because when the time before addition of ammonium hydroxide is increased during the synthesis, the silica has more time to self-assemble around the template prior to gelation.

The tubes that form after 6 hours are hollow inside but closed at the ends (Figure 3.9). After 12 hours silica fragments start to form instead of tubes (Figure 3.10). This occurs presumably because the silica framework that initially forms before NH_4OH is added has not completely hydrolysed or

condensed (i.e. has not completely formed Si-O-Si bonds). The underlying silica structure is hence 'chemically' active. This result reveals the importance of obtaining appropriate condensation reactions for formation of the silica structure.

Table 3.4. Effect of varying time before the addition of NH_4OH

Time [hrs]	Particle size [μm][a]	Structure[b]
0.25	L: 8.5 – 9.5 D: 1 - 2 S: 0.2 – 0.4	Tubes (80%) + filled spheres (20%)
0.5	L: 0.75 – 8.5 D: 0.5 – 0.6 S: 0.2 – 0.4	Tubes (75%) + filled spheres (25%)
1.5	L: 2.8 – 15 D: 0.6 – 0.9 S: 0.2 – 0.45	Tubes (68%)+ filled spheres (32%)
6	L: 17 - 20 D: 0.75 – 0.85 S: 0.75 – 0.85	Hollow tubes (40%)+ filled spheres (60%)
12	-	Fragments
24	-	Fragments

[a]L = length of tube, D = outer diameter of tube, S = diameter of sphere

[b]% in brackets gives an estimate of the amount of material formed as determined by TEM

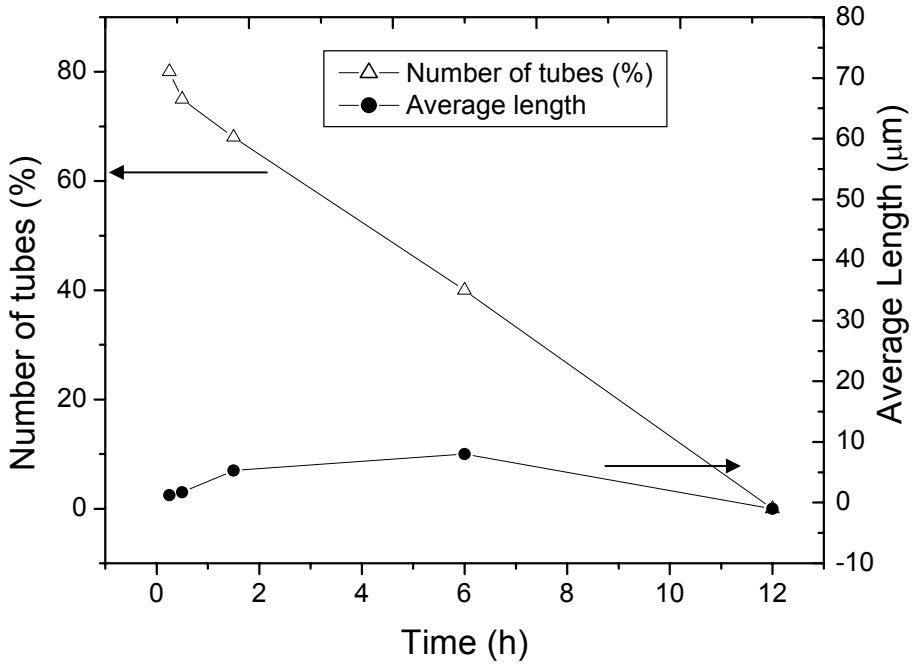

Figure 3.8. Effect of time before the addition of NH_4OH on the amount (Δ) and average length (●) of tubes formed.

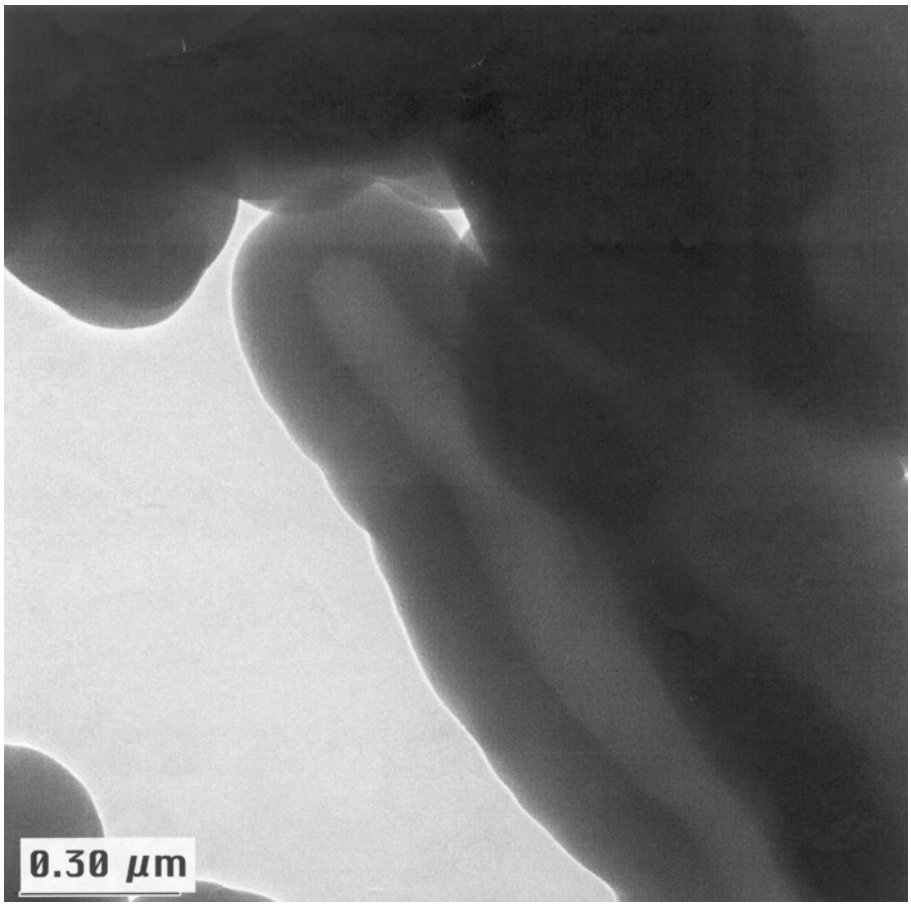

Figure 3.9. TEM image of a hollow tube obtained after 6 hours.

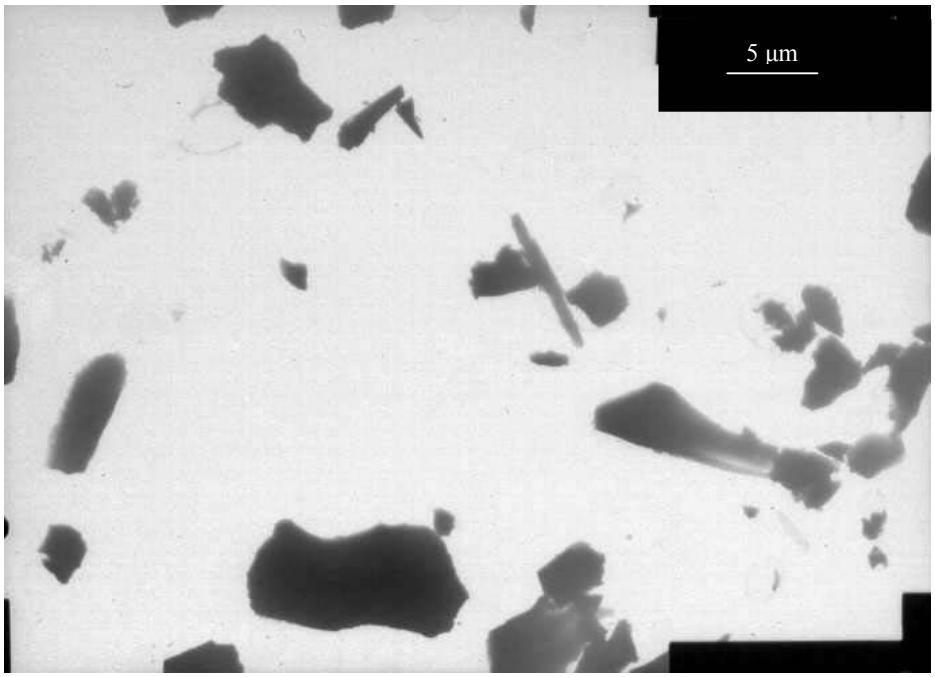

Figure 3.10. TEM image of silica fragments obtained after 12 hours.

Table 3.5 shows that stirring influences the formation and amount of tubes formed. More tubes are formed under stirred conditions and the tubes are also longer than the ones formed under non-stirred conditions. Table 3.6 and Figure 3.11 show that the yield of tubes increases as the stirring rate increases and the yield of tubes is at a maximum at 200 rpm. However; at 300 rpm no tubes are formed. Therefore the effect of stirring has two outcomes; break-up of the assembled template or increase of TEOS diffusion to the template. The interplay between these two effects is thus subtle and has to be determined for every system.

Table 3.5. Effect of adding NH_4OH under both static and stirring conditions (rapid addition)

	Non-stirring		**Stirring**	
Sample	Particle size[a] [μm]	Structure[b]	Particle size[a] [μm]	Structure[b]
15 min	L: 10 - 13 D: 1 – 1.5	Tubes (80%)	L: 7 - 60 D: 0.5 – 0.7	Tubes (95%)

[a]L = length of tube, D = diameter of tube, S = diameter of sphere

[b]% in brackets gives an estimate of the amount of material formed as determined by TEM

Table 3.6. Effect of stirring rate on the amount of tubes that form

Stirring rate (rpm)	Tubes formed (%)[b]
0	70
100	80
200	97
300	0

[b]% in brackets gives an estimate of the amount of material formed as determined by TEM

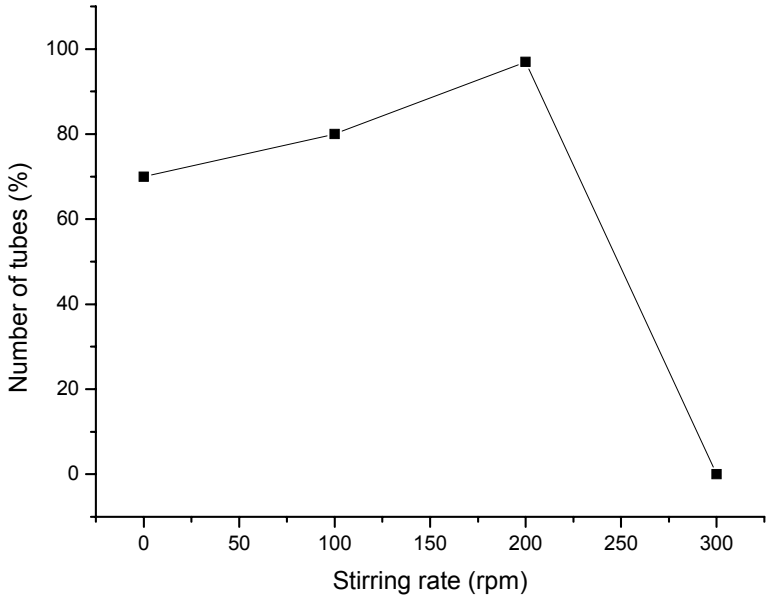

Figure 3.11. Effect of stirring rate on the number of tubes formed.

The solvent also plays a role in the formation of nanotubes and this is shown in Table 3.7. A high yield of 97% is obtained when ethanol/water (1.1%) solvent is used. The Table shows that when ethanol is used 70% of the silica is in tubular form whereas when water alone is used only spheres are obtained. Spherical particles are obtained when methanol is used while 10% of the tubes are formed when iso-propanol is used. The use of different solvents affects the pH of the reactant solution and this influences the tube/sphere formation.

Table 3.7. Effect of solvent on structure and number of tubes formed

Solvent	Particle size (μm)[a]	Structure[b]
Ethanol	L: 0.6 - 11	Tubes (70%) + filled spheres (30%)
	D: 0.4 – 0.6	
	S: 0.2 – 0.45	
H_2O/EtOH	L: 0.75 – 8.5	Tubes (97%) + filled spheres (3%)
	D: 0.5 – 0.6	
	S: 0.3 – 0.5	
Water	S: 0.06 – 0.08	Spheres
Methanol	S: 0.13 – 0.24	Spheres
Iso-propanol	L: 1.7 – 2.4	Tubes (10%) + filled spheres (90%)
	D: 0.6 – 0.8	
	S: 0.2 – 0.7	

[a]L = length of tube, D = diameter of tube, S = diameter of sphere

[b]% in brackets gives an estimate of the amount of material formed as determined by TEM

The average BET surface area of all the synthesized materials was about 47 m^2/g. The nitrogen adsorption-desorption isotherm of SiO_2 (ethanol/water, 0 ºC) (Figure 3.12) shows a type IV isotherm with a H4 hysteresis loop, indicating the existence of narrow slit-like pores in the material. The isotherm shows that the sample is mesoporous with some contribution of micropores. The t-plot diagram shows that the microporous volume represented 38% of the total porous volume. The BJH pore size distribution reveals pores that range from 1.7 – 3.1 nm in diameter (Figure 3.13). The peak at 1.7 nm is due

to the micropores that are present in the silica and the peaks at 2.4 and 2.6 nm are due to the mesopores that occur within the silica nanotube walls.

The powder XRD data reveals that the silicas produced are amorphous. The XRD and IR results are similar to materials obtained when using tartaric acid (see Chapter 2, Figures 2.15 and 2.16).

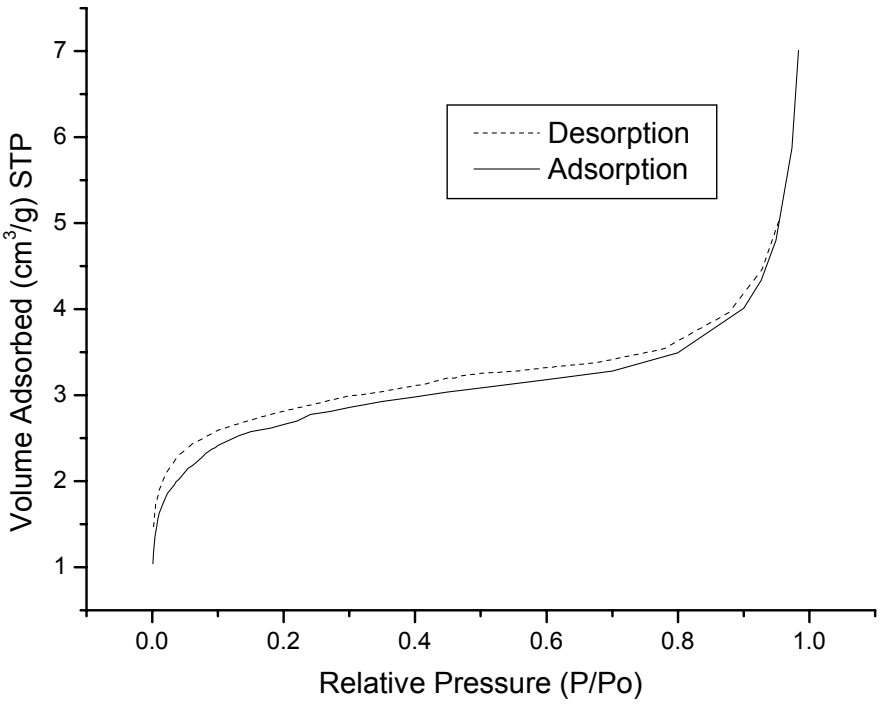

Figure 3.12. N_2 adsorption-desorption isotherm of SiO_2 (ethanol/water, 0 ºC).

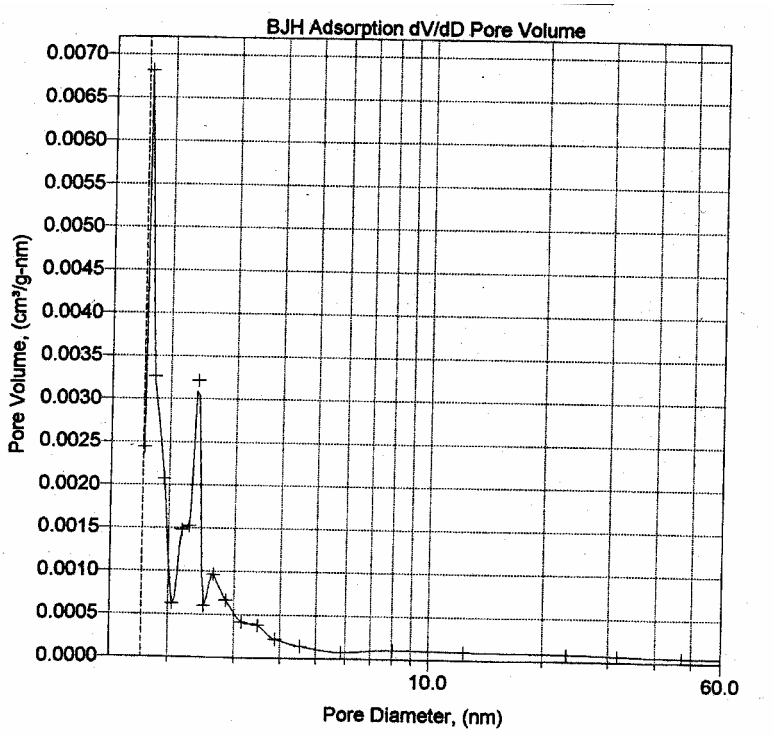

Figure 3.13. BJH pore size distribution plot (adsorption mode).

The TGA curve (Figure 3.14) shows that the silica materials obtained are thermally stable and even at 900 °C only 22% of the original weight is lost.

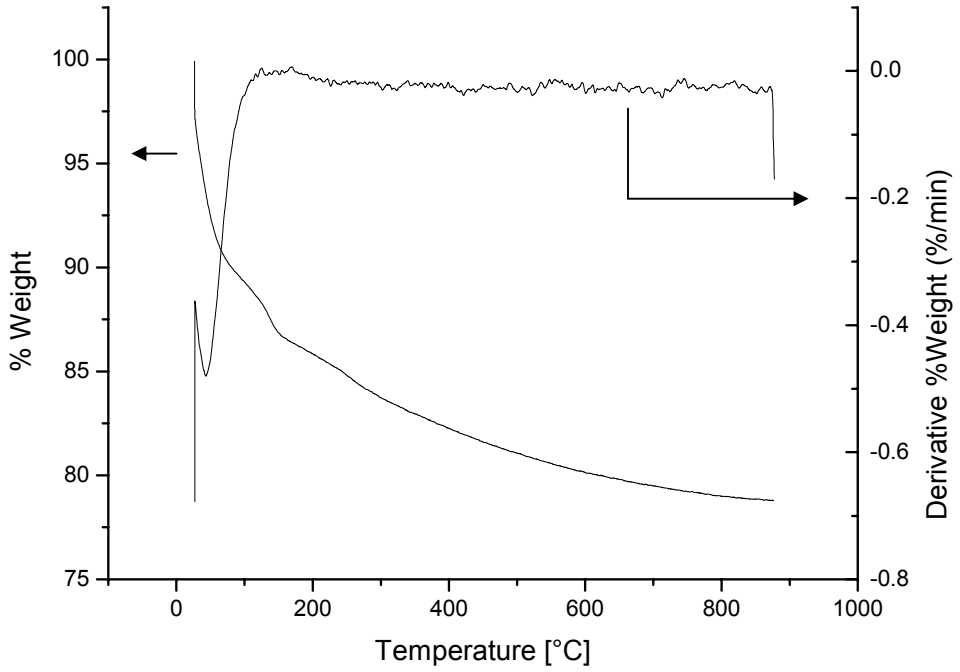

Figure 3.14. TGA curve of silica obtained at 0 °C.

Mechanism of formation

Our study reveals that the morphology of the final silica materials relies on the self-assembly of the template and the interaction between the inorganic silica precursors and the aggregates. The self-assembly of the template is highly influenced by synthesis conditions. Sphere formation is a competitive reaction to tube formation. Sphere shaped templates are formed under certain synthesis conditions (e.g. at 75 °C) while rod-like templates are formed are favoured under certain synthesis conditions (e.g. low temperatures). Thus the template ions (ammonium citrate ions) can form two types of templates depending on the conditions. The formation of rod-like crystals (as found in chapter 2 and by others[14]) leads to the formation of tubular silica materials.

In line with our study in the previous chapter and by others[14] our data are consistent with the following:

iv) formation of rod-like or sphere-like crystals (from template molecules) by a slow aggregation process,

v) interaction of the template with the TEOS,

vi) condensation/hydrolysis of the TEOS.

Our data do not establish whether a coil like growth of the silica occurs in the reaction.[14] (Refer to Appendix 2 for coil-like growth)

Comparison of citric acid with DL-tartaric acid

DL-Tartaric acid influences the formation of longer and more uniform tubes compared to citric acid. Tubes that are formed in DL-tartaric acid are hollow and open ended; however the ones formed in citric acid are a mixture of filled and hollow but closed tubes. Hollow spheres are exclusively formed when citric acid is used under certain conditions while only filled spheres are formed when DL-tartaric acid is used. The surface areas for the silica formed from DL-tartaric acid are lower that the areas obtained from citric acid.

Hence it appears that the template also plays a role in the formation of various silica morphologies. This can be attributed to the fact that crystals formed for each template are slightly different. (The size of the molecule, orientation of the hydroxyl groups and inter-molecular H-bonding etc. contribute to this). Both templates can be used depending on the morphology required since they are relatively inexpensive with comparable prices. (100 g of citric acid cost about R 140 while 100 g of DL-tartaric acid cost R 130)

3.4 Conclusions

The study reveals that synthesis conditions influence the formation of particular silica morphologies. It is thus important to carefully control these synthesis conditions. Temperature, water/ethanol dilution, stirring rate and solvent play a large role in structure formation. The formation of tubes is enhanced at lower temperatures relative to elevated temperatures. This effect can be related to diffusion and stability of the template. Only hollow spheres are formed at 70 °C. The formation of tubes is sensitive to the amount of water (water/ethanol dilution) present during the reaction. More tubes were formed under stirred conditions and the tubes were also longer than the ones formed under non-stirred conditions.

Pore size measurements indicate the existence of mesopores and some micropores in the formed silica materials. The powder XRD data reveals that the silicas produced are amorphous. The IR spectra of the calcined silica materials is typical for silica derived from TEOS as reported in the literature. TGA data shows that the silica materials obtained are thermally stable.

3.5 References

1. S. Mann, S.L. Burkett, S.A. Davis, C.E. Fowler, N.H. Mandelson, S.D. Sims, D. Walsh and N.T. Whilton, *Chem. Mater.*, **9**, 2300, (1997).
2. C.G. Göltner, S. Henke, M.C. Weisenberger and M. Antonietti, *Angeur. Chem. Int. Ed.*, **37**, 613, (1998).
3. D. Zhao, J. Feng, Q. Huo, N. Melosh, G.U. Fredrickson, B.F. Chmelka and G.D. Stucky, *Science*, **279**, 548, (1998).
4. A. Imhof and D.J. Pine, *Nature*, **389**, 948, (1997).
5. M. Antonietti, B. Berton, C.G. Göltner and H.P. Hentze, *Adv. Mater.*, **10**, 154, (1998).
6. S.A. Davis, S.L. Burkett, N.H. Mandelson and S. Mann, *Nature*, **385**, 420, (1997).
7. S. Baral and P. Schoen, *Chem. Mater.*, **5**, 145, (1992).
8. W. Shenton, T. Douglas, M. Young, G. Stubbs and S. Mann, *Adv. Mater.*, **11**, 253, (1999).
9. Y. Ono, K. Nakashima, M. Sano, Y. Kanckiyo, K. Inoue, J. Iiojo and S. Shinkai, *Chem. Commun.*, 1477, (1989).
10. H. Nakamura and Y. Matsui, *J. Am. Chem. Soc.*, **117,** 2651, (1995).
11. L. Wang, S. Tomura, F. Ohashi, M. Maeda, M. Suzuki and K. Inukai, *J. Mater. Chem.*, **11**, 1465, (2001).
12. E.P. Barret, L.G. Joyner and P.P. Halenda, *J. Am. Chem. Soc.*, **73**, 373, (1951).
13. W.D. Harkins and G. Jura, *J. Chem. Phys.*, **11**, 431, (1943).

14. F. Kleitz, F. Marlow, G.D. Stucky and F. Schüth, *Chem. Mater.*, **13**, 3587, (2001).

CHAPTER FOUR

TEMPLATES CONTAINING COOH AND/OR OH GROUPS FOR THE PREPARATION OF SILICA MATERIALS*

4.1 Introduction

Since the exciting discovery of the novel M41S family of molecular sieves by the scientists at Mobil Corporation,[1,2] the synthesis and application of mesoporous materials have been studied extensively.[3-7] Many synthetic routes and strategies have been developed to yield a wide diversity of materials of various framework, chemical composition and pore structures. Recently, there have been reports of mesoporous materials with various particle shapes such as fibers, spheres, ropes, discoids, toroids, hollow tubes, hollow spheres and dodecahedra having being synthesized.[8-17] So far, most of these materials were synthesized using templates for directing the formation of mesopores, which relied on the self-assembly of the templates and the interaction between the inorganic precursors and the aggregates.[18]

***To be submitted for publication**

The templates that have been used to date are surfactants, organogelators, hydroxy carboxylic acids, as well as porous or fibrous materials such as carbon nanotubes and membranes. Of all the templates that have been used, hydroxy carboxylic acids seem to be the desired choice because of the low cost and environmental friendliness of the materials.

In this study we have used mucic and tartronic acids (simple hydroxy carboxylic acids) as structural modifiers for the formation of silica tubes and spheres for the first time. We have also used simple carbohydrates (mostly sugars) as templates for the formation of silica materials. Sugars are environmentally friendly (biodegradable) and come from a cheap, renewable and widely available resource: carbohydrates. The structures of the templates used in this study are shown in Figure 4.1.

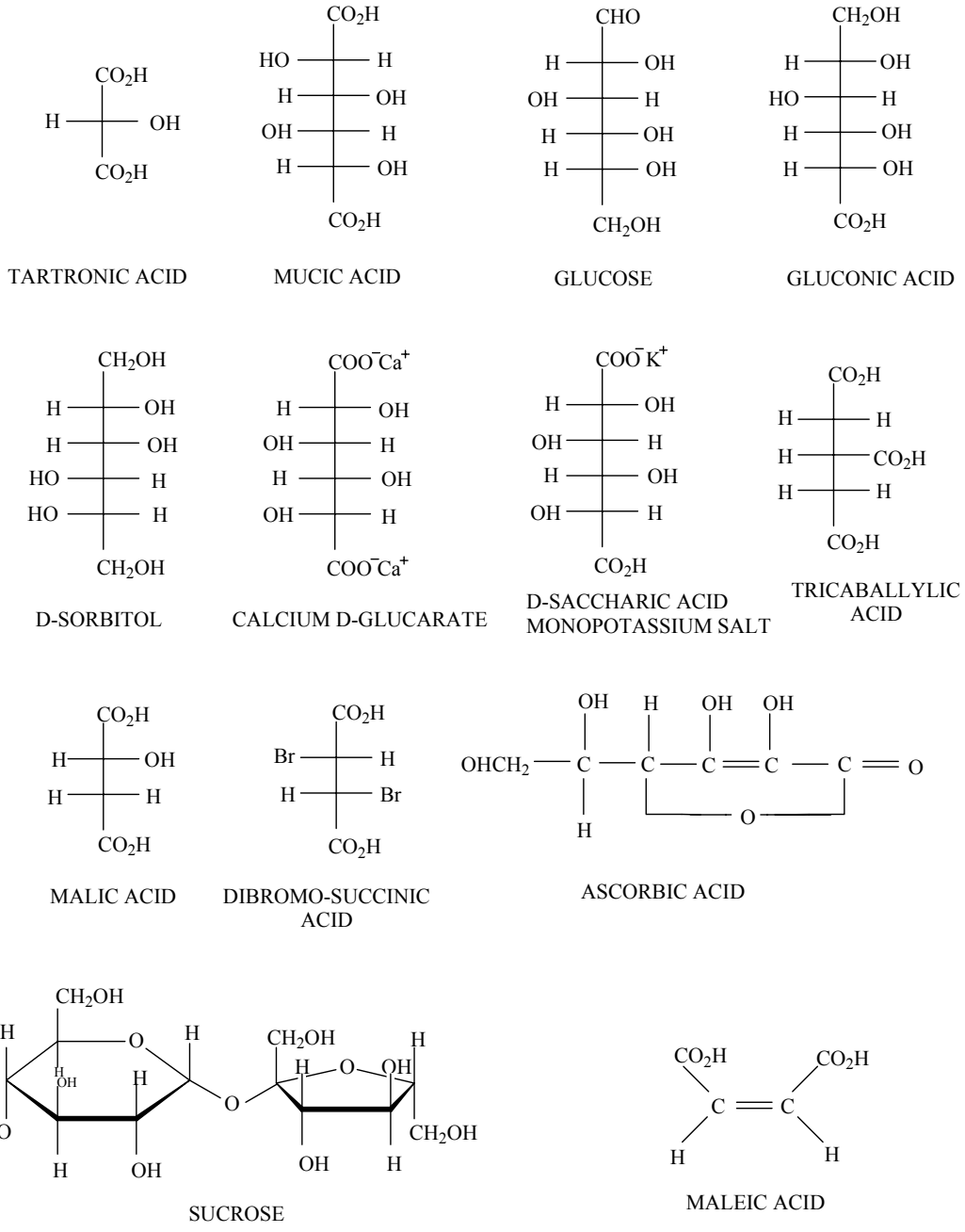

Figure 4.1. Structures of all templates used.

4.2 Experimental

4.2.1 Preparation

Ethanol, butanol, diethyl ether and ethylmethyl ketone (Saarchem), water, tetraethyl orthosilicate (TEOS); (Aldrich), templates (i.e. mucic acid, tartronic acid, glucose, ascorbic acid, gluconic acid, dibromo-succinic acid, maleic acid, DL-malic acid, calcium D-glucarate, D-saccharic acid monopotassium salt, tricaballylic acid, D-sorbitol and sucrose) from different suppliers and ammonium hydroxide (Fluka) were used as chemical sources.

The synthesis procedure followed a standard approach. The template (0.2 g) was dissolved in a mixture of 50 ml solvent and 0.6 ml water. To this mixture was added TEOS (7.3 g). The solution was left to stand for 30 minutes and during this time a silica sol formed. Finally 20 ml of NH_4OH (28% NH_3 solution) was added to the sol to form a gel. The gel was aged for 2 hours and then dried in an oven at 100 ºC. The products were calcined at 550 ºC for 4 hours. The silica was synthesized at three different temperatures, 0 ºC, room temperature and 75 ºC. The reactions were performed under both stirred and non-stirred conditions.

4.2.2 Characterization

The materials were characterised using the same techniques as those described in chapters two and three (sections 2.2.2 and 3.2.2).

4.3 Use of Mucic and Tartronic Acids as Templates

4.3.1 Solvent Effects

a) Mucic Acid

Table 4.1 shows the effect of using mucic acid as a template, at room temperature, on the structure of the silica material formed using different solvents. The table shows that spherical structures are generated in ethanol and butanol while fragmented tubes are formed in diethyl ether and ethyl methyl ketone (EMK). This shows that beside the template, the solvent also plays an important role in determining the resulting morphology of the silica, presumably due to the different polarity of the solvents. This is consistent with what was seen in the previous chapters i.e. changing or altering synthesis conditions such as solvent changes the resulting silica morphology.

The properties of a solvent that contribute to its ability to stabilise ions by solvation are not fully understood but are related to the polarity of the solvent. Solvent polarity is usually expressed in terms of dielectric constants, ε, which measure the ability of a solvent to act as an insulator of electric charges.[19] Solvents of low dielectric constant such as hydrocarbons are non-polar, whereas solvents of high dielectric constant such as water are polar. Table 4.2 lists the dielectric constants of solvents used (water is listed for comparison purposes). The results in Table 4.1 show that tube formation is mainly favoured when mucic acid is used with a non-polar solvent (diethyl ether).

Table 4.1. Effect of solvent on the particle size and structure of silica at 25 ºC[a]

Solvent	Particle size [μm][b]	Structure[c]
Ethanol	S: 0.33 – 0.67	Spheres
Butanol	S: 0.33 – 0.50	Spheres
Diethyl ether	L: 1.13 – 3.51 D: 0.22 – 0.41 S: 0.11 – 0.33	Fragmented tubes (10%) + spheres (90%)
Ethyl methyl ketone	L: 1.25 – 2.54 D: 0.13 – 0.19 S: 0.13 – 0.18	Fragmented tubes (2%) + spheres (98%)

[a]Prepared at 25 °C under a non-stirring condition with mucic acid as a template

[b]L = length of tube, D = outer diameter of tube, S = diameter of sphere

[c]% in brackets gives an estimate of the amount of material formed as determined by TEM

Table 4.2. Dielectric constants of solvents used[15]

Solvent	Dielectric constant
Water	80.4
Ethanol	25.3
Butanol	17.3
Diethyl ether	4.3
Ethyl methyl ketone	18.6

Table 4.3 shows the effect of solvent dilution, at room temperature, on the structure of silicas. The table shows that when a small amount of water (1.1%, vol %) is added to the solvent without changing other synthesis conditions the particle sizes for the silica produced in ethanol and butanol tend to differ only slightly. However in diethyl ether more dramatic structural changes were noted. In general the addition of small amounts of water to a solvent has a modest effect on the morphology and particle size of the silica.

Table 4.3. Effect of solvent dilution (1.1% water, vol %) on the morphology of silica at 25 ºC[a]

Solvent	Particle size [µm][b]	Structure[c]
Ethanol	S: 0.33 – 0.67	Spheres
Ethanol-water	S: 0.25 – 0.63	Spheres
Butanol	S: 0.33 – 0.50	Spheres
Butanol-water	0.17 – 0.67	Spheres
Diethyl ether	L: 1.13 – 3.51	Tubes (5%) + fragments (95%)
	D: 0.22 – 0.41	
	S: 0.11 – 0.33	
Diethyl ether-water	S: 0.40 – 0.65	Spheres (4%) + fragments (96%)

[a]Prepared at 25 °C under a non-stirring condition with mucic acid as a template

[b]L = length of tube, D = outer diameter of tube, S = diameter of sphere

[c]% in brackets gives an estimate of the amount of material formed as determined by TEM

b) Tartronic Acid

Table 4.4 shows the effect of using different solvents on the structure and particle size of the silica when using tartronic acid as a template. Tube formation is favoured when ethanol and diethyl ether are used, but not with EMK. However, the tubes formed when diethyl ether was used as a solvent are fragmented.

It is interesting to note that when tartronic acid is used as a template, tube formation is favoured in both a slightly polar (ethanol) and non-polar (diethyl ether) solvent. Hence it appears that besides synthesis conditions such as solvents, the template still plays a critical role in determining the final structure of the silica.

Table 4.4. Effect of solvent on the morphology of the silica at 25 ºC[a]

Solvent	Particle size [µm][b]	Structure[c]
Ethanol	L: 1.5 – 1.75 D: 0.75 – 0.92 S: 0.6– 0.85	Tubes (70%) + spheres (30%)
Diethyl ether	L: 0.63 – 0.88 D: 0.13 – 0.63 S: 0.10 – 0.52	Fragmented tubes (95%) + spheres (5%)
Ethyl methyl ketone	S: 0.15 – 0.32	Spheres

[a]Prepared at 25 °C under a non-stirring condition with tartronic acid as a template

[b]L = length of tube, D = outer diameter of tube, S = diameter of sphere

[c]% in brackets gives an estimate of the amount of material formed as determined by TEM

4.3.2 Temperature Effects

a) Mucic Acid

Table 4.5 shows that tube formation is favoured at lower temperatures when diethyl ether and EMK are used as solvents. When ethanol is used spheres are formed at all temperatures with the particle size remaining almost the same. Spheres that are formed at 75 °C are smaller than the ones formed at 25 °C. The yield of the tubes is higher at lower temperatures and the tubes are longer. This is because at lower temperatures there is little/less mobility of template and TEOS. Under these conditions the template crystals and TEOS are stable and assemble into tubes or rod-like structures.

Table 4.5. Effect of temperature on the morphology of silica when using various solvents

Solvent	Temperature [ºC]	Particle size [µm][a]	Structure[b]
Ethanol	0 ºC	S: 0.22 – 0.35	Spheres
	25 ºC	S: 0.33 – 0.67	Spheres
	75 ºC	S: 0.20 – 0.33	Spheres
Diethyl ether	0 ºC	L: 1.24 – 4.33	Fragmented tubes
		D: 0.22 – 0.39	(90%) + spheres
		S: 0.13 – 0.30	(10%)
	25 ºC	L: 1.13 – 3.51	Fragmented tubes
		D: 0.22 – 0.41	(10%) + spheres
		S: 0.11 – 0.33	(90%)
	75 ºC	-	Fragments
Ethyl methyl	0 ºC	L: 1.25 – 5.0	Fragmented tubes
ketone		D: 0.13 – 0.24	(20%) + spheres
		S: 0.13 – 0.20	(80%)
	25 ºC	L: 1.25 – 2.54	Fragmented tubes
		D: 0.13 – 0.19	(2%) + spheres (98%)
		S: 0.13 – 0.18	
	75 ºC	S: 0.10 – 0.16	Spheres

[a]L = length of tube, D = outer diameter of tube, S = diameter of sphere

[b]% in brackets gives an estimate of the amount of material formed as determined by TEM

b) Tartronic Acid

Table 4.6 shows the effect of using different solvents at different temperatures on the structure and particle size in the formation of silica when using tartronic acid as a template. Tube formation is favoured when ethanol and diethyl ether are used but not when EMK is used. When ethanol and diethyl ether are used as solvents only tubes form at 0 ºC and 25 ºC but the yield of the tubes is higher at 0 ºC than at 25 ºC; only spheres are formed at 75 ºC. This can be related to the inability of the template and silica to assemble as the temperature is raised, therefore resulting in sphere formation. The tubes that are obtained at 0 ºC when using ethanol are hollow (Figure 4.2) with outer diameters ranging from 0.5 to 0.75 µm. Changing the temperature does not seem to have an adverse effect on the structure when EMK is used; it is only the particle size that changes

Table 4.6. Effect of temperature on the structure and particle size of the silica when using different solvents

Solvent	Temperature [ºC]	Particle size [µm][a]	Structure[b]
Ethanol	0 ºC	L: 1.0 – 1.80 D: 0.5 – 0.75 S: 0.4 – 0.68	Hollow tubes (90%) + Spheres (10%)
	25 ºC	L: 1.5 – 1.75 D: 0.75 – 0.92 S: 0.6 – 0.85	Fragmented tubes (70%) + spheres (30%)
	75 ºC	S: 0.13 – 0.75	Spheres
Diethyl ether	0 ºC	L: 5.0 – 7.0 D: 0.63 – 0.67 S: 0.10 – 0.48	Fragmented tubes (95%) + spheres (5%)
	25 ºC	L: 0.63 – 0.88 D: 0.13 – 0.63 S: 0.10 – 0.52	Fragmented tubes (10%) + spheres (90%)
	75 ºC	S: 0.10 – 0.22	Spheres
Ethyl methyl ketone	0 ºC	S: 0.17 – 0.25	Spheres
	25 ºC	S: 0.23 – 0.40	Spheres
	75 ºC	S: 0.15 – 0.38	Spheres

[a]L = length of tube, D = outer diameter of tube, S = diameter of sphere

[b]% in brackets gives an estimate of the amount of material formed as determined by TEM

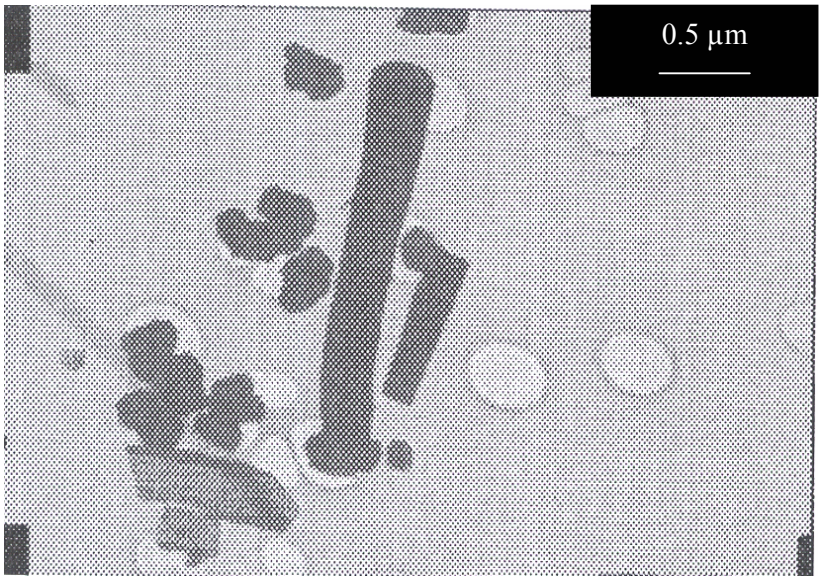

Figure 4.2 TEM image of SiO_2 obtained at 0 ºC when ethanol is used as a solvent.

4.3.3 **Stirring vs Non-stirring Conditions**

Stirring enhances the formation of tubes for all solvents used (Tables 4.7a and b) regardless of the template used. This is because when the diffusion rate is increased molecules move and assemble more easily. The nature and type of solvent also influences the morphology of the silica materials.

Table 4.7a. Effect of stirring on the structure and particle size of silica at 25 °C for mucic acid.

Solvent	Condition	Particle size [μm][a]	Structure[b]
Diethyl ether	Non-stirring	L: 1.13 – 3.51 D: 0.22 – 0.41 S: 0.11 – 0.33	Fragmented tubes (10%) + Spheres (90%)
	Stirring	L: 2.0 – 4.0 D: 0.25 – 0.38 S: 0.25 – 0.30	Fragmented tubes (40%) + Spheres (60%)
EMK	Non-stirring	L: 1.25 – 2.54 D: 0.13 – 0.19 S: 0.13 – 0.18	Fragmented tubes (2%) + spheres (98%)
	Stirring	L: 1.25 – 3.92 D: 0.38 – 0.63 S: 0.30 – 0.41	Fragmented tubes (35%) + spheres (65%)

[a]L = length of tube, D = outer diameter of tube, S = diameter of sphere

[b]% in brackets gives an estimate of the amount of material formed as determined by TEM

Table 4.7b. Effect of stirring on the structure and particle size of silica at 25 °C for tartronic acid.

Solvent	Condition	Particle size [μm][a]	Structure[b]
Ethanol	Non-stirring	L: 1.5 – 1.75 D: 0.75 – 0.92 S: 0.6 – 0.85	Fragmented tubes (70%) + Spheres (30%)
	Stirring	L: 2.0 – 4.0 D: 0.25 – 0.38 S: 0.25 – 0.30	Fragmented tubes (90%) + Spheres (10%)
Diethyl ether	Non-stirring	L: 0.63 – 0.88 D: 0.13 – 0.63 S: 0.10 – 0.52	Fragmented tubes (10%) + spheres (90%)
	Stirring	L: 0.63 – 1.75 D: 0.38 – 0.63 S: 0.30 – 0.53	Fragmented tubes (35%) + spheres (65%)

[a]L = length of tube, D = outer diameter of tube, S = diameter of sphere

[b]% in brackets gives an estimate of the amount of material formed as determined by TEM

4.3.4 Surface Area and Pore Analysis

Table 4.8 shows the effect of solvent and temperature on the surface area of the silica materials obtained. When diethyl ether was used as a solvent and mucic acid used as a template, the product formed gave high surface areas compared to those given when ethanol and EMK were used as solvents under the same synthesis conditions. The surface area that was obtained when tartronic acid was used in all solvents, was very low < 20 m^2/g. In general the materials formed from tartronic acid as a template have lower surface areas compared to the mucic acid derived ones. The textures were also different. The tartronic acid derived silica was fluffy and light, while the mucic acid derived silica was dense and crystal like.

Table 4.8. Summary of BET surface area results*

Template	Solvent	Temperature [ºC]	BET Surface Area [m^2/g]
Tartronic acid	Ethanol	0	8.5
		25	5.3
		75	10.1
	Diethyl ether	0	9.7
		25	15.6
		75	19.4
	Ethylmethyl ketone	0	8.7
		25	11.9
		75	18.4
Mucic acid	Ethanol	0	198.4
		25	188.2
		75	163.5
	Diethyl ether	0	268.1
		25	263.5
		75	187.7
	Ethylmethyl ketone	0	180.3
		25	179.1
		75	106.7

*** Calcined at 550 ºC for 4 hours**

The pore analyses of the materials obtained when using mucic acid and diethyl ether; and tartronic acid and ethanol were carried out because the materials gave tubes and/or spheres at certain temperatures. The nitrogen adsorption-desorption isotherm of SiO_2 synthesised from mucic acid (diethyl ether, 25 ºC) (Figure 4.3) shows a type IV isotherm with a H2 hysteresis loop, indicating the presence of mesopores with an interconnected network of pores of different shapes and sizes.[20] The BJH pore size distribution (Figure 4.4) also reveals that the material is mesoporous with an average pore diameter of 3.5 nm. TEM showed the material to consist mostly of spheres and some fragmented tubes (10%).

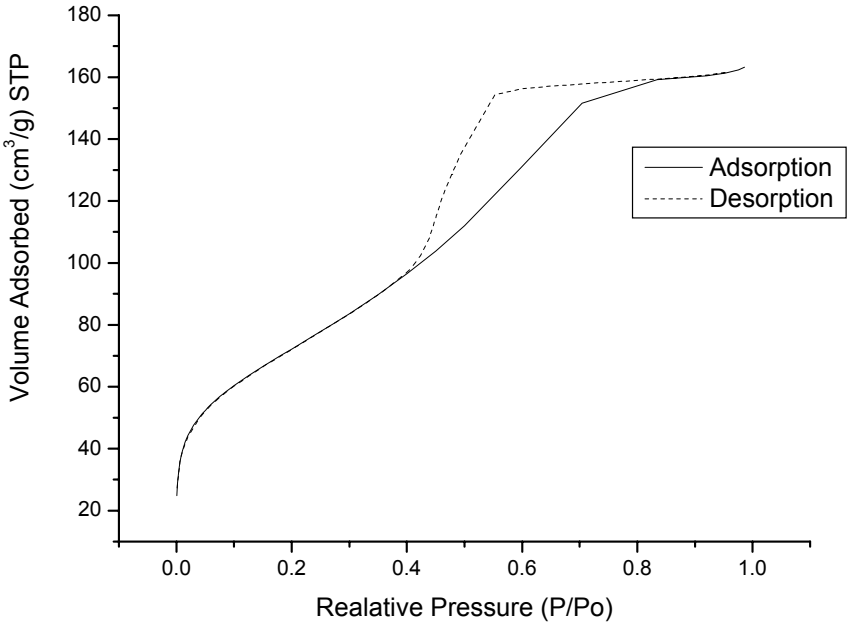

Figure 4.3. Nitrogen adsorption-desorption isotherm of SiO_2 synthesised from mucic acid (diethyl ether, 25 ºC).

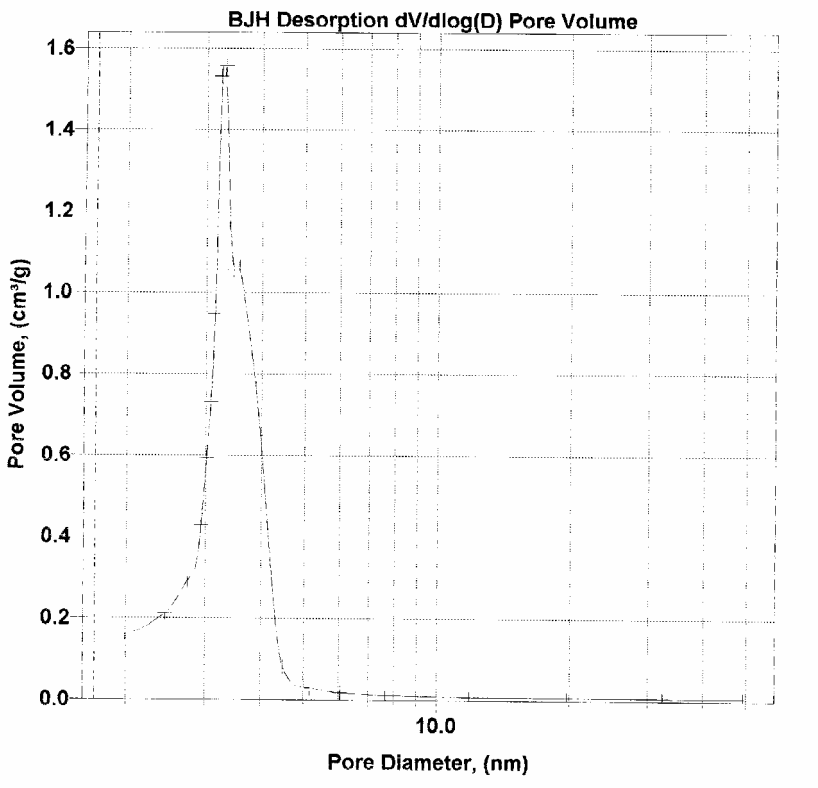

Figure 4.4. BJH pore size distribution for SiO_2 synthesised from mucic acid (diethyl ether, 25 ºC), desorption mode.

The nitrogen adsorption-desorption isotherm of SiO_2 formed from mucic acid (diethyl ether, 75 ºC) (Figure 4.5) also shows a type IV isotherm with a H2 hysteresis loop, indicating the presence of mesopores with an interconnected network of pores of different shapes and sizes.[20] The BJH pore size distribution for the this sample (Figure 4.6) reveals a bimodal pore size distribution in the material: one with an average pore diameter of 3.3 nm and the other with a pore diameter of 4.4 nm. These different pore sizes can be attributed to different mesopores within the amorphous fragmented nanoparticles. TEM also showed that the material consisted of fragments with

different shapes and sizes. Altering synthesis conditions, in this case temperature, affected the morphology of the material, which in turn affected the pore size distribution.

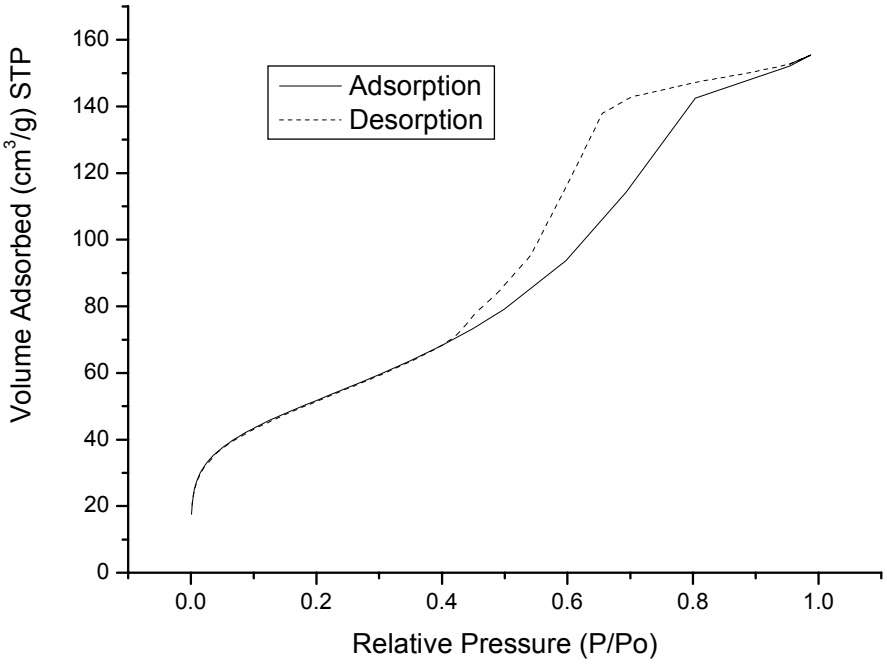

Figure 4.5. Nitrogen adsorption-desorption isotherm of SiO_2 synthesised from mucic acid (diethyl ether, 75 ºC).

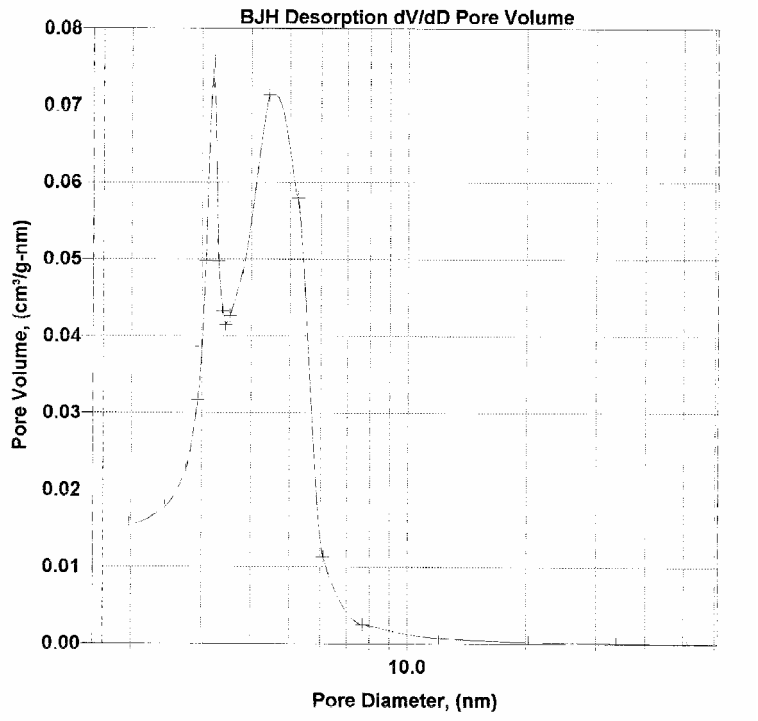

Figure 4.6. BJH pore size distribution for SiO_2 formed from mucic acid (diethyl ether, 75 ºC), desorption mode.

The nitrogen adsorption-desorption isotherm of the sample formed from tartronic acid (ethanol, 25 ºC) (Figure 4.7) shows a Type IV isotherm with a H4 hysteresis loop, indicating the existence of narrow slit-like pores in the material. The BJH pore size distribution of the sample reveals that the pores range from 1.7 – 2.4 nm (Figure 4.8). The peak at 1.7 nm is due to the micropores that are present in the silica and the peak at 2.4 nm is due to the mesopores that occur within the silica nanotube walls.[13] The t-plot diagram showed that the microporous volume represented 46% of the total porous volume. TEM showed the material to consist of mostly fragmented tubes with some spheres.

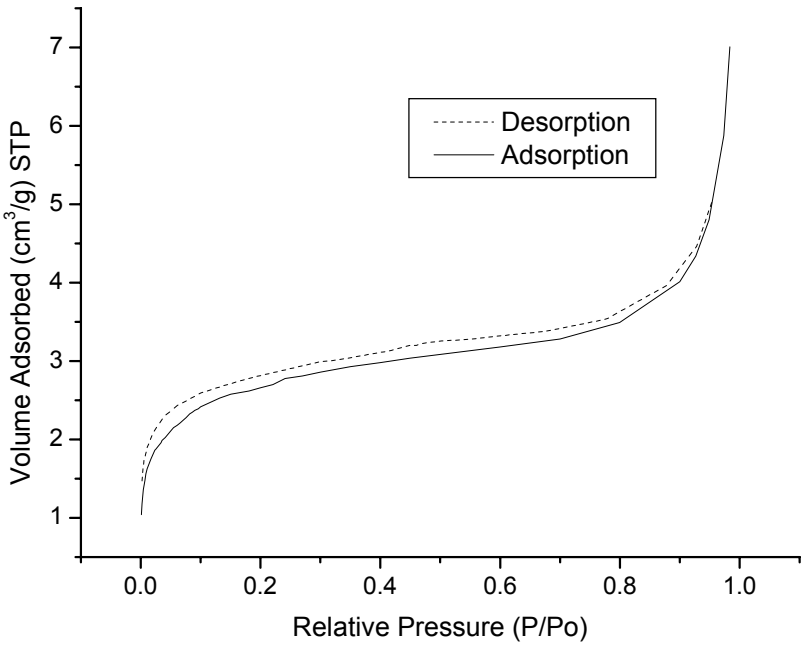

Figure 4.7. Nitrogen adsorption-desorption isotherm of SiO_2 formed from tartronic acid (ethanol, 25 ºC).

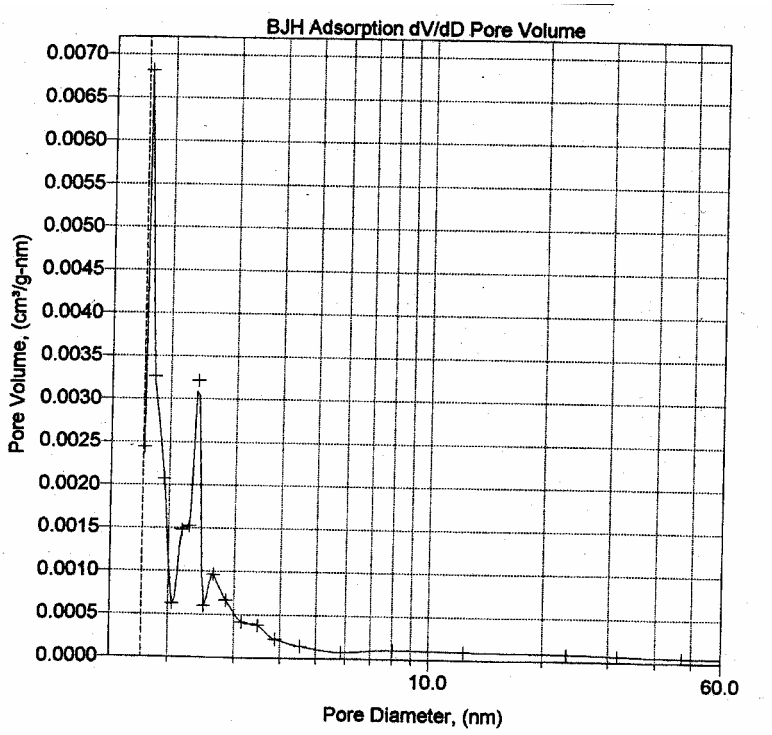

Figure 4.8 BJH pore size distribution for SiO_2 synthesised from tartronic acid (ethanol, 25 ºC).

The nitrogen adsorption-desorption isotherm of SiO_2 formed from tartronic acid, (ethanol, 75 ºC) also shows a Type IV isotherm with a H4 hysteresis loop, indicating the presence of not so well defined narrow slit-like mesopores in the material.[20] The BJH pore size distribution of the sample reveals that the pores range from 1.7 – 2.5 nm (Figure 4.10). The peak at 1.7 nm is due to the micropores that are present in the silica and the peak at 2.5 nm is due to the mesopores that occur in the silica. The t-plot diagram showed that the microporous volume represented 54% of the total porous volume. TEM showed the material to be only consisting of spheres.

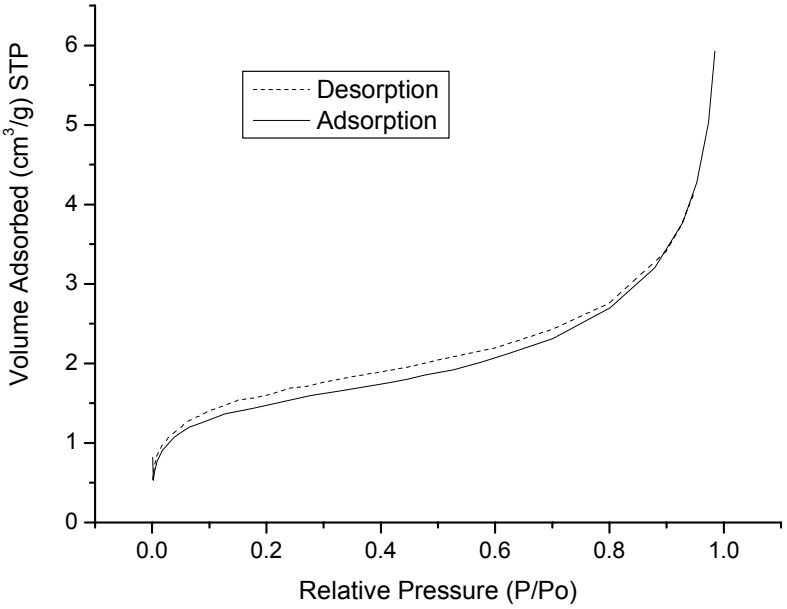

Figure 4.9. Nitrogen adsorption-desorption isotherm of SiO_2 formed from tartronic acid, ethanol, 75 ºC).

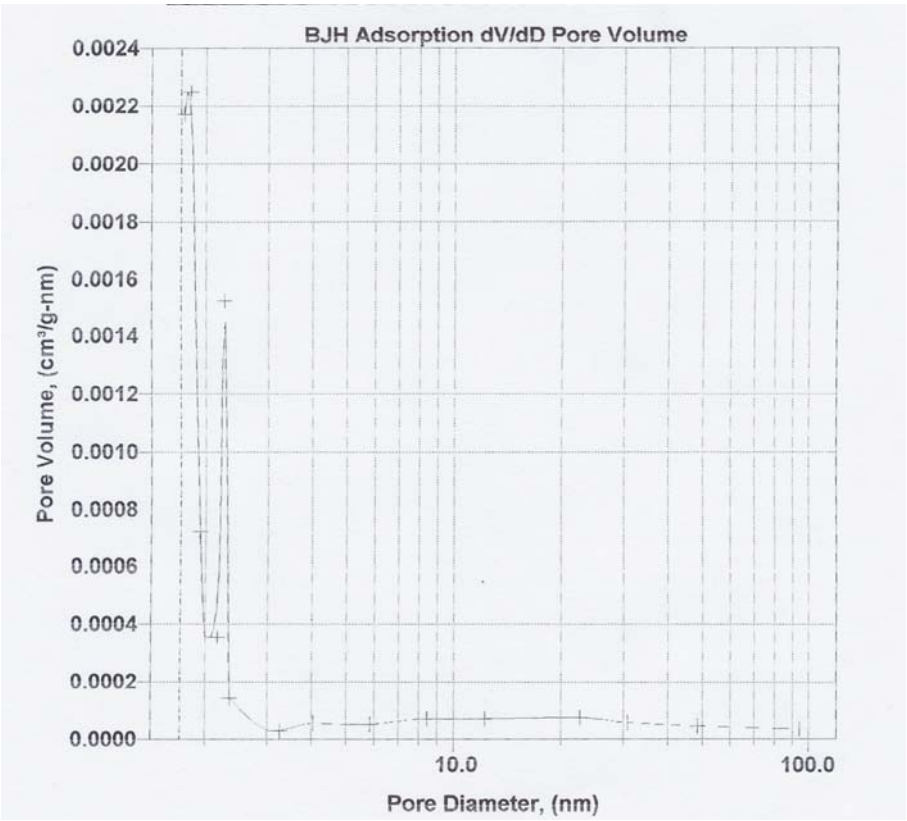

Figure 4.10. BJH pore size distribution plot for SiO_2 synthesised from tartronic acid (ethanol, 75 ºC), adsorption mode.

Table 4.9 gives a comprehensive summary of the results. From these results one can conclude that mucic acid tends to influence the formation of materials with mesopores while tartronic acid influences the formation of materials with a combination of mesopores and micropores, hence the surface areas obtained with tartronic acid are lower.

Table 4.9. Tabular summary of results discussed in this section.

Sample	Structure[a]	Types of pores	Surface Area (m^2/g)
Mucic, diethyl ether, 25 °C	Fragmented tubes (10%) + spheres (90%)	Meso pores	263
Mucic, diethyl ether, 75 °C	Fragments	Meso pores	187.7
Tartronic, ethanol, 25 °C	Fragmented tubes (70%) + spheres (30%)	Meso + micro pores	5.3
Tartronic, ethanol, 75 °C	Spheres	Meso + micro pores	10.1

[a]% in brackets gives an estimate of the amount of material formed as determined by TEM

4.3.5 Thermal Analysis

The TGA data below (Tables 4.8 and 4.9) show that the silica materials obtained are moderately stable. Only about 16% of the original weight is lost when the samples are heated to 900 ºC. These losses are attributed to the loss in moisture and template respectively in the samples.

Table 4.10. TGA data of the material obtained when using mucic acid as a template and diethyl ether as a solvent.

Temperature (°C)	1st weight loss temperature (°C)	% Weight lost at 1st temperature	2nd weight loss temperature (°C)	% Weight lost at 2nd temperature	Total % weight loss at 900 °C (%)
0	115	9.8	303	4.8	14.4
25	120	10	310	4.8	14.8
75	112	12	271	5	17.0

Table 4.11. TGA data of the material obtained when using tartronic acid as a template and ethanol as a solvent.

Temperature (°C)	1st weight loss temperature (°C)	% Weight lost at 1st temperature	2nd weight loss temperature (°C)	% Weight lost at 2nd temperature	Total % weight loss at 900 °C (%)
0	133	6.6	290	12.5	19.1
25	126	9.6	320	15.5	25.1
75	120	8.5	302	13.6	18.2

4.4 Use of Sugars as Templates

The reason that these templates were used is that it was seen in the previous chapters of this thesis that simple organic acids such as DL-tartaric, citric and tartronic acids acted as templates during the formation of silica nanotubes. Matsui *et al*[12] suggested that the hydrogen bonding that existed in these molecules played an important role in the reaction mechanism. However a recent article by Miyaji *et al*[21] suggests that needle-like ammonium DL-tartrate crystals which form almost simultaneously with polycondensed silica when NH_3 aq. is added, play the role of template. Hence it appears that NH_3 aq. plays a dual role during the synthesis, first as a source of template crystals, and then as a basic catalyst for silica hydrolysis and polycondensation. (It is important to note that it is only the template that was varied, not the synthesis conditions. The synthesis in this study was carried out at room temperature without any stirring with ethanol as a solvent).

Table 4.12 shows results obtained when carbohydrates, mostly sugars, were used as templates. (See Figure 4.1 for the chemical structures of templates used). In all cases the silica materials obtained had spherical morphology (Figure 4.12) but had different sizes and surface areas. The particle sizes ranged from 0.003 to 3 μm and the surface areas ranged from 3.6 to 61.7 m^2/g.

Table 4.12. Effect of different templates on the surface area and particle size

Template	BET Surface Area [m^2/g]	Particle Size [μm]
Glucose	17.6	0.3 – 0.5
Gluconic acid	5.2	0.003 – 0.01
Ascorbic acid	3.6	0.3 – 0.5
D-Sorbitol	6.2	0.09 – 0.12
Dibromo-succinic acid	5.9	0.2 – 0.45
Maleic acid	61.7	0.4 – 0.7
DL-Malic acid	3.5	0.05 – 0.4
Calcium D-glucarate	5.8	0.012 – 0.014
D-Saccharic acid monopotassium salt	6.9	0.02 – 0.024
Sucrose	13.4	0.25 – 0.5
Tricaballylic acid	28.4	1 - 3

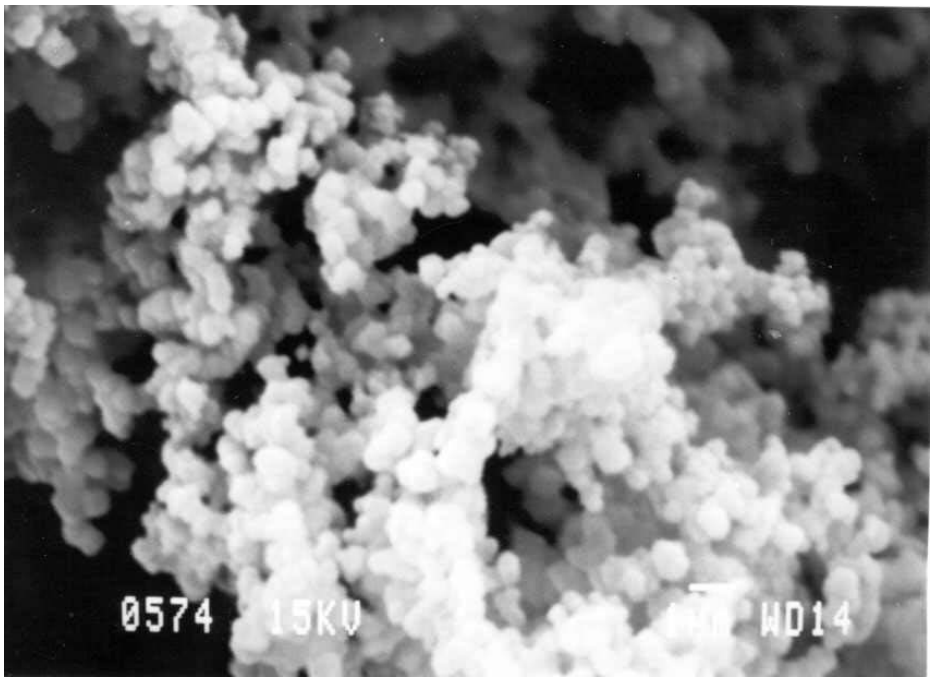

Figure 4.11. SEM image showing the spherical particles obtained when using glucose as a template.

Gluconic acid, D-sorbitol, calcium D-glucarate and D-saccharic acid monopotassium salt gave particles that are very small (in the nano-scale). These particle sizes are much smaller than the ones that are normally obtained by the sol-gel method. A classical example is that of silica materials obtained by Stöber and co-workers where their particle size was in the range 0.05 - 2 μm.[22] On the other hand glucose, ascorbic acid (commonly known as vitamin C), dibromo-succinic acid, maleic acid, DL-malic acid, sucrose (common sugar) and tricarballyic acid gave bigger particles (in the micro-scale).

The results show that all the materials obtained from the templates used in this section have a spherical morphology. These templates are unlike the

ones that were used in earlier studies, i.e. DL-tartaric, citric, mucic and tartronic acids, which generated a combination of tubes and spheres at room temperature.

It is possible that tubes did not form here because NH_3 aq. was added after TEOS addition and so the silica hydrolysed and polycondensed before the template crystals could be formed. It is also possible that the NH_3 solution that was added was not in excess and hence there were not enough template crystals formed and hence the hydrolysis and condensation proceeded without template formation. The unique combination of hydroxyl groups and carboxylic acid groups that is found in DL-tartaric, citric, mucic and tartronic acids, is not found in sugars (refer to chemical structures in Figures 2.1, 3.1 and 4.1) and that might play a role in assisting with the rapid formation of template crystals before the hydrolysis and polycondensation of the silica.

The N_2 adsorption-desorption isotherms of the silicas produced from these templates all showed Type IV isotherms with H4 hysteresis loops (e.g. data for glucose is shown in Figure 4.12), indicating the presence of not so well defined narrow mesopores in the materials.[20] The t-plot diagrams showed that the microporous volume represented about 50% of the total porous volume in these materials.

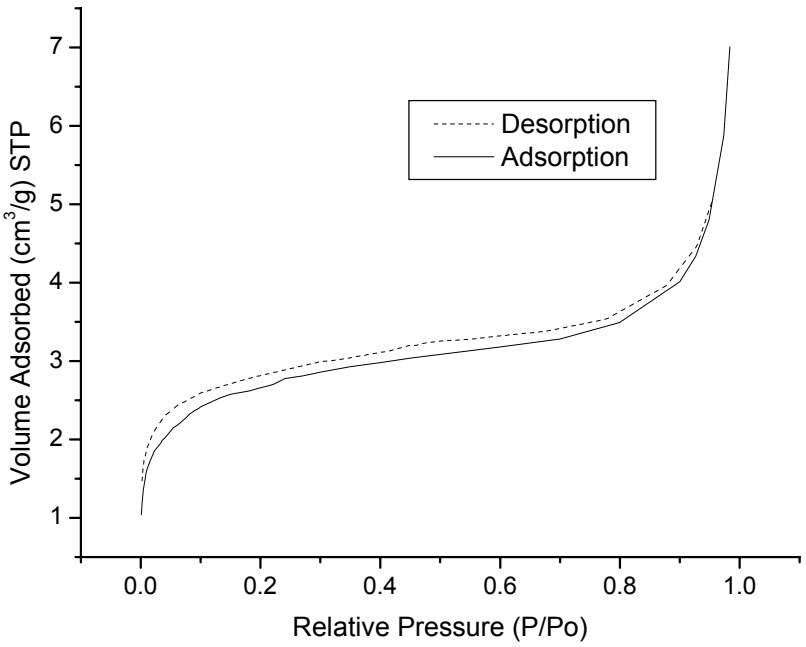

Figure 4.12. N_2 adsorption-desorption isotherm of SiO_2 that was obtained when glucose was used as a template.

Powder XRD diffraction patterns for all the silica materials obtained show that only one broad peak appears between 23 – 24º, indicating that the silica framework is amorphous (see Fig. 4.13).

The IR spectra (Figure 4.14) of these materials showed the absorption bands to be typical of the silica derived from TEOS as reported in the literature.[23,24] A broad band around 3414 cm^{-1} is caused by the O-H stretching vibration mode of the adsorbed water molecules, whose bending vibration mode is responsible for the band recorded at 1627 cm^{-1}. The intense peak at 1098 cm^{-1} is due to the Si-O-R stretching vibration ($\upsilon 1$) of ethoxy groups directly

bonded to silicon while the peaks at 805 and 445 cm^{-1} are caused by the SiOH bending bands $\upsilon 2$ and $\upsilon 3$ modes respectively.

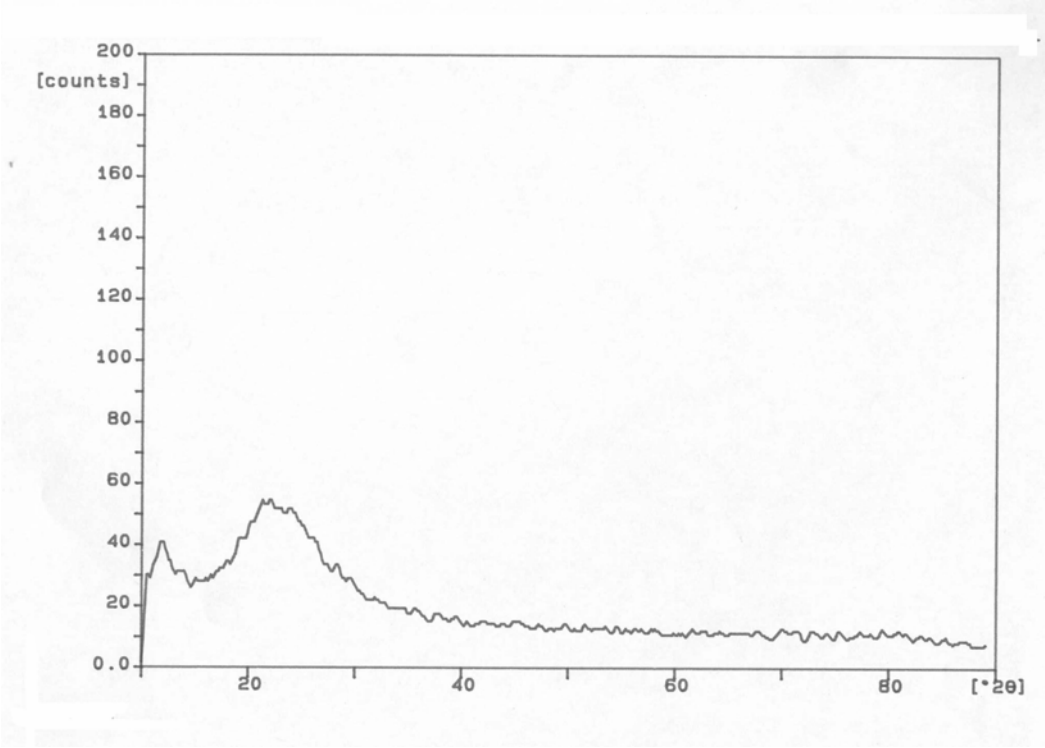

Figure 4.13. Powder XRD pattern of silica produced when sucrose was used as a template.

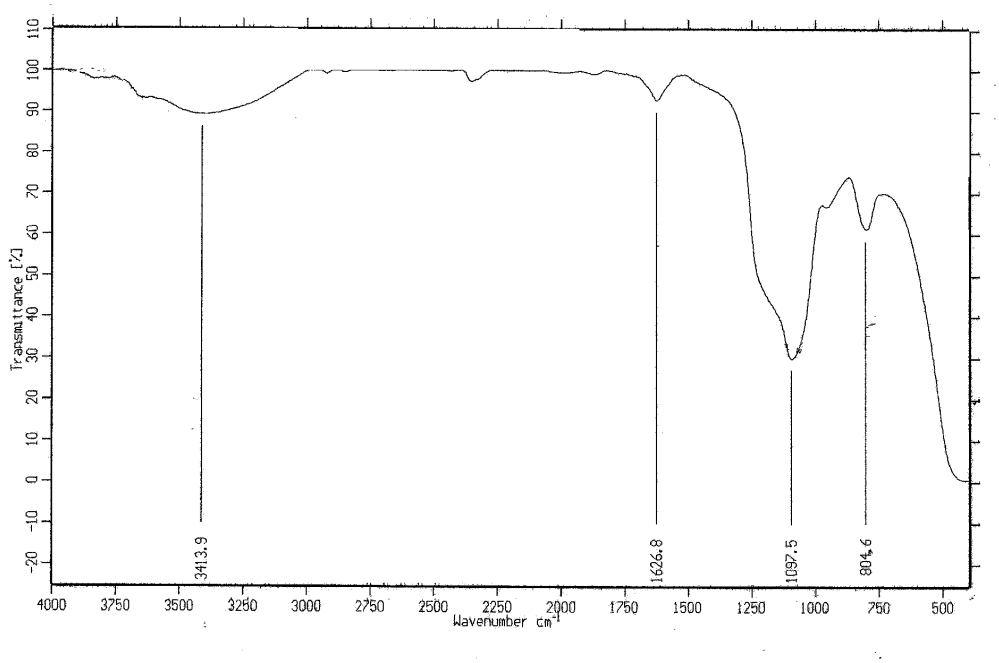

Figure 4.14. IR spectrum of a silica material formed from sucrose (recorded in KBr).

4.5 Conclusions

In this study it was also shown that the template together with synthesis conditions affect the resulting morphology of the silica. Mucic acid influences the formation of silica materials with high surface areas, mesopores and a morphology that reveals fragmented tubes. Tartronic acid influences the formation of hollow tube materials with low surface areas and a combination of micro- and mesopores. The yield of the tubes was higher at lower temperatures for both templates. When sugars were used only spherical particles were obtained and some sugars gave particle sizes that are smaller than the ones that are normally obtained by the sol-gel method. Therefore it appears that a combination of both COOH and OH groups are needed in a template in order to obtain tubular structures.

4.6 References

1. C.T. Kresge, M.E. Leonowicz, W.J. Roth, J.C Vartuli and J.S. Beck, *Nature*, 359, 710, (1992).
2. J.S. Beck, J.C Vartuli, W.J. Roth, M.E. Leonowicz, C.T. Kresge, K.D. Schmitt, C.T.W. Chu, D.H. Olson, E.W. Sheppard, S.B. McCullen, J.B. Higgins and J.L. Schlenker, *J. Am. Chem. Soc*., 114, 10834, (1992).
3. J.Y. Ying, C.P. Mehnert and M.S. Wong, *Angew. Chem. Int. Ed*., 38, 56, (1999).
4. N.K. Raman, M.T. Anderson and C.J. Brinker, *Chem. Mater*., 8, 1682, (1996).
5. A. Corma, *Chem. Rev*., 97, 2373, (1997).
6. U. Ciesla and F. Schuth, *Micro. Meso. Mater*., 27, 131, (1999).
7. S. Biz, M.L. Occelli, *Catal. Rev. Sci. Eng*., 40, 329, (1998).
8. P.J. Bruinsma, A.Y. Kim, J. Liu and S. Baskaran, *Chem. Mater*., 9, 2507, (1997).
9. S.S. Park, C.H. Lee, J.H. Cheon and D.H. Park, *J. Mater. Chem*., 11, Advance Article, (2001).
10. (a) M. Trau, N. Yao, E. Kim, Y. Xia, G.M. Whitesides and I.A. Aksay, *Nature*, 390, 674, (1997). (b) H. Yang, N. Coombs and G.A. Ozin, *Adv. Mater*., 9, 811, (1997).
11. S. Oliver, A. Kuperman, N. Coombs, A. Lough and G.A. Ozin, *Nature*, 1995, 378, 47, (1995).
12. H. Nakamura and Y. Matsui, *J. Am. Chem. Soc*., 117, 2651, (1995); (b) H. Nakamura and Y. Matsui, *Adv. Mater*., 7, 871, (1995).

13. L. Wang, S. Tomura, F. Ohashi, M. Maeda, M. Suzuki and K. Inukai, *J. Mater. Chem.*, 11, 1465, (2001).
14. Y. Zhang, Y. Bando, K. Wada and K. Kurashima, *J. Mater. Sci. Lett.*, 18, 1911, (1999).
15. L. Sudheendra and A.R. Raju, *Bull. Mater. Sci.*, 22, 1025, (1999).
16. F. Miyaji, S.A. Davis, J.P.H. Charmant and S. Mann, *Chem. Mater.*, 11, 3021, (1999).
17. C.E. Fowler, D. Khushalani and S. Mann, *J. Mater. Chem.,* 11, 1968, (2001).
18. J.B. Pang, K.Y. Qiu and Y. Wei, *J. Non-Cryst. Solids*, 283, 101, (2001).
19. J. McMurry, Organic Chemistry, 3rd edition, (Brooks/Cole Publishing Company, Pacific Grove, California, 1992).
20. W.C. Conner, S. Christensen, H. Topsøe, M. Ferrero and A. Pullen in *Characterization of Porous Solids III* (Eds: J. Rouquerol, F. Rodriguez-Reinoso, K.S.W. Sing, K.K. Unger), Elsevier, Amsterdam, 151-160, (1994).
21. F. Miyaji, Y. Tatematsu and Y. Suyama, *J. Cer. Soc Japan*, 109(11), 924-928, (2001).
22. W. Stöber, A. Fink and E. Bohn, *J. Coll. Int. Sci.*, 26, 62, (1968).
23. D.L. Wood and E.M. Rabinovich, *Appl. Spectrosc.*, 43, 263, (1989).
24. H. Izutsu, F. Mizukami, Y. Kiyozuma and K. Maeda, *J. Mater. Chem.*, **7(8)**, 1519 – 1525, (1997).

PART II

THE APPLICATION OF NOVEL SILICA MATERIALS IN THE FISCHER-TROPSCH SYNTHESIS

CHAPTER FIVE

THE FISCHER-TROPSCH SYNTHESIS: AN OVERVIEW

5.1 Introduction

The Fischer-Tropsch (F-T) synthesis is a method for the production of liquid hydrocarbons from synthesis gas (CO and H_2) [derived from either coal or natural gas] [1]. It can hence be considered as an alternative to crude oil for the production of both liquid fuels (gasoline and diesel) and chemicals (in particular, 1-alkenes).[2]

The F-T synthesis was first discovered by Fischer and Tropsch in 1923 when it was found that carbon monoxide and hydrogen reacted at high pressure in the presence of alkalised iron catalysts to yield higher hydrocarbons.[3] The F-T synthesis has since this time been utilised at an industrial level and some economically viable projects are in existence. The three plants run by Sasol in South Africa[4] and the Shell F-T process in Malaysia[5,6] are examples.

There is an abundance of literature on various aspects of the F-T synthesis. Consequently no attempt has been made in this chapter to give a comprehensive literature review of the F-T synthesis reaction. Instead, a general overview of the F-T synthesis will be given which concentrates on the effect that various metals, supports and promoters have on the catalytic properties of the F-T catalysts. Particular emphasis will be placed on studies

entailing iron as a catalyst, since this is the metal that has been studied in this thesis.

5.2 The Fischer-Tropsch Synthesis

The F-T synthesis is a surface-catalysed polymerisation process that uses CH_2 monomers, formed by the hydrogenation of adsorbed CO, to produce hydrocarbons with a broad range of chain length and functionality.[7] The major overall reactions encountered in the synthesis are shown below:[8,9]

Product forming reactions

Olefins

$$2nH_2 + nCO \rightarrow C_nH_{2n} + nH_2O \quad (5.1)$$

Paraffins

$$(2n + 1)\ H_2 + nCO \rightarrow C_nH_{2n+2} + nH_2O \quad (5.2)$$

Alcohols

$$2nH_2 + nCO \rightarrow C_nH_{2n+2}O + (n - 1)\ H_2O \quad (5.3)$$

Side reactions

Water-gas shift

$$H_2O + CO \rightarrow CO_2 + H_2 \quad (5.4)$$

Surface carbonaceous material

$$(x + (y/2))\ H_2 + xCO \rightarrow C_xH_y + xH_2O \quad (5.5)$$

Boudouard disproportionation

$$CO + CO \rightarrow CO_2 + C \quad (5.6)$$

Catalyst oxidation-reduction

a. $$yH_2O + xM \rightleftharpoons M_xO_y + yH_2 \quad (5.7)$$

b. $$yCO_2 + xM \rightleftharpoons M_xO_y + yCO \quad (5.8)$$

Bulk carbide formation

$$yC + xM \rightarrow M_xC_y \quad (5.9)$$

Equations 5.1 - 5.3 provide a simplistic view of the synthesis of alkanes, alkenes and alcohols. The water-gas shift reaction (equation 5.4) and the Boudouard reaction (equation 5.6) [which results in the deposition of carbon] are the main side reactions.[1]

The F-T synthesis is considered to be a chain polymerisation reaction and thus the product spectrum can be described by a chain polymerisation kinetic model.[10] The equation describing the model proposed by Anderson, Schulz and Flory (ASF model) which explains the product spectrum is shown in equation 5.10.[1]

$$W_n/n = (1-\alpha)^2 \alpha^{n-1} \quad (5.10)$$

where n is the carbon number, W_n is the weight fraction of product containing n atoms and α is the chain growth probability. Equation 5.10 can be rewritten to give equation 5.11 which can be used to determine the chain growth probability for a given product spectrum.

$$\ln (W_n/n) = \ln (1-\alpha)^2 + (n-1)\ln\alpha \quad (5.11)$$

Note that α is defined in terms of the rate of chain propagation (r_p) and chain termination (r_t) as shown in equation 5.12.[11]

$$\alpha = r_p/(r_t + r_p) \quad (5.12)$$

The value of α typically lies between 0 and 1 with a higher value indicating a greater selectivity towards waxy products.

The products from the F-T synthesis may vary depending on the catalyst formulation and process conditions.[12] Typical product distributions for low temperature F-T (LTFT) and high temperature F-T (HTFT) are shown in Table 5.1. The product slates follow the Schultz-Flory distributions with, for LTFT, alpha values ranging up to 0.95 or higher for LTFT reactions.

Table 5.1. Selectivity (carbon basis) of Sasol processes[12]

Product	LTFT	HTFT
CH_4	4	7
C_2 to C_4 olefins	4	24
C_2 to C_4 paraffins	4	6
Gasoline	18	36
Middle distillate	19	12
Heavy oils and waxes	48	9
Water soluble oxygenates	3	6

5.3 Process Reactors

There are a number of commercial reactors that are currently used for the F-T reaction. The types of reactors used can be divided into two categories, those used for high temperature F-T (HTFT) and those used for low temperature F-T (LTFT) reactions. The LTFT process is geared to high wax production and the HTFT process is geared mainly for the production of alkenes and gasoline.[13,14]

Originally, tubular fixed bed reactors (TFBR) were used for LTFT (Figure 5.1 (A)) at Sasol. These are the ARGE reactors that were commissioned at Sasol in 1955.[4] These reactors had various disadvantages; high pressure drops, difficulty in replacing spent catalyst and temperature profiles in the reactors were all disadvantages that could not be avoided.[4]

Consequently in 1993 a different type of LTFT reactor was commissioned (Figure 5.1 (C)), the Sasol slurry bed reactor (SSBR).[4] It consists of a shell with cooling coils. The catalyst is suspended in a wax medium through which the feed gas is bubbled. The reactant molecules diffuse through the liquid phase to the catalyst particles. The products would then either diffuse back into the bubbles and be removed as a gaseous product (light hydrocarbons and water) or remain in the slurry and be removed as a wax (heavy hydrocarbon products).

The SSBR has a number of advantages over the TFBR. The temperature control is much better due to the well mixed state of the reactor, the pressure

drop is lower, the catalyst can be added and removed online, scale up is relatively easy, and less capital is required for the SSBR.[4,15] Low temperature operation of the reactors facilitates wax production and thus high quality diesel fuel[5] whilst low molecular weight alkenes are favoured by high temperature operation. Consequently the slurry reactor can be used for the synthesis of gasoline from coal.[16] Due to the promise shown by the slurry reactor, a lot of research has been performed using slurry reactors. The research ranges from the modelling of the slurry reactor,[17,18] to catalyst testing,[19-22] testing different starting media in the reactor[23] and kinetic studies.[24-28]

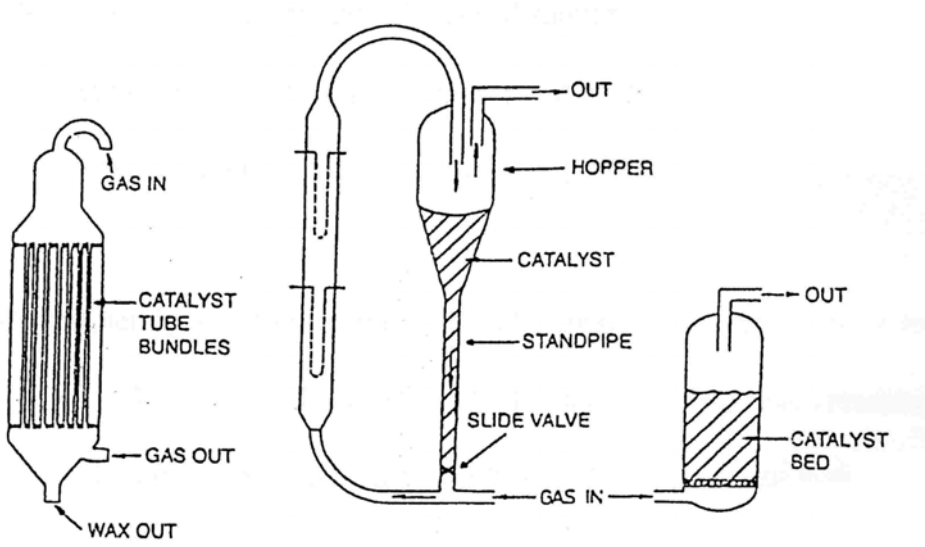

Figure 5.1. Various F-T reactors. (A) Multi-tubular ARGE fixed-bed, (B) Circulating fluidised synthol, (C) Fixed fluidised or slurry phase[14]

The reactors used for HTFT are the circulating fluidised bed (CFB) reactors. Sasol operates Synthol reactors at Sasol 2 and 3 (now called Sasol Synfuels) which are of the fluidised bed type.[13] These are shown in Figure 5.1 (B). The feed gas enters the bottom of the reactor where it entrains a stream of catalyst. The catalyst and feed gas move into the reactor zone and then to the hopper section where the product and the catalyst disengage. The product leaves from the top of the reactor whilst the catalyst gets recycled to the bottom of the reactor. Due to the nature of the reactor, it is possible to replace the old catalyst online. The reactor temperature is controlled by means of heat exchangers in the reactor.

In 1990, Sasol commissioned a fixed fluidised bed (FFB) reactor (Figure 5.1 (C)), the Sasol Advanced Synthol (SAS) reactor for HTFT[15]. The reactor consists of a vessel with a gas distributor, a fluidised bed containing the catalyst, cooling coils in the bed and a cyclone or filter system to remove the catalyst from the product. This reactor is a lot simpler to run than the conventional CFB reactors with the FFB reactor being a lot less complex and smaller than the traditional circulating fluidised bed reactors. The FFB reactor was found to give high oil selectivities and higher conversions than that obtained for an equivalent CFB reactor.[8]

5.4 Fischer-Tropsch Catalysts

The most common catalysts for CO hydrogenation (F-T synthesis) are group 8 – 10 elements: in particular iron, cobalt, ruthenium and nickel. Historically, iron has been the catalyst of choice in industrial applications due to its low cost.[8]

Of late, cobalt has been shown to be a good catalyst for the F-T reaction as it displays greater stability than iron[5] and can be used at lower temperatures and pressures.[29,30] Cobalt based catalysts provide the best compromise between performance and cost for the synthesis of hydrocarbons.[7] However, the choice of catalyst is largely dictated by the synthesis gas feed composition, i.e., by the raw material used for synthesis gas production. Due to the high water-gas-shift (WGS) activity of the iron catalyst, it is the preferred choice for F-T synthesis with coal-derived syngas ($H_2/CO = 0.5 – 0.7$).[31] (Iron catalysts are currently being utilised in the commercial operations at Sasol because Sasol obtains most of the syngas used from coal since large coal reserves are available in South Africa). For natural gas derived syngas ($H_2/CO = 1.6 – 2.2$) and high single pass conversions, the cobalt based catalyst is the preferred catalyst.[31]

The research presented in this thesis has concentrated on the use of iron catalysts. Some current literature on the use of Fe catalysts will hence be reviewed. A brief mention of Co, Ru, Ni, and other metals that have been used to catalyse the F-T synthesis, will also be given, below.

5.4.1 Iron[32]

Iron catalysts have been used extensively for the F-T synthesis and are currently the catalysts utilised in the commercial operations at Sasol and PetroSA (old name was Mossgas) in South Africa.[33] The iron catalyst permits the production of olefinic products when operated in either the low or high alpha mode.[34]

F-T iron catalysts need alkali promotion to attain high activity and stability (e.g. ~ 0.5 wt.% K_2O). Addition of Cu for metal reduction promotion, addition of SiO_2 and Al_2O_3 for structural promotion and even manganese can be applied to Fe catalysts for selectivity control (e.g. high olefinicity). The working catalyst is only obtained after reduction of the iron oxide with hydrogen, CO or syngas. In the initial period of synthesis several iron carbide phases and elemental carbon are formed[35-40] while iron oxides are still present in addition to some metallic iron.[41] With iron catalysts two directions of selectivity have been pursued.

One direction has aimed at a low molecular weight olefinic hydrocarbon mixtures produced in an entrained phase or fluid bed process (Sasol Synthol Process). Due to the relatively high reaction temperature (~ 340 ºC), the average molecular weight of the product is so low that no liquid product phase occurs under reaction conditions. The catalyst particles moving around in the reactor are small (d_p ~100µm)[38] and carbon deposition on the catalyst does not disturb the reactor operation. Thus a catalyst with low porosity and with small pore diameters as obtained from fused magnetite (plus promoters) after reduction with hydrogen is used.

The second direction in iron catalyst development has aimed at high catalyst activity to be generated at low reaction temperatures (~ 230 °C) where most of the hydrocarbon product is in the liquid phase under reaction conditions. Typically, such catalysts are prepared by precipitation from nitrate solutions. A high content of carrier or support provides mechanical strength and wide

pores for easy mass transfer of the reactants with the liquid product filling the pores. The main product fraction then is paraffin wax, which is refined at Sasol,[41] or selectively hydrocracked to a high quality diesel fuel.

Thus iron catalysts are very flexible. Selective F-T synthesis of linear terminal olefins only seems possible with iron catalysts. Alkalised iron F-T catalysts exhibit water-gas shift activity (in contrast to cobalt catalysts). This is a favourable feature for F-T synthesis with CO-rich syngas; as obtained from high temperature coal- or heavy-oil-gasification, through partial oxidation (H_2/CO molar ratio < 1). However, it is undesirable for F-T synthesis with hydrogen-rich syngas as produced from natural gas.

5.4.2 Cobalt

Cobalt catalysts yield mainly straight-chain hydrocarbons. Water is the principal oxygenate formed with alcohol production being rare.[5] Water-gas-shift activity over cobalt is low, unlike over iron catalysts where it is considerable.

The classical cobalt catalysts used in the first German industrial plants had very low activity.[35] One way that is used to improve the activity is to add small amounts of a second metal such as Pt or Re[42-45] to cobalt. Also due to its cost, cobalt is typically used in the form of a supported catalyst. A number of different supports have been used and these supports have different effects on the CO hydrogenation activity and hydrocarbon selectivity. In this thesis however, no experimental work was performed using a cobalt catalyst, and it

is therefore outside the scope of this study to review the use of cobalt catalysts in detail. The reader is referred to a number of reviews on the role of cobalt catalysts in the F-T reaction such as references 46 and 47.

5.4.3 Ruthenium[32]

Ruthenium as a F-T catalyst is of scientific interest. It is the most active working catalyst and can be used at low reaction temperatures. It produces the highest molecular weight hydrocarbons. It acts as a F-T catalyst as a pure metal, without any promoters, thus providing the simplest catalytic system for F-T synthesis. Mechanistic conclusions are thus easier to achieve – much easier than e.g. with iron as the catalyst. Like with nickel, the selectivity changes to mainly methane at elevated temperatures. The high price of ruthenium and the limited world resource exclude industrial application. Systematic F-T studies with ruthenium catalysts contribute substantially to the further exploration of the fundamentals of F-T synthesis.

5.4.4 Nickel

Nickel is generally regarded as a methanation catalyst with its use in the F-T synthesis being limited.[5] Nickel has been shown to be active for the methanation of synthesis gas both as an alloy[48] and as a supported catalyst; typically the support used is SiO_2[49] or Al_2O_3.[50] There has been limited work reported using nickel as a F-T catalyst. Nickel has been shown to be active for F-T synthesis when supported on TiO_2,[51] SiO_2 or Al_2O_3.[52,53]

5.4.5 Other F-T Catalysts

Vannice[54] determined the specific activity of a number of group 8 – 10 metals and found that they could be ranked in the order: Ru > Fe > Ni > Co > Rh > Pd > Pt. These measurements were performed between 240 ºC and 280 ºC and at atmospheric pressure. From this list it is obvious as to why most attention has been given to ruthenium, iron, nickel and cobalt as catalysts.

There has been much interest in bimetallic catalysts of late. A major objective has been to find metals that combine to form bimetallic clusters such that the metals are intimately connected both electronically and geometrically and the resultant activity is greater than the sum of the two metal components.[55] Most of the group 8 – 10 metals mentioned earlier have been used in various combinations in both supported and un-supported bimetallic systems. Iron bimetallic systems have elicited the most interest due to its industrial significance.[56–61] Cobalt has also been used in a number of studies entailing bimetallic catalysts. Reference 46 has an excellent review of the cobalt based bimetallic catalysts.

5.5 Promoter Effects

The Fischer-Tropsch reaction is known to give a very large product distribution described by the Anderson-Schulz-Flory model.[62] It is possible to alter this distribution for F-T catalysts to favour certain areas of the product spectrum through the use of promoters. A promoter is regarded as a component of the catalyst that does not take part in the catalytic reaction but changes the catalytic properties the catalyst.

Promoter chemistry could be said to contribute in two major ways to catalysis. Firstly a promoter could improve catalyst structural[63] features such as by enhancing the catalyst surface area while maintaining its stability in a catalytic reaction. A structural promoter also acts as a barrier[64] or spacer between active metal crystallites, inhibiting sintering or crystallite growth. Typical structural promoters used in F-T catalysis include SiO_2, Al_2O_3, MnO and TiO_2. In many cases an increase is found in BET surface area as a function of increasing levels of promoter content.[38]

The second way in which promoters affect catalysts is electronic in nature. This occurs as a result of a change in the electronic environment of the catalyst surface. This could lead to enhanced reactant gas–active site interactions which could lead to bonding destabilization of the reactant gas. This type of promotion is chemical[65] in nature, and the promoter is referred to as a 'chemical promoter'. Chemical promoters also have the ability to increase catalyst reduction levels. For example the Ruhrchemie[66] precipitated iron catalyst is promoted with Cu, which decreases the temperature of the iron reduction. The increased reduction level results in an activity enhancement and a shift in the product selectivity of the catalyst.

The presence of promoters, notably alkali metals on transition metal surfaces alters the binding energy as well as the sticking probability of the reactant molecules.[67] For iron-based catalysts the probability of chain growth increases with alkali promotion in the order Li, Na, K and Rb.[68] Because of the high price of Rb, potassium salts are generally used in practice.

Potassium and copper have been used as promoters in this study; therefore they will be discussed in detail.

5.5.1 Potassium[68]

Potassium has long being used as a promoter for iron catalysts. It provides an increase in the alkene yield and a decrease in the fraction of methane that is produced.[69,41] Potassium can also increase the catalytic activity for FTS and WGS reactions.[70]

Dry reported the effect of potassium on iron catalysts utilized in a fixed bed and a fluidised bed reactor that operated at different temperatures.[41] According to Dry, the low temperature FTS catalytic activity decreased as the loading of potassium increased but the high temperature reaction showed the opposite effect. As shown in Figure 5.2, at 200 °C, the relative catalyst activity decreased from 64 to 29 when the relative K_2O content increased from 0 to 2.6. At 330 °C, the catalytic activities first increased and then stabilized at a certain level as the relative K_2O content was increased above 2 - 3. For use at high temperature conditions, Figure 5.2 indicates that the catalytic activity can be enhanced by potassium when its loading was lower than 3 relative to Fe, but a further increase in K_2O loading does not enhance the iron catalytic activity.

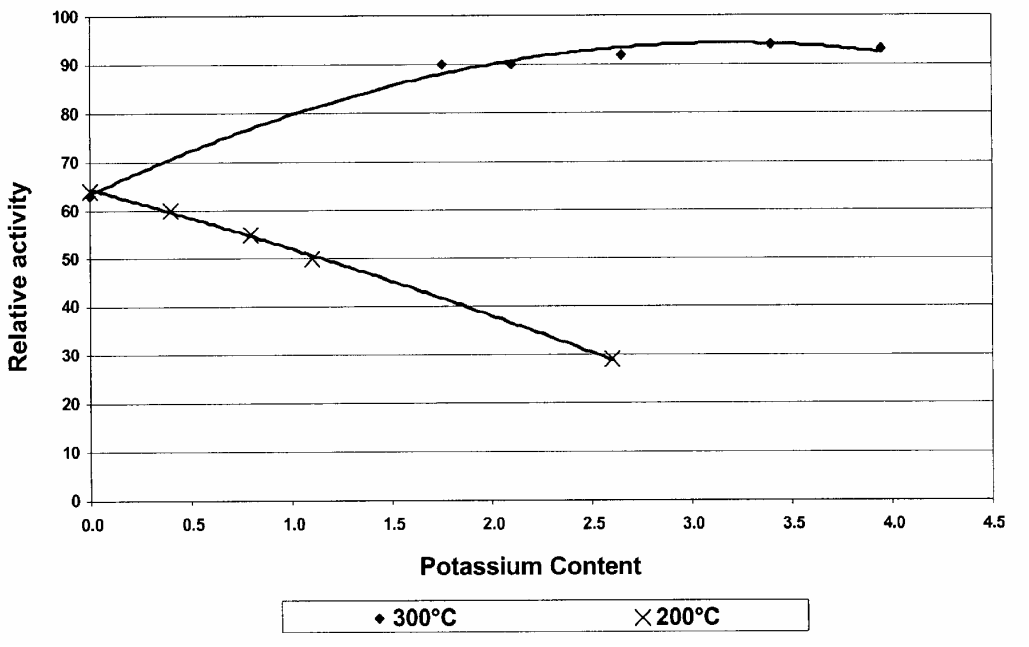

Figure 5.2. Potassium effect on relative activity (drawn from data in ref. 41)

The influence of potassium on iron catalysts has also been investigated by other researchers (e.g. references 71 – 73). It is believed that strong bases of Group I metals have significant effects on both FTS activity and product selectivity. Bell and co-workers found that potassium enhances the adsorption of CO but decreases the adsorption of H_2; therefore, potassium decreases olefin hydrogenation.[74,75] As the most effective promoter, potassium salts are widely used in iron catalysts; however, the readiness to form an alkali compound with common catalyst supports, or structural promoters such as alumina or silica, complicates the situation. Although, potassium enhanced the FTS activity and heavy product fraction, high potassium loadings may cover too large of a fraction of the surface of the iron catalyst, resulting in a limited promotion effect or even a decrease in FTS conversions. In a study by Davis and co-workers,[68] a potassium loading resulting in a K/Fe atomic ratio of

greater than 5 failed to further enhance the CO conversion. Bonzel and Kerbs[76] claimed that potassium lowered the methane formation rate and increased the carbon deposition rate. It was also found that the deposited carbon was covered by potassium compounds rather than carbon sitting on top of the promoter. Huang and Xue Xue Bao[71] studied potassium promoted iron catalysts with X-ray photoelectron spectroscopy (XPS) and found that two-thirds of the catalyst surface was covered by K_2O and SiO_2. Wang and Xue Xue Bao[72] applied the temperature programmed (TPR) technique to study the effects of potassium. They suggested that potassium facilitates the desorption process of carbon monoxide and strengthens the Fe-C bond. Thus, potassium enhanced the selectivity of long chain products, i.e. it resulted in a high-alpha product distribution.

The effects of potassium on the behaviour of iron catalysts are summarized below.[9] The presence of potassium leads to:

1. Higher α, resulting in an increase in the average molecular weight (chain length) of hydrocarbon products (i.e. decrease in production of methane and light gases).
2. Increased olefin/paraffin ratio in the hydrocarbon product.
3. Increased activity for the WGS reaction.
4. Increased catalyst deactivation rate resulting from a higher carbon deposition on the catalyst.
5. Increased FTS activity at low potassium concentrations, followed by a decrease at higher levels of promotion.

5.5.2 Copper

Copper is widely used as a promoter for iron FTS catalysts. It is introduced into the catalyst material as a promoter to facilitate the reduction of the precursor to an active catalyst. Copper nitrate is added in the requisite proportion to the ferric nitrate solution prior to precipitation in the approximate proportion 100Fe/ 3Cu.[41]

Copper is a more effective promoter than potassium in increasing the rate of FTS, whereas the opposite applies to the WGS activity.[70] Copper facilitates the reduction of iron and thus decreases the time required to achieve steady state in FT synthesis. The average molecular weight of the product hydrocarbons is increased in the presence of copper, although copper is less effective than potassium in this respect.[16] Copper can also minimize the sintering of iron catalysts by lowering the reduction temperature.[41]

The precipitated iron catalyst developed by Ruhrchemie and used in the fixed bed reactors at Sasol contains about 5% wt. copper.[76] Dry[41] states that the role of copper is to enhance the rate of reduction, allowing lower reduction temperatures and yielding catalysts with a higher activity than monometallic iron catalysts. Shah and Perrotta[30] have found that Fe-Cu catalysts afford the formation of a higher amount of C_{5+} (hydrocarbons containing more than five carbon atoms) than does a pure iron catalyst. Anderson[77] and Wachs *et al*.[78] concluded that the presence of copper does not alter the activity and selectivity of an iron catalyst. On the other hand, a number of patents have been published claiming that copper markedly enhances the selectivity for

oxygenated products.[79] Anderson[77] and others[80] have found that the presence of copper lowers the rate of carbon formation on iron. According to Dry[41] however, studies at Sasol have not confirmed this conclusion. Wachs *et al.*[78] have also found that the rate of carbon formation is not affected by the presence of copper (or other group 12 metals such as silver). These authors proposed that this arose as a result of a poor contact between the respective metals during the Fischer-Tropsch reaction.

According to a study on the effect copper on the F-T synthesis by Wielers and co-workers[76] the following conclusions can be made about iron catalysts containing copper:

1. Fe-Cu catalysts containing a small amount of Cu exhibit a markedly higher activity in the F-T reaction than monometallic Fe catalysts. This is due to the fact that copper markedly enhances the reducibility of the iron ions and as a result a higher degree of iron reduction is obtained in the catalysts containing Cu. However, with increasing copper content the activity decreases as expected.
2. In a broad compositional range, the selectivity is not affected by the presence of copper. At high copper levels (> 60 wt.%) the selectivity for CO_2, CH_4 and paraffins (at the expense of olefins) increases. This can be explained by assuming that with increasing copper content side reactions such as the WGS (producing CO_2) and hydrogenation reactions (favouring production of methane and parrafins) become more pronounced.

5.6 Support Effects

The choice of support can have a considerable effect on the final activity and selectivity of the catalysts due to interactions between the support and the active metal.[81] Generally a support with a high surface area is used to maximise the dispersion of the metal and reduce the costs. Typically inorganic oxides such as alumina, silica, titania, zirconia and magnesia have been used.[82] Zeolites have also been investigated as supports for F-T catalysts.[6]

Silica seems to be the best support for Fe-based catalysts, at least in terms of activity and wax production.[6] Alumina, partly because of its amphoteric nature, provides a variety of interesting features especially in the isomerisation of straight chain hydrocarbons. However in an alkali environment both silica and alumina, although endowed with high surface areas (100 – 1000 m^2/g) suffer significant deterioration.[83] Titania-supported catalysts on the other hand can deliver relatively high hydrogenation activities due to strong-metal support interactions.[83-86]

Silica is not generally used as frequently as alumina as a support, but it has been found to be useful in some cases in which alumina cannot be used.[87] For example, it is more resistant to acidic media[88] than alumina and it is more sensitive to pressure changes than alumina. This review will focus mainly on silica since it is the support that was used in this study.

Silica is a structural promoter added to maintain the surface area[16,89-90] and it can also have a chemical effect on the catalyst properties or modify the

texture of the catalyst.[89,91-93] The presence of silica may lead to the following effects:[16]

1. Reduction in the bulk concentration of iron in the catalyst, which may hinder mass transfer of gas to liquid as solids loadings are increased to maintain metal concentrations.
2. Possible increase in the concentration of active metal sites by maintaining higher metal dispersions.
3. Influence as a structural promoter in improving the aging characteristics of the catalyst.

Egiebor and Cooper[94] conducted a study of a precipitated iron catalyst on the influence of a silica support in the F-T reaction on the selectivity to 1-olefins, internal olefins and branched hydrocarbons in the gasoline range (C_5-C_{11} hydrocarbons) of a precipitated iron catalyst. They found that the 1-olefin and branched hydrocarbon selectivities decreased whereas the internal olefin selectivity increased with an increase in the silica content of the catalyst. On the other hand, the aromatic and alcohol contents of the products remained relatively constant for all three catalysts tested (100Fe/ 4.2Cu/ 6.7K/ *x*SiO_2) in parts per weight, where x = 21, 50 or 73). Bukur and co-workers[100] also undertook a study to determine the effects of silica and alumina as binders (supports) and process conditions on the activity and product selectivity of precipitated iron catalysts. They found that the addition of silica or alumina to the precipitated unsupported iron catalyst (100Fe/ 5Cu/ 4.2K) influenced the catalyst's activity, stability and selectivity during the Fischer-Tropsch synthesis. The specific activity decreased with increasing support content;

however, the catalyst stability improved with the addition of silica. Product selectivities also changed markedly with increasing silica content of the catalyst, whereas no significant changes were observed with the alumina-containing catalyst. The total olefin content and the fraction of branched hydrocarbons both decreased, whereas the fraction of internal olefins increased with an increase in the silica content of the catalyst. These observations by Burkur and co-workers reflected the expected trends arising from the reduction of surface basicity of the catalyst with increasing silica content and were in agreement with the results obtained in previous studies with similar catalysts.[41,94]

Reuel and Bartholomew[96] showed that the support could significantly influence the extent of reduction, morphology, adsorption and activity/selectivity properties of the active phase, especially in well-dispersed catalysts. Yoshoka *et al*[97] using silica gel as a support for iron, reported that the support has no influence on the oxidation state of iron, but it did influence the degree of dispersion. These workers found that in a silica gel sample, both the surface area and the pore volume increased when the iron concentration was increased. These interesting results suggest that the iron dispersion is not only affected by the surface area of the support, but also by the pore structure of the support. Vanhove *et al*.[98] also observed that the chain length of hydrocarbons was related to the mean pore diameter of the supports in Co/Al_2O_3 catalysts. Thus the porosity of supports for chain growth and reactive products diffusion seems to be very important in the F-T synthesis. However, the non-uniform pore size distribution of supports such

as alumina, silica, titania and zirconia, etc., might lead to a wide distribution of hydrocarbon products.[99]

Recently there have been a considerable number of papers and reviews dealing with the synthesis and characterization of highly uniform mesoporous materials, particularly the hexagonal pore silica-based MCM-41.[100-102] The so-called M41S materials possess a periodic framework of regular mesopores, whose size depends on the alkyl chain length of the organic template and suitable adjustment of the preparation procedure, and is generally ca. 2 and 4 nm. The obtained materials possess interesting physical properties that make them potentially attractive as supports or catalysts. [They usually have high surface areas (~1000 m^2/g), uniform pore size with average pore dimensions between 1.5 and 10 nm and high thermal and hydrothermal stability][99,103]. Indeed the use of periodic mesoporous silicas as F-T supports has recently been explored.[99,103-107] The use of MCM-41 as metal catalyst support has resulted in several cases in significant improvements compared to conventional commercial catalyst due to superior dispersion of the active metals[105-107]. Goodwin and co-workers[103] showed that MCM-41 supported cobalt catalysts have higher activities on a gram catalyst basis for F-T synthesis at 220 °C and 1 atm than conventional silica-supported ones. Pillared clays which are bi-dimensional porous materials[108] and zeolites[5,109-110] such as ZSM-5 have also been used as supports. These materials also have interesting characteristics when compared with conventional supports.

5.7 Fischer-Tropsch Mechanism and Kinetics[5]

The F-T synthesis has long been recognised as a polymerisation reaction with the steps

i) reactant adsorption

ii) chain initiation

iii) chain growth

iv) chain termination

v) product desorption

vi) re-adsorption and further reaction

being the key sequence of events in the reaction.

While most of the mechanistic proposals still remain within the original four classes put forward over the decades, namely; the surface carbide, enolic intermediate, CO-insertion and alkoxy intermediate mechanisms,[31] recent investigators have proposed some useful generalisations which have given rise to important 'hybrid' mechanisms capable of explaining the full hydrocarbon product distribution and also the formation of alcohols, aldehydes and acids.[111] Wojciechowski[112] has inferred that any F-T mechanism must have the following characteristics:

1. Adsorption of all species on the catalyst surface onto one set of sites resulting in the decomposition of H_2 and CO to hydrogen atoms, adsorbed C and O respectively. The interaction between these surface species leads to the formation of CH_x, OH, etc.

2. The monomeric species for oligomerisation is the CH_2 unit and its formation from adsorbed C and H is the rate-determining step for CO hydrogenation kinetics.
3. The growing chain on the surface is immobile except for C_1 – C_4 species. Chain growth proceeds only from a monomer situated near the growing chain. This monomer can either be formed next to the chain or migrate via surface diffusion among an appropriate set of sites.
4. Surface chain growth can produce spontaneous 1 – 2 shift attachments leading to branched hydrocarbons.
5. The termination event and hence product type is determined by the type of occupant on the site adjacent to a growing chain. This occupant may be an appropriate species such as a hydrogen atom, adsorbed OH or even an empty site. If, however, termination occurs after the growing chain has undergone one or more successive 1 – 2 shifts, internal functional groups will arise yielding β-alkenes, 2-alcohols, etc.
6. All classical distributions consist of product species that are primary and each has its own chain length distribution on the Anderson-Schulz-Flory (ASF) plot. This distribution is the property of a co-location grouping of growth, monomer and termination sites which constitute a 'growth location' for that molecular species. The locations are stable in composition and continue to produce only one type of molecule at a given set of reaction conditions.

7. System temperature, total pressure and the H_2/CO ratio are fundamental governing factors which affect both kinetics and product distribution.

Analysis of the F-T product distribution shows that Anderson-Schulz-Flory (ASF) polymerisation kinetics are followed (Figure 5.3), in agreement with a reaction involving stepwise polymerisation of C_1 units. It is generally agreed today that the C_1 units are surface methylenes ($>CH_2$), formed by the hydrogenation of dissociated CO.[113] Fischer and Tropsch were the first to propose the involvement of surface methylene.[114] This concept was later developed by Pettit and Biloen and their collaborators who proposed an "alkyl mechanism" (Figure 5.4) in which the chains grow by the insertion of a surface methylene into the M-C bond of a surface alkyl, and terminate by a β-hydride elimination from the surface alkyl to release the 1-alkene product.[115-117] However, this theory has a number of shortcomings: For example, it cannot easily account for the formation of small amounts of branched chain products or for the formation of anomalously low amounts of C_2 products. The β-hydride elimination step is also unexpected under such strongly hydrogenating conditions. Maitlis and co-workers,[118,119] and others[120,121] have felt that the "alkyl mechanism" has significant inadequacies that require a modification.

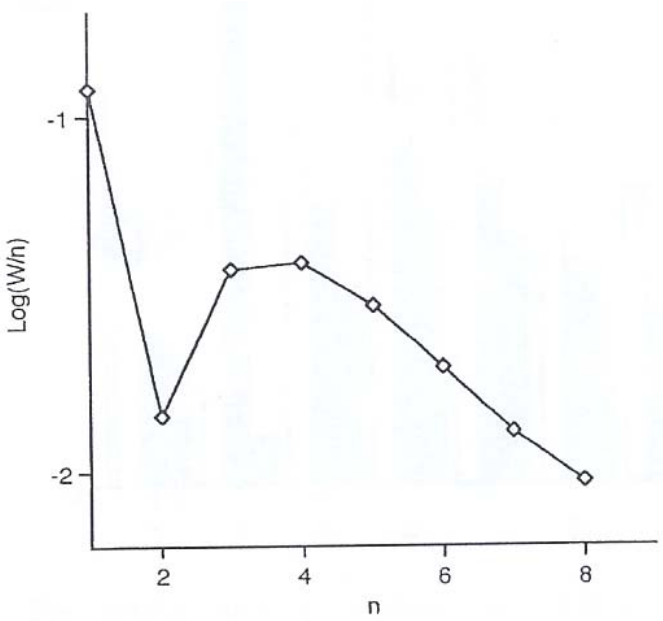

Figure 5.3. Anderson-Schulz-Flory plot of the formation of hydrocarbons from CO hydrogenation, where W is the weight fraction of products having n carbon atoms.

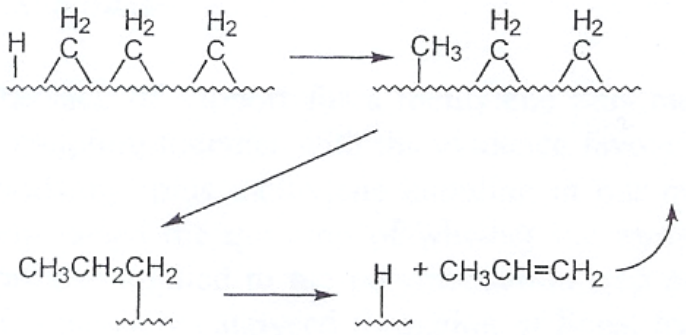

Figure 5.4. Schematic of the alkyl mechanism for the polymerisation of surface methylenes to surface alkyls.[85]

Maitlis and co-workers have used the ideas of organometallic chemistry and homogeneous catalysis derived from model systems, combined with the results of experiments using $^{13}CH_2=^{13}CH_2$-X (X = H, Br, etc) compounds as probes to investigate the heterogeneously catalysed hydrogenation of CO over metal catalysts. From these studies they proposed the "alkenyl mechanism" for the F-T reaction, in which chain growth is initiated by a vinyl + methylene coupling, proceeds by alkenyl + methylene coupling, and terminates via hydrogenation of the alkenyl to yield the 1-alkene.[122] This mechanism, shown in Figure 5.5, has a number of advantages over the alkyl mechanism, since it can explain the formation of branched products (for example, by allyl isomerisation); the low amount of C_2 products (the mechanism for the formation of the C_2 initiator is different from the subsequent chain growth steps); and the release of 1-alkenes as primary products (by a favourable hydrogenation reaction). Some of this work has been reviewed recently.[123] Labelling probe studies also suggest that oxygenates such as ethanol arise from CO but not via methylenes in F-T reactions.

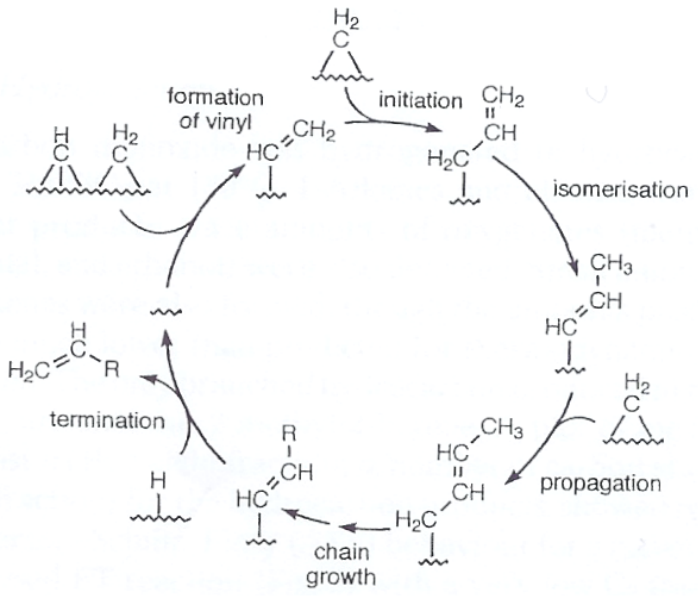

Figure 5.5. The alkenyl mechanism for the stepwise polymerisation methylenes in the Fischer-Tropsch reaction.[122]

However, even the mechanistic proposal made by Maitlis has been controversial.[124,125]

5.8 Aims of This Study

$Fe/Cu/K_2O/SiO_2$ catalysts have been used as commercial catalysts in the Fischer-Tropsch reaction because silica was found to be the best support in terms of both activity and selectivity.[5,41,126] So far the studies that have been carried out on these catalysts used relate to silica prepared by traditional procedures.

Recently it has been reported in the literature that silica with various shapes and sizes (e.g. spherical, tubular, porous and non-porous, mesoporous, etc.) can be synthesized. Indeed the first part of this thesis described the synthesis

of these types of silicas. In this thesis we have thus investigated the effect of silica type (i.e. hollow nanotubes, hollow and closed spheres) and content on the activity and selectivity of $Fe/Cu/K_2O/SiO_2$ catalysts. The size and geometry of the support are expected to influence the final distribution of the catalyst, which in turn will affect the activity and selectivity of the catalyst.

5.9 References

1. C.H. Bartholomew, *New Trends in CO Activation, Studies in Surface Science and Catalysis*, No. 64, (Elsevier Science Publishers, Amsterdam, 1991), 158.
2. M.E. Dry, *Appl. Catal. A: General*, **189**, 185, (1999).
3. F. Fischer and H. Tropsch, *Brennst. Chem.*, **4**, 276, (1923).
4. B. Jager and R. Espinoza, *Catalysis Today*, **23**, 17, (1995).
5. A. A. Adesina, *Appl. Catal. A: General*, **138**, 345, (1996).
6. J. Eilers, S.A. Posthuma and S.T. Sie, *Catalysis Letters*, **7**, 253, (1997).
7. E. Iglesia, *Appl. Catal. A: General*, **161**, 59, (1997).
8. M.E. Dry, *Catalysis Today*, **6**, 183, (1990).
9. R.D. Srivastava, V. U. Rao, G. Cinquegrane and G.J. Stiegel, *Hydrocarbon Processing*, 59, Feb, (1990).
10. H.G. Stenger and C.F. Askonas, *Ind. Eng. Chem. Fundam.*, **25**, 410, (1986).
11. X. Zhang and P. Biloen, *J. Catal.*, **98**, 468, (1986).
12. B. Jager, Natural Gas Convention V, *Studies in Surface Science and Catalysis*, vol. 119, (Elsevier Science Publishers, Amsterdam, 1998), 26
13. M.E. Dry, *Appl. Catal. A: General*, **138**, 319, (1996).
14. B. Jager, Natural Gas Convention IV, *Studies in Surface Science and Catalysis*, vol. 107, (Elsevier Science Publishers, Amsterdam, 1997), 219.
15. B. Jager, M.E. Dry, T. Shingles and A.P. Steynberg, *Catal. Lett.*, **7**, 293, (1990).

16. V.U.S. Rao, G.J. Stiegel, G. Cinquegrane and R.D. Srivastava, *Fuel Proc. Tech.*, **30**, 83 - 96, (1992).

17. S. C. Saxena, *Cat. Rev. Sci. Eng.*, **37**, 227, (1999).

18. J.R. Turner and P.L. Mills, *Chem. Eng. Sci.*, **45**, 2317, (1990).

19. J.R. Inga and B.I. Morsi, *Energy and Fuels*, **10**, 566, (1996).

20. C.N. Satterfield and G.A. Huff, *J. Catal.*, **73**, 187, (1982).

21. G.A. Huff and C.N. Satterfield, *Ind. Eng. Chem. Fundam.*, **21**, 479, (1982).

22. D.B. Bukur, L. Nowicki and X. Lang, *Chem. Eng. Sci.*, **49**, 4615, (1994).

23. R.J. Gormley, M.F. Zarochak, P.W. Deffenbaugh and K.R.P.M. Rao, *Appl. Catal. A: General*, **161**, 263, (1997).

24. G.A. Huff and C.N. Satterfield, *Ind. Eng. Chem. Process Des. Dev.*, **23**, 696, (1984).

25. I.C. Yates and C.N. Satterfield, *Energy and Fuels*, **5**, 168, (1991).

26. W.H. Zimmerman and D.B. Burkur, *Can. J. Chem. Eng.*, **68**, 292, (1990).

27. W.H. Zimmerman, D.B. Burkur and S. Ledakowicz, *Chem. Eng. Sci.*, **47**, 2707, (1992).

28. H.P. Withers, K.F. Eliezer and J.W. Mitchell, *Ind. Eng. Chem. Res.*, **29**, 1807, (1990).

29. R.B. Anderson, *The Fischer-Tropsch Synthesis*, (Academic Press, New York, 1984), 103.

30. Y.T. Shah and A.J. Perotta, *Ind. Eng. Chem. Prod. Res. Dev.*, **15**, 123, (1976).

31. D.B. Bukur, and X. Lang, *Ind. Eng. Chem. Res.*, **38**, 3270, (1999).

32. H. Schulz, *Appl. Catal. A: General*, **186**, 6 – 7, (1999).

33. M.E. Dry, *CHEMTECH*, **22**, 744, (1982).

34. V.U.S. Rao, G.J. Stiegel, A.C. Bose and G.J. Cinquegrane, *Prepr. Pap.-Am. Chem. Soc. Div. Fuel Chem*., **37**, 184, (1982).

35. H.H. Storch, N. Golumbic and R.B. Anderson, *The Fischer-Tropsch and Related Synthesis*, (Wiley, New York, 1951).

36. C.D. Frohning, H. Kölbel, M. Ralek, W. Rottig, F. Schnur and H. Schulz, in J. Falbe (Ed.), *Chemierohstoffe aus Kohle*, (Georg Thieme Verlag, Stuttgart, 1977), 219.

37. H. Schulz, G. Schaub, M. Claeys and T. Riedel, *Appl. Catal. A: General*, **186**, 215, (1999).

38. J.W. Niemantsverdriet, A.M. van der Kraan, W.L. van Dijk and H.S. van der Braan, *J. Phys. Chem*., **54**, 3363, (1980).

39. C.N. Satterfield, R.T. Hanlon, S.E. Tung, Z. Zou and G.C. Papaefthymiou, *Ind. Eng. Chem. Prod. Res. Dev*., **25**, 401, (1986).

40. O.G. Malan, J.D. Louw and L.C. Ferreira, *Brennstoff-Chem*., **42**, 209, (1961).

41. M.E. Dry, in J.R. Anderson and M. Boudart (Eds.), *Catalysis Science and Technology IV*, (Springer, Berlin, 1981), 159 - 255.

42. S. Vada, A. Hoff, E. Adnanes, D. Schanke and A. Holmen, *Topics Catal*., **2**, 155, (1995).

43. D. Schanke, S. Vada, E.A. Blekkan, A.-M. Hilmen, A. Hoff and A. Holmen, *J. Catal*., **155**, 40, (1995).

44. S. Eri, J.G. Goodwin, G. Marcelin and T. Riis, *US Patent 4801573*, (1989).

45. S. Eri, G. Marcelin and J.G. Goodwin, *WO 90/07377*, (1990).

46. T. Chronis, *A Fischer-Tropsch Study of Co/Ru Catalysts*, PhD Thesis, University of the Witwatersrand, Johannesburg, (1999).

47. J.G. Price, *An Investigation into Novel Bimetallic Catalysts For Use in the Fischer-Tropsch Reaction*, PhD Thesis, University of the Witwatersrand, Johannesburg, (1994).

48. H. Habazaki, M. Yamasaki, B. Zhang, A. Kawashima, S. Kohno, T. Takai and K. Hashimoto, *Appl. Catal. A:General*, **172**, 131, (1998).

49. C. Louis, Z.X. Cheng and M. Che, *J. Phys. Chem.*, **97**, 5703, (1993).

50. S.L. Chen, H.L. Zhang, J. Hu, C. Contescu and J.A. Schwarz, *Appl. Catal.*, **73**, 289, (1991).

51. S. Ho, J.M. Cruz, M. Houalla and D.M. Hercules, *J. Catal.*, **135**, 173, (1992).

52. C.H. Bartholomew, R.B. Pannell and J.L. Butler, *J. Catal*, **65**, 335, (1980).

53. Y. Huang and J.A. Schwarz, *Appl. Catal.*, **32**, 59, (1987).

54. M.A. Vannice, *J. Catal.*, **37**, 449, (1975).

55. J.H. Sinfelt and J.A. Cusumano, *Advanced Materials in Catalysis*, in J.J. Burton and R.L. Garten, eds., (Academic Press, New York, 1977).

56. D.J. Duvenhage, *The Preparation, Characterisation and Evaluation of Titania Supported Fe:Co Bimetallic Catalysts for the Hydrogenation of CO*, PhD Thesis, University of the Witwatersrand, Johannesburg, (1994).

57. J.B. Butt, L.H. Schwartz, M. Baerns and R. Malessa, *Ind. Eng. Chem. Prod. Res. Dev,* **23**, 51, (1984).

58. Z. Liu, Y. Li, J. Zhou abd B. Zhang, *J. Chem. Soc. Faraday Trans*., **91**, 3255, (1995).

59. L. Guczi, Z. Schay, K. Matusek and I. Bogyay, *Appl. Catal*., **22**, 289, (1986).

60. F. Stoop and and K. van der Wiele, *Appl. Catal*., **23**, 289, (1986).

61. T. Ishahara, K. Eguchi and H. Arai, *Appl. Catal*, **30**, 225, (1987).

62. C.H. Bartholomew, Edited by Guczi, *New Trends in CO Activation, Studies in Surface Science and Catalysis*, Vol. 64, Ch. 5, 158, (1991).

63. P. Forzatti, G. Buzzi-Ferraris, M. Morbidelli and S. Carrá, *Int. Chem. Eng*., **24(1)**, 60, (1984).

64. J. Oudar, *Chem. Ind*., **20**, 62, (1985).

65. M.E. Dry, J.A.K. du Plessis and G.M. Leuteritz, *J. Catal*., **6**, 194, (1966).

66. J.T. Richardson, *Principles of Catalyst Development*, eds. M.V. Twigg and M.S. Spencer, (Plenum Press, New York, 1989).

67. G. Broyden, T.N. Rhodin, C.F. Brucker, R. Benbow and Z. Hurych, *Surf. Sci*., **59**, 593, (1976).

68. M. Luo, R.J. O'Brien, S. Bao and B.H. Davis, *Appl. Catal*., **239**, 111 – 120, (2003).

69. R.J. O'Brien, L. Xu, R.L. Spicer and B. Davis, in: *Proceedings of the Symposium on Syngas Convesrion to High Value Chemicals Presented at the 211th ACS Annual Meeting*, New Orleans, 24 – 29 March 1996, pp. 252/253.

70. D.B. Bukur, D. Mukesh and S.A. Patel, *Ind. Eng. Chem. Res.*, **29**, 194, (1990).

71. Z.E. Huang, *Journal of Fuel Chemistry and Technology (in Chinese)*, **18**, 143, (1990).

72. X.Z. Wang, *Journal of Fuel Chemistry and Technology (in Chinese)*, **18**, 137, (1990).

73. D.B. Bukur, L. Nowichi, X. Lang, *Energy Fuels*, **9**, 620, (1995).

74. H. Arakawa, A.T. Bell, *IEC Proc. Des. Dev.*, **22,** 97, (1986).

75. A.D. Ronald, A. T. Bell, *J. Catal.*, **97**, 121, (1986).

76. A.F.H. Wielers, G.W. Koebrugge and J.W. Geus, *J. Catal.*, **121**, 376, (1990).

77. R.B. Anderson, in *Catalysis*, (P. H. Emmett, Editor), Vol. 4, p. 1, (Reinhold, Baltimore, 1956).

78. I.E. Wachs, D.J. Dwyer and E. Eglesia, *Appl. Catal.*, **12**, 201, (1984).

79. Deutsches Patentschrift 923127, (1955), Deutsches Patentschrift 937706, (1956).

80. US Patent 644.313, (1975).

81. M.A. Vannice, *Cat. Today*, **12**, 255, (1992).

82. G.S. Sewell, E. van Steen and C.T. O'Connor, *Catalysis Letters*, **37**, 255, (1996).

83. S. Bessell, *Appl. Catal. A: General*, **96**, 253, (1993).

84. H. Brumberger, *J. Catal.*, **92**, 199, (1985).

85. Y.C. Liu, G. L. Griffin, S.S. Chan and I.E. Wachs, *J. Catal.*, **94**, 108, (1985).

86. M.S. Spencer, *J. Catal.*, **93**, 261, (1985).

87. G.L. Haller, et al., *J. Catal.*, **84**, 477, (1983).

88. C. Satterfield, *Heterogeneous Catalysis in Practice*, (McGraw Hill, New York, 1980), 93.

89. M.E. Dry, in: B.E. Leach (Editor), *Applied Industrial Catalysis*, vol. 2, (Academic Press, New York, 1983), 167.

90. C.D. Frohning, in: J. Falbe (Editor), *New Synthesis with Carbon Monoxide,* (Springer-Verlag, New York, 1980), 353.

91. C. Li, *Effect of potassium and copper promoters on reduction behaviour of precipitated iron catalysts*, PhD Thesis, Texas A&M University, (1988).

92. J.L. Rankins and C.H. Bartholomew, *J. Catal*., **100**, 533, (1986).

93. J.A. Dalmon, R. Dutartre, G.A.C.R. Martin, *Acad. Sci.*, Ser. C 287, 557, (1978).

94. N.O. Egiebor and W.C. Cooper, *Can. J. Chem. Eng*., **63**, 81 – 85, (1985).

95. D.B. Bukur, X. Lang, D. Mukesh, W.H. Zimmerman, M.P. Rosynek and C. Li, *Ind. Eng. Chem. Res*., **29**, 1588 – 1599, (1990).

96. R.C. Reuel and C.H. Bartholomew, *J. Catal*., **85**, 78, (1984).

97. T. Yoshoka, J. Koezuka and H. Ikoma, *J. Catal*., **16**, 264, (1970).

98. D. Vanhove, Z. Zhang, L. Makambo and M. Blanchard, *Appl. Catal*., **9**, 327, (1984).

99. D. Yin, W. Li, W. Yang, H. Xiang, Y. Sun, B. Zhong and S. Peng, *Micropor. Mesopor. Mater*., **47**, 16, (2001).

100. C. T. Kresge, M.E. Leonnowicz, W.J. Roth, J.C. Varuli and J.S. Beck, Nature, **359**, 710, (1992).

101. J.S. Beck, J.C. Vartuli, W.J. Roth, M.E. Leonnowicz, C.T. Kresge, K.D. Schmitt, C.T. Chu, D.H. Oslon, E.W. Sheppard, S.B. McCullen, J.B. Higginsand J.L. Schlemker, *J. Am. Chem. Soc*., **114**, 10834, (1992).

102. X.S. Zhao, G.Q. Lu and G.J. Miller, *Ind. Eng. Chem. Res*., **35**, 2075, (1996).

103. J. Panpranot, J.G. Goodwin and A. Sayari, *J. Catal*., **211**, 530, (2002).

104. J. Panpranot, J.G. Goodwin and A. Sayari, *Catal. Today*, **269**, (2002).

105. A. Corma, V. Martines and V. Soria, *J. Catal*., **169**, 480, (1997).

106. C. Song and K.M. Reddy, *Appl. Catal. A*, **176**, 1, (1999).

107. F. Schuth, A. Wingen and J. Sauer, *Microporous Mesoporuos Mater.*, **44 - 45**, 465, (2001).

108. K. Sapag, S. Rojas, M. López Granados, J.L.G. Fierro and S. Mendioroz, *J. Molecular Catal. A: Chem*., **167**, 81 – 89, (2001).

109. N.O. Egiebor, W.C. Cooper and B.W. Wojciechowski, *Appl. Catal*., **55**, 47, (1989).

110. S. Bessell, *Appl. Catal. A*, **126**, 235, (1995).

111. A.T. Bell, *Cat. Rev. Sci. Eng*., **23 (1 & 2)**, 203, (1981).

112. B.W. Wojciechowski, *Cat. Rev. Sci. Eng*., **30(4)**, 629, (1988).

113. M.P. Kamisky, N. Winograd, G.L.Geoffroy and M.A. Vannice, *J. Am Chem. Soc*., **108**, 1315, (1986).

114. F. Fischer and H. Tropsch, *Brennstoff Chem*., **7**, 97, (1926).

115. P. Biloen, J.N. Helle and W.M.H Bennet, *J. Catal*., **58**, 95, (1979).

116. R.C. Brady III and R.J. Pettit, *J. Am. Chem. Soc*., **102**, 6181, (1981).

117. R.C. Brady III and R.J. Pettit, *J. Am. Chem. Soc*.,**103**, 1287, (1881).

118. H.C. Long, M.L. Turner, P. Fornasiero, J. Kăspar, M. Graziani and P.M. Maitlis, *J. Catal.*, **167**, 172-179, (1997).

119. P.M. Maitlis, R. Quyoum, H.C. Long and M.L. Turner, *Appl. Catal. A: General*, **186**, 363-374, (1999).

120. L.E. McCandlish, *J. Catal*., **83**, 362, (1983).

121. R.W. Joyner, *Catal. Lett*., **1**, 307, (1988).

122. M.L. Turner, H.C. Long, A. Shenton, P.K. Byers and P.M. Maitlis, *Chem. Eur. J*., **1***,* 549, (1995).

123. P.M. Maitlis, H.C. Long, R. Quyoum, M.L. Turner and Z. Q. Wang, *J. Chem. Soc., Chem. Commun.,* **1**, (1996).

124. B. Shi and B.H. Davis, *Catal. Today*, **58**, 255 – 261, (2000).

125. S.B. Ndlovu, N.S. Phala, M. Hearshaw-Timme, P. Beagly, J.R. Moss, M. Claeys and E. van Steen, *Catal. Today*, **71**, 343 – 349, (2002).

126. D.B. Bukur, L. Mukesh and X. Lang, *Chem. Eng. Sci*., **49**, 4615, (1990).

CHAPTER SIX

EXPERIMENTAL METHOD

6.1 Introduction

The Fischer-Tropsch (F-T) reaction system is possibly one of the most complex reaction systems that can be studied due to the large number of products that are formed. It is known that a large variety of factors influence both the activity and selectivity of catalysts in this system. There are a large number of experimental techniques that may be used to examine both the catalysts and their activity in the F-T system.

The catalysts prepared in this study were tested in a plug flow reactor system. Various techniques were used to characterize the catalysts and to correlate and quantify the physical properties with the observed catalyst selectivities and activities.

This chapter describes both the synthesis and characterization of a series of silica-supported iron catalysts.

6.2 Materials and Chemicals Used

The chemicals and gases that were used for the synthesis and characterisation of the catalysts are detailed below.

6.2.1 Support

The silica supports used in this study were synthesized by the templated sol-gel method that was described in the first part of this thesis. The hollow spheres were obtained when citric acid was used as a template (at 70 ºC) while the hollow nanotubes were obtained when DL-tartaric acid was used as a template at 0 ºC. Stöber/closed spheres were obtained when no template was used.

A Ruhrchemie[1] catalyst, where the silica source was produced from potassium silicate, was studied to permit comparison of the new catalysts with a known catalyst standard.

6.2.2 Metals

Ferric nitrate ($Fe(NO_3)_3.9H_2O$, Saarchem), cupric nitrate ($Cu(NO_3)_2$ Saarchem) and potassium nitrate (KNO_3, ACE chemicals) were used as sources of iron, copper and potassium respectively. The precipitating agent used was anhydrous sodium carbonate (Na_2CO_3, Labchem).

6.2.3 Gases

All the gases used were supplied by African Oxygen (AFROX). The gases used for the BET surface area determination and catalyst reduction prior to

the F-T synthesis were Ultra High Purity (UHP) grade gases (>99.997% purity). The synthesis gas used in the reactor experimental runs was a pre-mixed gas (from Afrox) with a composition of 10 % Ar, 30% CO and 60% H_2. Dry air, UHP hydrogen and wet CO_2 (for cooling the column to –30 ºC) were used in the gas chromatograph (G.C).

6.3 Catalyst Preparation

In preparing the precipitate, 300 ml of 0.716 M $Fe(NO_3)_3.9H_2O$ and 100 ml of 0.0314 M $Cu(NO_3)_2$ (both at 80 ºC) were added to a vigorously strirred solution containing 600 ml Na_2CO_3 (0.7 M solution) also at 80 ºC. The precipitation was stopped at pH 6.9. The experimental set-up is shown in Figure 6.1. After aging, the precipitate was washed by successive centrifugation steps, the pellet being re-suspended in deionised water between washings. The washing was stopped once the conductivity of the supernatant was less than 200 µS (a Siemens conductometer was used). The iron-copper slurry was then mixed with the SiO_2-KNO_3* slurry. In the case of the Ruhrchemie catalyst an appropriate amount of dilute potassium silicate solution was added to an iron-copper paste. The catalysts were dried overnight at 120 ºC in a fan oven. After drying, the resulting solids were crushed and sieved and particles between 850 – 1180 µm were collected.

*The types of silica used were hollow spheres, hollow nanotubes and Stöber/closed spheres.

The catalysts were prepared such that at the end the nominal compositions were:

(i) 9% SiO_2/ 83% Fe/ 4% Cu/ 4% K

(ii) 18% SiO_2/ 74% Fe/ 4% Cu/ 4% K

(iii) 27% SiO_2/ 65% Fe/ 4% Cu/ 4% K

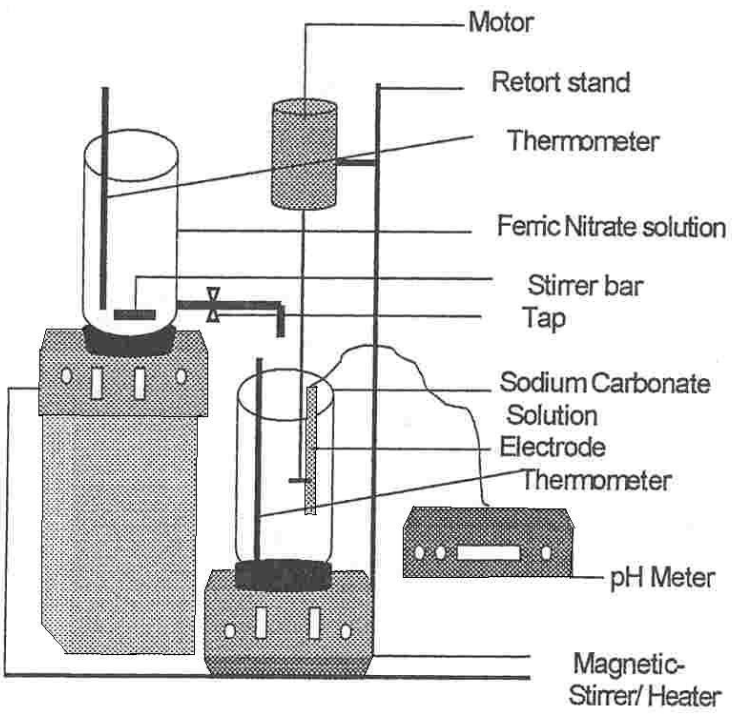

Figure 6.1. Experimental set-up used for the precipitation of the iron catalyst.[2]

6.4 Reactor System

The catalysts were evaluated for F-T activity in three plug flow reactors. The products were analysed using a shared on-line G.C. (C_1 – C_9) together with an off-line G.C. (C_7 – C_{30}).

The plug flow reactor (PFR) system is shown in Figure 6.2 and is similar to that used by Duvenhage.[3] A series of on/off valves are used to feed air, hydrogen or synthesis gas to the system. The pressure of the system was set using the feed gas regulators.

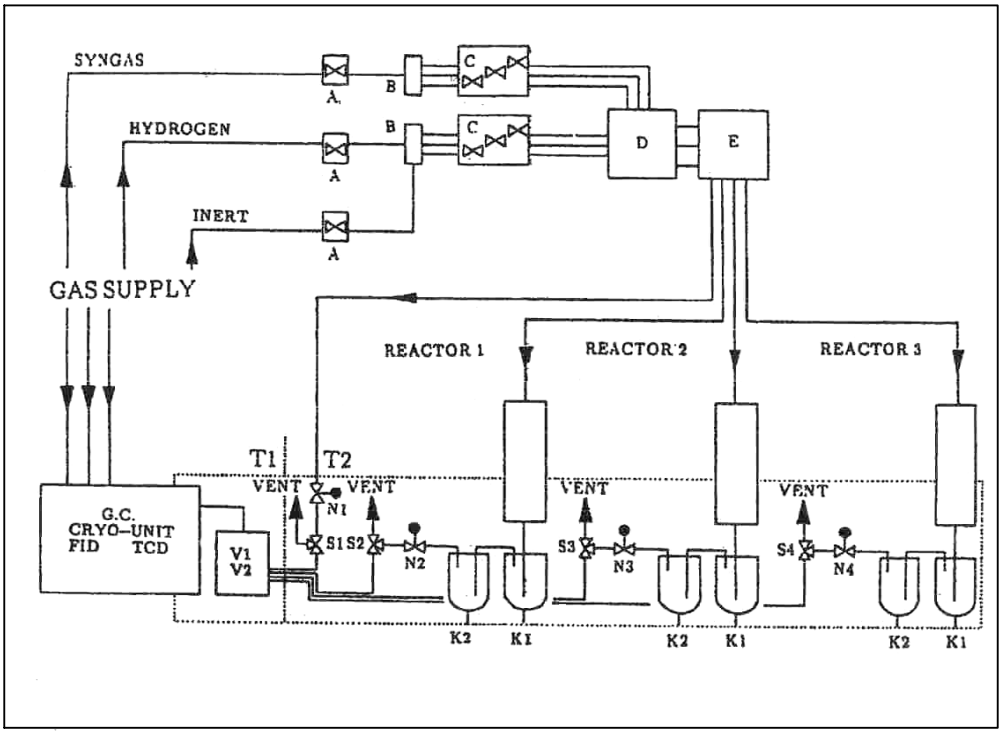

A Pressure regulator; B Manifold; C Shut-off valve; D Manifold; E Gas mixing; F Flow indicator; K1 Wax knockout (120 ˚C); K2 Liquid knockout (25 ˚C); N Needle valve; P Pressure indicator; S Selection valve; T1 Valve **box at 170 ˚C; T2 Product lines at 170 ˚C; V1 10 port valve; V2 6 port valve**

Figure 6.2. The plug flow reactor system configuration.[3]

The three plug flow reactors were run in parallel with the supply gases being split in a manifold that directed the gases to each reactor. In addition, a bypass line was present that bypassed syngas through a solenoid valve that allowed the analysis of the feed.

The plug flow reactor design is shown in Figure 6.3 and is similar to that described by Snel.[4] In the reactor, there are three zones, the pre-heating zone where the gas is heated to the reaction temperature, the reactor bed and the region below the catalyst bed. The feed gas entered through the top of the reactor and then flowed through the catalyst bed.

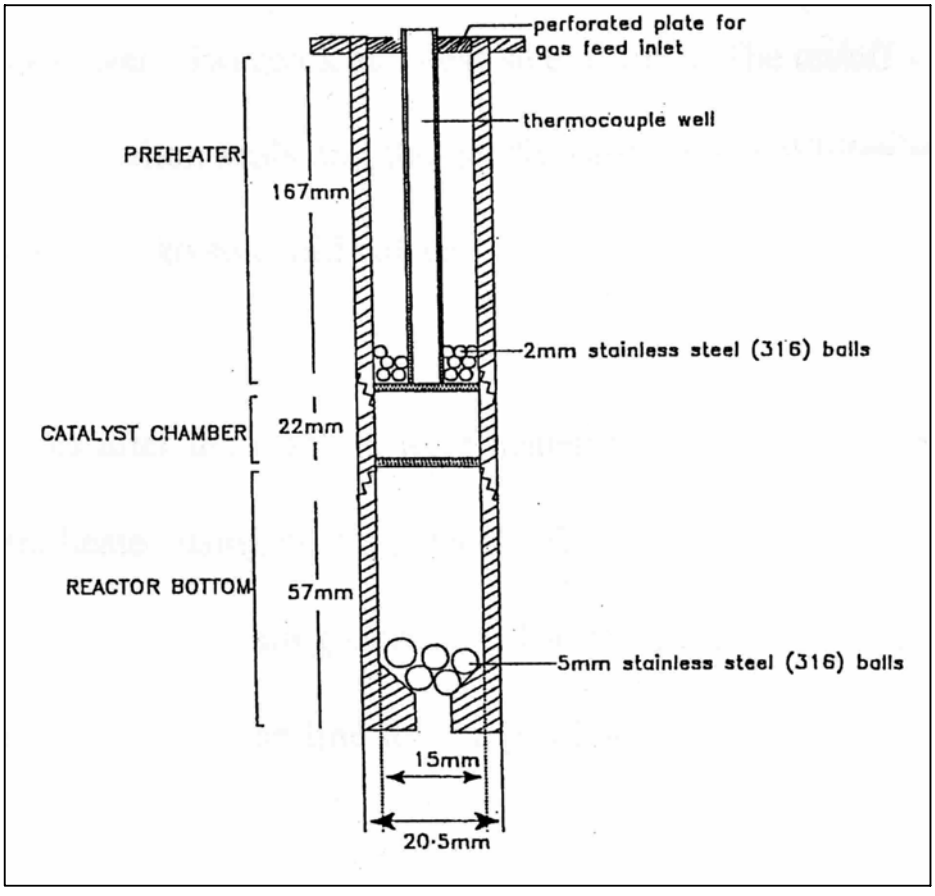

Figure 6.3. The plug flow reactor.[5]

Two knockout pots were placed below the reactor bed. The first, kept at approximately 150 °C, was used to collect the wax fraction. The second, kept at ambient temperature, was used to collect the water and liquid oil fraction.

A needle valve was installed after the knockout pots and was used to control the volumetric flow through the reactor and also to maintain a backpressure in the system. The flow-rate through the reactor was measured using soap bubble meters. Two solenoid valves were placed in the line after this valve. The solenoid valves were run in such a way that when the one was open the other was closed. In this way, the gaseous product from the reactor was directed either to the G.C. for analysis or vented to atmosphere. These valves were connected to the timers that automated the sampling of the gaseous sample. Each sample was analysed individually and the system automatically cycled between the reactors and the feed. All the lines used in the system were 1/4" or 1/8" stainless steel tubing and the fittings used were Swagelok stainless steel fittings. The on/off valves were SS Valco valves with viton seals and the needle valves were Whitey valves. The selection valves were Usko solenoid valves.

All the lines after the reactors were heated at 150 ºC using a heating tape. The reactors were heated using heating jackets. RKC Rex-C100 P.I.D. controllers were used to control all the heating elements. The controlling thermocouples were placed between the tape and the line for the gas lines, and inside the catalyst bed for the reactors.

6.5 Fischer-Tropsch Synthesis

The catalysts were first calcined at 400 ºC for 16 hours in an oven (i.e. *ex-situ*). They were pressed and crushed to sizes between 1180 – 850 µm. In all cases 2 ml of catalyst was loaded into each plug flow reactor. The system was pressurised and left for a few hours. If a pressure drop was observed, a leak in the system was indicated which was then rectified. The catalyst was then reduced in UHP hydrogen at 400 ºC and a GHSV of 500 hr^{-1}, at 1 bar for 16 hours.

After reduction, the reactors were cooled to 250 °C, checked for leaks and the synthesis gas was introduced to the system at a GHSV of 400 hr^{-1} and a pressure of 8 bar. Synthesis was performed for a stabilisation period of 120 hours after which the mass balance period was started. The mass balance had a duration of approximately 120 hours. Throughout this period, the selectivity and conversion analysis was performed as described in the product analysis section.

6.5.1 Product Analysis

The analysis of the product spectrum was divided into two parts. The first part entailed the on-line analysis of the gaseous product and the second part entailed the off-line analysis of liquid and wax samples.

The vapour product from each reactor was sequentially analysed. The samples were directed to the dedicated G.C. as described earlier. The product streams to be analysed were sampled and directed to the relevant column

using the sample valve configuration similar to that described by Duvenhage[3]. A ten-port valve fed the sample to the Thermal Conductivity detector (TCD) side of the analysis whilst a six-port valve was used to feed the sample to the Flame Ionisation Detector (FID) side of the system. A TCD detector connected to a 2 m carbosieve IIS column was used to simultaneously analyse the sample for argon, carbon monoxide and carbon dioxide. A typical TCD trace is shown in Figure 6.4. A FID connected to a 2 m PPQ column was used to analyse the hydrocarbons from the vapour product (from C_1 up to C_9). A typical product trace is shown in Figure 6.5.

During the mass balance period the PPQ column was replaced with a 25 m SPB1 megabore capillary column. This column allowed the separation of paraffin and olefin fractions and permitted the determination of the paraffin to olefin ratios when the G.C. was operated in cryogenic mode (starting temperature -30 ºC). A G.C. trace is shown in Figure 6.6.

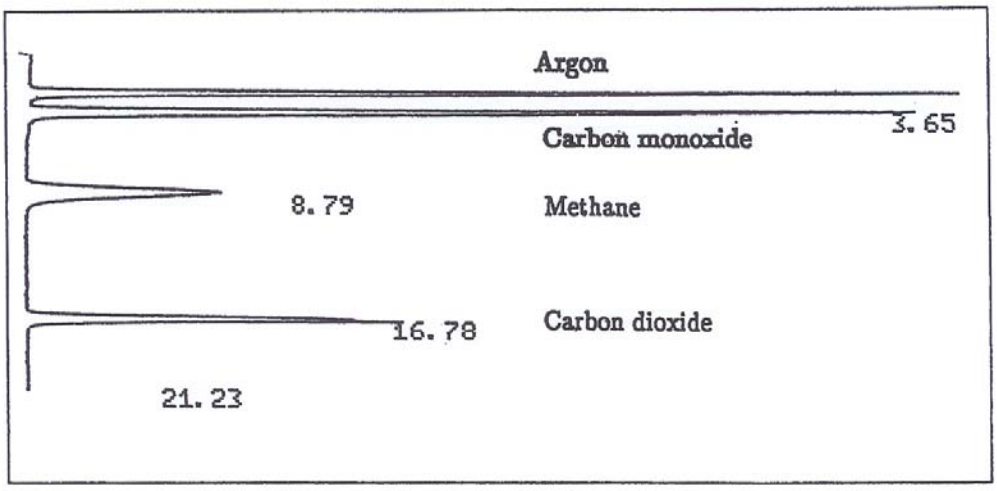

Figure 6.4. A typical spectrum using a TCD and a Carbosieve IIS column.

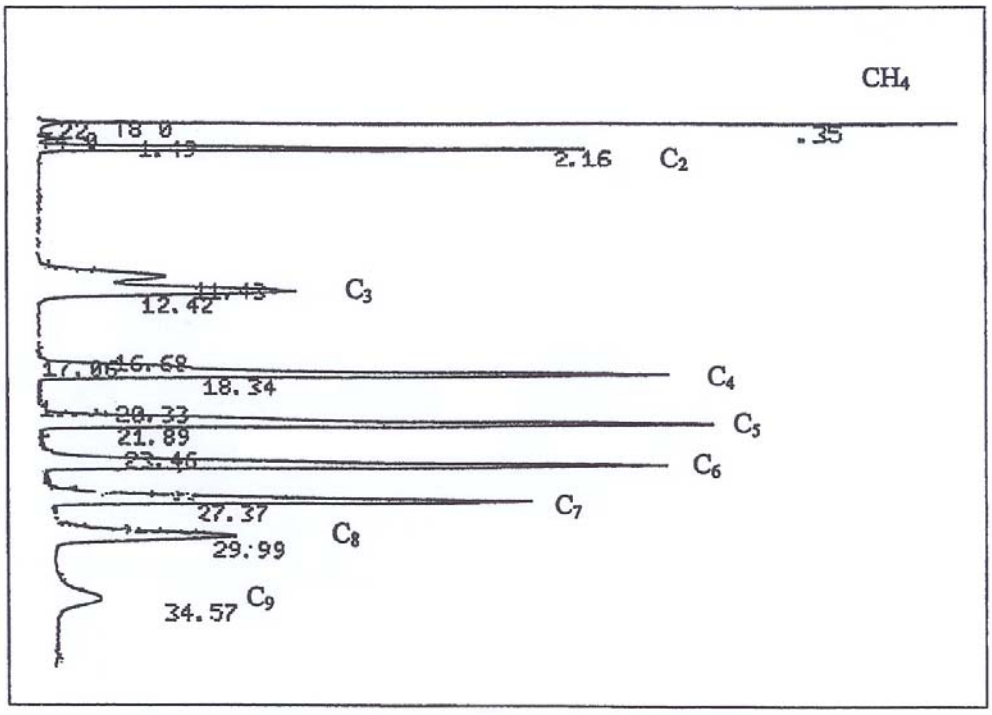

Figure 6.5. The hydrocarbon separation using a Porapak Q column.

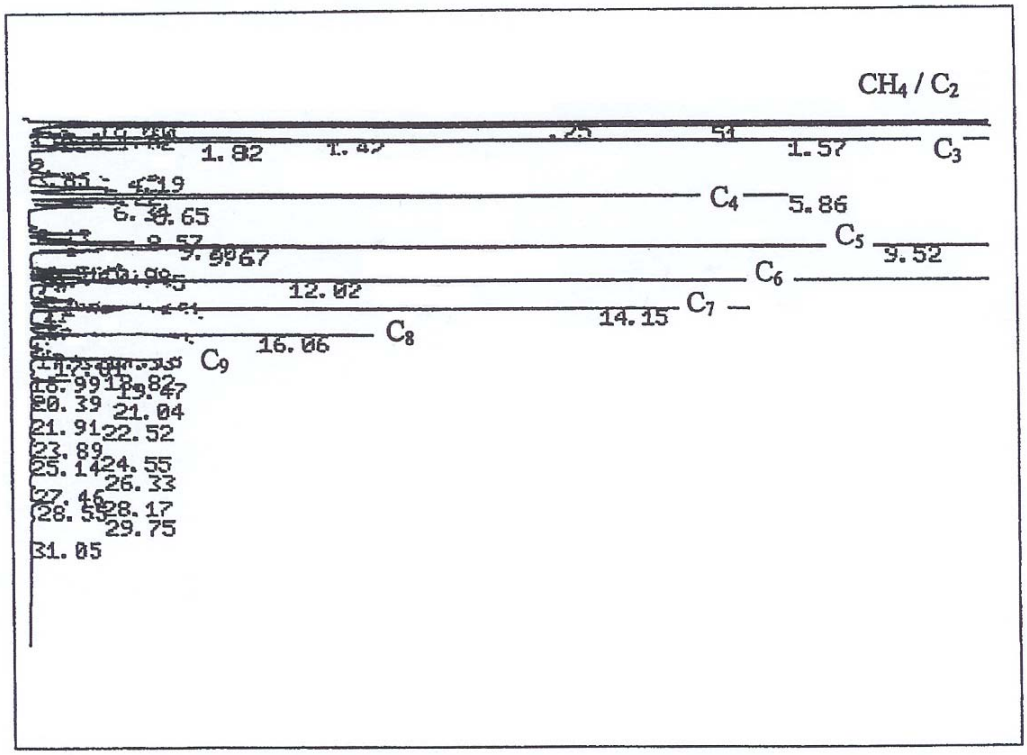

Figure 6.6. The separation obtained using a BP1 Megabore capillary column.

The actuated 6 port and 10 port valves were controlled using a Varian Sp 4200 integrator and the data was collected using the same integrator.

The off-line analysis of the wax and liquid fractions was performed in a G.C. equipped with a SPB5 column connected to a FID.

6.5.2 Mass Balance Calculations

The calculations used to determine the mass balance are similar to those used by Nijs et al.,[6] Duvenhage[3], Price[5] and Chronis.[7] The mass balance was performed on carbon and the analysis was carried out as follows:

The TCD and FID data for the gaseous products were converted to data that gave the composition by mole of the product. A calibration gas containing hydrogen, carbon monoxide, carbon dioxide, methane, ethane and ethylene was used to calibrate the TCD and FID data. Response factors were obtained from Deitz[8] and converted to allow calculation of molar compositions for the different components using the method described by Scanlon.[9] The equation then used to determine the molar composition is given below:

$$X_{HC,i} = \frac{A_{HC,i}\, RF_i\, X_{C2,cal}}{A_{C2,cal}} \qquad (6.1)$$

where $X_{HC,I}$ is the mole fraction of the ith hydrocarbon, $X_{C2,cal}$ is the mole fraction of the C2 hydrocarbon in the calibration gas, $A_{HC,I}$ is the area of the ith hydrocarbon, $A_{C2,cal}$ is the area of the relevant C2 hydrocarbon and RF_i is the response factor of the ith hydrocarbon. The area from a G.C. trace, for ethane in the calibration gas was used to calibrate for alkanes and similarly that of ethene in the calibration gas was used to calibrate for the olefins.

This molar composition thus obtained could then be used to determine the number of carbon atoms in the vapour product stream. The masses of product for the wax and liquid fraction were determined in the same way and added to the gaseous product breakdown to give the product spectrum for a catalytic reaction. The response factors of the liquid and wax stream components were taken to be one. The mass fraction of each component is thus determined by

dividing its peak area by the total of all the peak areas combined. In this way the number of carbon atoms in the two off-line streams could be determined.

The carbon monoxide conversion was determined using equation 6.2.

$$\text{Conversion} = \frac{CO_{in} - (CO_{out} \; x \; Ar_{in}/Ar_{out})}{CO_{in}} \; x \; 100\% \qquad (6.2)$$

where CO_{in} is the area of the CO peak in the feed, CO_{out} is the area of the CO peak in the gaseous product stream, Ar_{in} is the area of the argon peak in the feed and Ar_{out} is the area of the argon peak in the product stream.

As no mass flow controllers were used, the gas flow into the reactor had to be determined by a mass balance of argon. The equation to determine the flow-rate into the reactor in terms of the outlet flow-rate is present in the equation 6.3.

$$F_{in} = F_{out} \; x \; Ar_{out}/Ar_{in} \qquad (6.3)$$

where F_{in} and F_{out} are the gas flow-rates into and out of the reactor in ml/s.

Once the composition of all streams, both on-line and off-line, had been determined, it was a relatively simple task to determine the mass balance on carbon. Additional information required for this task was the composition and

flow of the inlet stream as well as the flow of the product stream and the total time for the mass balance was determined using equation 6.4.

$$\% \text{ Mole Balance} = \frac{(M_{CO,in} - M_{C,vap} - M_{C,oil} - M_{C,wax} - M_{CO,out} - M_{CO_2})}{M_{CO,in}} \quad (6.4)$$

where M refers to the total moles of carbon atoms in that category for the mass balance period. CO in the subscript refers to carbon monoxide, C to carbon and CO_2 to carbon dioxide.

Carbon atoms that enter the reactor must equal the sum of carbon atoms (reactant and product) that exit from the reactor. Inaccuracy in the mass balance is expected so a mass balance of 100 ± 5% was deemed as acceptable.

The product distributions were calculated using equation 6.5. which represents the selectivity of the reaction to a specific component.

$$S_i = m_i/\sum m_n \quad (6.5)$$

where S_i is the mass fraction of component i and m_i is the mass of component i.

The Schulz-Flory parameter was obtained by performing a least squares fit on a Schulz-Flory plot of the gaseous product. Equation 6.6 was fitted with the exponential of the slope giving the required parameter.

$$\ln(W_n/n) = n\ln(\alpha) + \ln((1 - \alpha)^2/ \alpha) \quad (6.6)$$

where W_n is the mass fraction of the hydrocarbon with n carbon units and α is the Shultz-Flory parameter.

The olefinity of products was defined by the olefin to paraffin ratio:

$$[(m_{olefin})/m_{olefin} + m_{paraffin})] \; x \; 100 \quad (6.7)$$

for carbon numbers greater than two.

6.6 Catalyst Characterization

6.6.1 BET Surface Area Measurement

The BET surface area of the catalysts was measured using an ASAP 2010 Porosimeter. The sample was degassed overnight at 120 °C under vacuum prior to analysis. The surface area was then determined at liquid nitrogen temperature.[9]

6.6.2 Temperature Programmed Reduction (TPR)

The TPR apparatus used was the same as that used by Duvenhage.[2] The catalyst (50 mg) was loaded into a quartz U tube that was heated using a furnace. Initially, the catalyst was heated in a nitrogen atmosphere at 150 °C for half an hour. This was done to remove H_2O from the catalyst. The catalyst was then heated to 800 °C at 10 °C per minute under flowing hydrogen (5%

H_2/N_2 mixture) in a quartz U-tube. The various reduction steps were recorded using a low temperature dual filament thermal conductivity detector.

6.6.3 Transmission Electron Microscopy

Transmission electron microscopy images were observed with JEOL-100S and JEOL-2010 electron microscopes. Samples for TEM analysis were prepared by sonicating about 1 mg sample into 1 ml ethanol for at least 4 minutes. A few drops of the suspension were added to a holey Cu grid coated with a carbon film (made in the Wits Electron Microscope Unit or purchased from Ted Pella Inc, USA).

6.6.4 Mössbauer Spectroscopy

The Mössbauer experiments were performed with a 50 mCi ^{57}Co source in a rhodium matrix. The analyses were performed at approximately 25 ºC with the catalysts still in the wax medium to prevent re-oxidation. The data was analysed using a least-square fitting routine that models the spectra as a combination of quadruple doublets and sextuplets based on a Lorentzian line-shape profile. The spectral components were identified based on their isomeric shift (IS), quadruple splitting (QS) and hyperfine magnetic field (B_{hf}). The isomeric shift values are reported relative to metallic iron (α-Fe) and the iron content of each phase is determined from their relative peak areas, assuming that these phases have similar recoil free fraction (*f*).

6.7 References

1. C.D. Frohning, Fischer-Tropsch-Synthese, Chemierohstoffe aus Kohle, (J. Falbe, ed.), Stuttgart:Thieme, (1977).
2. K.L. Revombo, *The Synthesis, Characterization and Catalytic Behaviour of Precipitated Iron Catalysts Containing Sulphur*, MSc Dissertation, University of the Witwatersrand, Johannesburg, (2001).
3. D.J. Duvenhage, *The Preparation, Characterisation and Evaluation of Titania Supported Fe:Co Bimetallic Catalysts for the Hydrogenation of CO*, PhD Thesis, University of the Witwatersrand, Johannesburg, (1994).
4. R. Snel, *Chemica Scripta*, **20,** 99, (1982).
5. J.G. Price, *An Investigation into Novel Bimetallic Catalysts For Use in the Fischer-Tropsch Reaction*, PhD Thesis, University of the Witwatersrand, Johannesburg, (1994).
6. H.H. Nijs and P. A. Jacobs, *J. Chronm. Sci*., **19 (1)**, 40, (1981).
7. T. Chronis, *A Fischer-Tropsch Study of Co/Ru Catalysts*, PhD Thesis, University of the Witwatersrand, Johannesburg, (1999).
8. W.A. Deitz, *J. Gas Chrom*., Feb, 62, (1967).
9. J.T. Scanlon and D.E. Willis., *J. Chrom. Sci*., **23**, 333, (1985).
10. G. Leofanti, M. Padovan, G. Tozolla and B. Venturelli, *Cat. Today*, **41**, 207, (1998).

CHAPTER SEVEN

SILICA WITH VARIOUS MORPHOLOGIES AS A BINDER / SUPPORT FOR IRON FISCHER-TROPSCH CATALYSTS

7.1 Introduction

Fischer-Tropsch synthesis (FTS) is recognized as a viable route for the conversion of syngas (derived from coal or natural gas) to liquid fuels and chemicals.[1] The use of an iron-based catalyst is attractive due to its FTS activity as well as its water-gas shift reactivity, which helps make up the deficit H_2 in the syngas from modern energy efficient coal gasifiers.[2] One major limitation relating to iron-based catalysts is that they tend to undergo attrition during use.[3] Therefore a catalyst support/binder is an essential structural additive for iron-based FTS catalysts to improve catalyst attrition resistance and the aging characteristics of the catalyst. The support may also have significant effects on the catalyst activity and selectivity due to strong metal-support interactions.[4,5]

$Fe/Cu/K_2O/SiO_2$ catalysts have been used as commercial catalysts in the Fischer-Tropsch reaction. Silica was used as it is reported to be the best support in terms of both activity and selectivity.[4,5] Also from the studies that

have been carried out, it is believed that the addition of silica improves the stability of the catalysts because it stabilises the iron crystallites during synthesis and also reduces the surface basicity of the catalysts. (A detailed description of the role of silica in silica supported catalysts is given in Chapter 5). So far the studies that have been carried out on these catalysts relate to silica in the amorphous spherical form.[2,5-13] (Conventional or traditional silica supports are known to have a spherical shape).

The effect of support and its porosity on F-T reaction rate and hydrocarbon selectivities still remains unclear. Mass transport limitations for carbon monoxide and hydrocarbons in the catalyst pores, pore filling and condensation of heavier hydrocarbons, different adsorption properties of metal particles located in narrow and wide pores are often employed to explain the effect of pore size on F-T reaction rates and selectivities.[14] Anderson *et al*.[15] for example, attributed the observed increase in methane selectivity with decreasing average pore diameter to mass transport phenomenon. It was suggested that the greater rate of diffusion of hydrogen inside pores filled with liquid products compared to that of carbon monoxide caused an increase in H_2/CO ratio in catalyst pores, and thus, a shift toward formation of lighter hydrocarbons. Lapszewicz *et al*.[16] showed that variation of product distribution as a function of catalyst pore diameter could be the result of changing adsorption patterns of hydrogen and carbon monoxide rather than mass transfer phenomenon. Vanhove *et al*.[17] found that textural properties of cobalt catalysts supported by alumina could modify the chain length of hydrocarbons. The effect was assigned to different residence times of

hydrocarbons in alumina pores due to pore condensation and filling. Ernst *et al*.[18] studied the F-T activity and selectivity of Co/SiO_2 catalysts prepared by a pseudo sol-gel technique in acid and base media. The activity for CO hydrogenation was found to increase with the specific surface area, and the selectivity for heavy hydrocarbons was favoured in the case of a catalyst with the pore diameter of a support less than 4 nm. Thus, even for the same kind of support, the surface properties and pore size were crucial for the chain growth and product distribution in F-T synthesis.

Since traditional mesoporous silica materials are irregularly spaced and their pore sizes are broadly distributed, it is rather difficult to establish in which pores Fischer-Tropsch synthesis takes place. Moreover, at F-T reaction conditions the products, wax and carbon deposits could easily block a part of the catalyst pores making them unavailable for reacting molecules. Recently it has been reported in the literature that silica with various shapes and sizes (e.g. spherical, tubular, porous and non-porous, mesoporous, etc.) can be synthesized.[19] (Indeed the first part of this thesis described the synthesis of these types of silica). These new types of silicas can be considered as model supports, which allow the effect of pore size and shape on catalytic behaviour of supported catalysts to be studied.

This chapter looks at the effect of silica type (i.e. hollow nanotubes, hollow and closed spheres) and Fe content on $Fe/Cu/K_2O/SiO_2$ catalyst activity and selectivity. It is expected that the size and geometry of the support will influence the final distribution of the catalyst, which in turn will affect the

activity and selectivity of the catalyst. The role of silica interactions will be studied by keeping the Cu and K loading constant and by only varying the Si (and Fe) content. A Ruhrchemie catalyst was also studied to permit comparison of the new catalysts with a known catalyst standard.

7.2 Experimental Procedure

7.2.1 Catalyst Synthesis

- The silica support/binder was first prepared by the templated sol-gel method. (Synthesis with DL-tartaric acid at 0 °C gave hollow nanotubes while synthesis with citric acid at 75 °C gave hollow spheres and synthesis without any template gave closed (Stöber) spheres). The reader is referred to Chapters 2 and 3 for a detailed description of the preparation method.
- Then $Fe(NO_3)_3.9H_2O$ and $Cu(NO_3)_2$ were precipitated at 80 °C, with sodium carbonate as a precipitating agent. A detailed catalyst preparation method is given in Chapter 6.
- The Fe-Cu slurry was mixed with a SiO_2-KNO_3* slurry. In the case of the Ruhrchemie catalyst an appropriate amount of dilute potassium silicate solution was added to an iron-copper paste.
- The resulting mixture was dried in an oven, and then calcined at 400 °C for 16 hours.
- The catalysts were pressed, crushed and sieved and the sizes between 850 and 1180 μm were collected.

*The types of silica used were hollow spheres, hollow nanotubes and Stöber/closed spheres.

The catalysts were prepared such that at the end the nominal compositions for each of the catalyst types were:

(i) 9% SiO_2/ 83% Fe/ 4% Cu/ 4% K

(ii) 18% SiO_2/ 74% Fe/ 4% Cu/ 4% K

(iii) 27% SiO_2/ 65% Fe/ 4% Cu/ 4% K

Throughout the chapter the 12 catalysts will be abbreviated for simplicity as follows:

- 9% SiO_2 (Ruhrchemie)/ 83% Fe/ 4% Cu/ 4% K – 9Ruhr
- 9% SiO_2 (Nanotubes)/ 83% Fe/ 4% Cu/ 4% K – 9Nano
- 9% SiO_2 (Stöber spheres)/ 83% Fe/ 4% Cu/ 4% K – 9Stob
- 9% SiO_2 (Hollow spheres)/ 83% Fe/ 4% Cu/ 4% K – 9Holo
- 18% SiO_2 (Ruhrchemie)/ 74% Fe/ 4% Cu/ 4% K – 18Ruhr
- 18% SiO_2 (Nanotubes)/ 74% Fe/ 4% Cu/ 4% K – 18Nano
- 18% SiO_2 (Stöber spheres)/ 74% Fe/ 4% Cu/ 4% K – 18Stob
- 18% SiO_2 (Hollow spheres)/ 74% Fe/ 4% Cu/ 4% K – 18Holo
- 27% SiO_2 (Ruhrchemie)/ 65% Fe/ 4% Cu/ 4% K – 27Ruhr
- 27% SiO_2 (Nanotubes)/ 65% Fe/ 4% Cu/ 4% K – 27Nano
- 27% SiO_2 (Stöber spheres)/ 65% Fe/ 4% Cu/ 4% K – 27Stob
- 27% SiO_2 (Hollow spheres)/ 65% Fe/ 4% Cu/ 4% K – 27Holo

7.2.2 Catalyst Characterization

The catalysts were characterized using BET surface area analysis, Temperature Programmed Reduction (TPR), Mössbauer Spectroscopy and Transmission Electron Microscopy (TEM) as described in Chapter 6.

7.2.3 Catalyst Evaluation

The catalysts were evaluated for F-T activity in a system of three stainless steel plug flow reactors (see Chapter 6 for details). A 2 ml (~1.5 g) charge of catalyst was loaded and tested in each of the reactors.

The catalysts were reduced in flowing hydrogen at 400 °C for 16 hours at a GHSV of 500 h^{-1} and a pressure of 1 bar. After reduction, the system was allowed to cool to 250 °C and the synthesis gas (60% H_2, 30% CO, 10% Ar) was introduced at a pressure of 8 bar. The GHSV was set at 400 h^{-1}. The gas flowrates were controlled using needle valves. The GHSV tended to vary by around 10%. The catalysts were initially allowed to achieve steady state over a period of 120 h followed by a 100 – 120 h mass balance period. The data recorded was analysed as described in Chapter 6.

7.3 Results and Discussion

7.3.1 BET Surface Area Analysis

The determination of surface area is considered to be an important requirement in catalyst characterization, although the catalytic activity may only be indirectly related to this "total" surface area.[20] In addition it is usually necessary to specify the pore structure since this may control the transport of the reactants and products of a catalytic reaction in this case the Fischer-Tropsch reaction.

The BET surface areas of as-prepared and calcined samples are listed in Table 7.1. As expected the surface areas of all the catalyst samples

decreased after calcination. This is caused by the collapse of pore structure due to removal of water of hydration from the highly porous $FeOOH/Fe_2O_3$ structure. The pore volume and diameter did not change substantially after calcination. The introduction of SiO_2 to the pores of the precipitate provided a rigid matrix that helped to prevent complete collapse of the original pore structure, during thermal treatment. (In general, the addition of silica to iron FT catalysts is known to improve the stability of the porous iron oxide / hydroxide network)[5]

The Ruhrchemie catalyst was found to have the highest surface area compared to the other catalysts (i.e. catalysts supported on nanotubes, Stöber spheres and hollow spheres). The catalysts with the composition of 18% SiO_2 had the highest surface areas in each category of silica used. In general a catalyst with a high surface area is a better catalyst because the metal is better dispersed onto the support. It is thus expected that the 18% silica catalyst for each silica type will perform better than the other catalysts.

From the observed surface area results, a proposed model explaining the structure of the catalysts is shown by pictures in Figures 7.1 a, b and c. In the 9% SiO_2 catalysts the iron particles are not well dispersed and hence pore blockage occurs which results in lower surface areas than in the other catalysts. The 18% SiO_2 catalysts have higher surface areas because the iron particles are well dispersed onto the supports and therefore not blocking the pores. It would have been expected that the 27% SiO_2 catalysts will have

higher surface areas than the 18% SiO_2 catalysts but that was not observed in the data.

Iron particles also contribute to the total surface area and if the iron particles are small they will have a larger effect on the surface area compared to when the particles are big.

a)

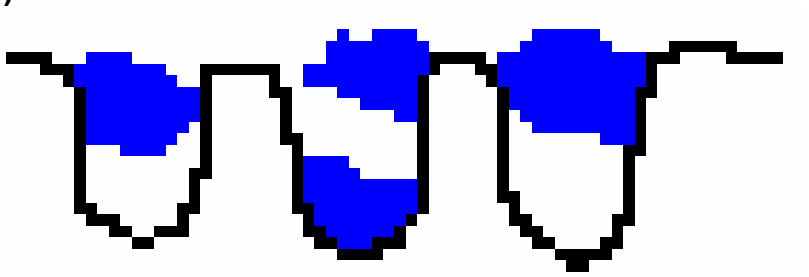

b)

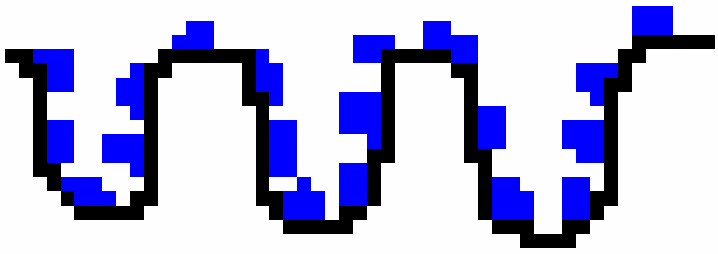

c)

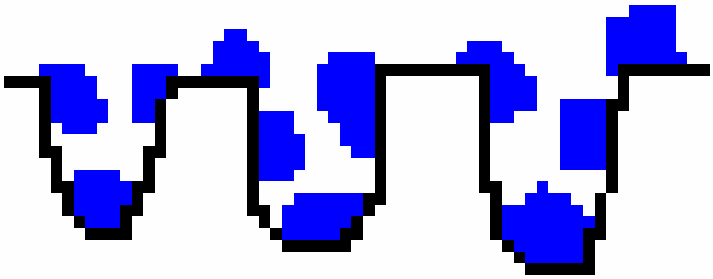

Figure 7.1. The proposed structure of a) 9% SiO_2, b) 18% SiO_2, c) 27% SiO_2 catalysts

Table 7.1. BET results of catalysts

Sample	As prepared			Calcined*		
	BET Surface Area (m^2/g)	Pore Volume (cm^3/g)	Pore Diameter (nm)	BET Surface Area (m^2/g)	Pore Volume (cm^3/g)	Pore Diameter (nm)
9Ruhr	130.4	0.42	10.2	106.7	0.45	14.3
9Stob	40.1	0.09	7.8	19.9	0.11	9.3
9Holo	43.7	0.10	8.7	22.9	0.14	11.2
9Nano	30.6	0.08	11.5	17.1	0.10	16.4
18Ruhr	179.2	0.48	8.5	142.6	0.51	12.3
18Stob	128.9	0.19	4.9	99.5	0.22	6.7
18Holo	86.5	0.10	5.3	56.2	0.15	7.9
18Nano	75.3	0.11	6.8	45.8	0.15	9.0
27Ruhr	161.3	0.41	8.1	128.8	0.45	11.6
27Stob	56.4	0.24	5.2	28.8	0.29	6.9
27Holo	39.7	0.16	4.3	17.5	0.20	5.4
27Nano	29.8	0.17	4.9	15.6	0.20	6.6

*Calcined at 400 °C for 16 hours

7.3.2 Temperature Programmed Reduction (TPR) Study

TPR is a powerful tool to trace the reduction of the oxide phases, it also provides information about the metal dispersion and metal-support interaction. For bulk oxides an increase in T_m (temperature at maximum) is expected with increasing particle size, whereas for supported metal oxides reduction may be hindered or promoted depending on the nature of the interaction between the oxide and support.[21]

The reduction of bulk hematite (α-Fe_2O_3) proceeds via magnetite (Fe_3O_4) and wustite (FeO) to metallic iron.[22,23] However, the formation of FeO is not observed, because wustite is metastable below 570 °C[22-24] at which temperature disproportionation into Fe_3O_4 and Fe proceeds. With supported iron catalysts the purely divalent state of iron can be stabilised well below the critical temperature by interaction with the support due to the formation of mixed oxides. For iron catalysts supported on SiO_2 the formation of ferrous silicates has also been reported.[23,25-28]

Figures 7.2 (a – d) show the TPR profiles of the catalysts after calcination (in air) at 400 °C. Figure 7.2a shows that all the Ruhrchemie catalysts (i.e. 9% SiO_2, 18% SiO_2 and 27% SiO_2) reduce in two steps. The first peak at 300 – 400 °C corresponds to the reduction of $Fe_2O_3 \rightarrow Fe_3O_4$, and the second peak with the maximum around 530 – 580 °C corresponds to the reduction of Fe_3O_4 to metallic iron.[2,10,19] These curves are similar to what others have reported in the literature.[2,10,18,22-24] The small shoulder that is visible on the left side of the first peaks results from reduction of the copper promoter ($CuO \rightarrow Cu$) which

subsequently facilitates the onset and increases the rate of iron reduction. (The reduction profile of copper on silica is shown in Figure 7.3) According to the nucleation theory, the reduction of oxide accelerates as the first metal nuclei are formed.[29] The lower reduction temperature required for copper oxide compared to iron oxide leads to the formation of nucleation sites in metallic copper at temperatures where metallic iron would not normally be formed. This increase in the number of nucleation sites accelerates the subsequent reduction of iron oxide.

Figures 7.2 b, c and d show that the reduction profiles of the 18% silicas (i.e. nanotubes, hollow spheres, Stöber spheres) are slightly different from the other catalysts. The first peak relates to the transitions of CuO → Cu and Fe_2O_3 → Fe_3O_4 that occur at slightly lower temperatures i.e. the temperature for the onset of reduction is 200 °C compared to 340 °C, which implies that the CuO is well mixed with the Fe_2O_3 phase, compared to the other catalysts. Since the 18% silicas reduce much earlier, they are expected to reduce to a greater extent than other catalysts during an isothermal reduction in the reactor prior to the FT reaction. The third peak that is observed for the 18% silicas at around 630 °C, which can be associated with the occurrence of metal-support interactions, is not expected to be observed during the isothermal reduction. Only the TPR reducibility of 30 – 450 °C is important since it correlates with the reducibility of the catalyst during the optimum standard reaction procedure. This reducibility is related to the amount of active Fe^0 available for catalysing FTS after standard reduction. The broad

peaks that represent the $Fe_3O_4 \rightarrow$ α-Fe phase transformation indicate that this is a slow process (more difficult step), which is consistent with the literature.[6]

a)

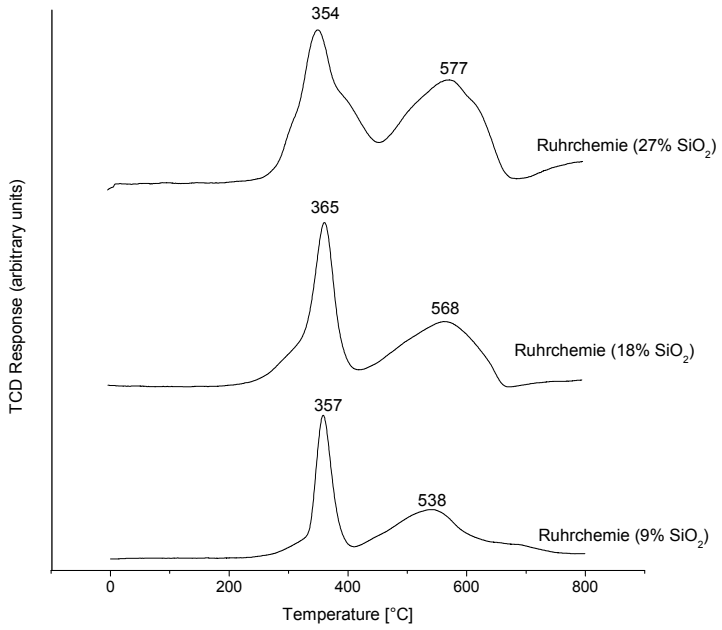

b)

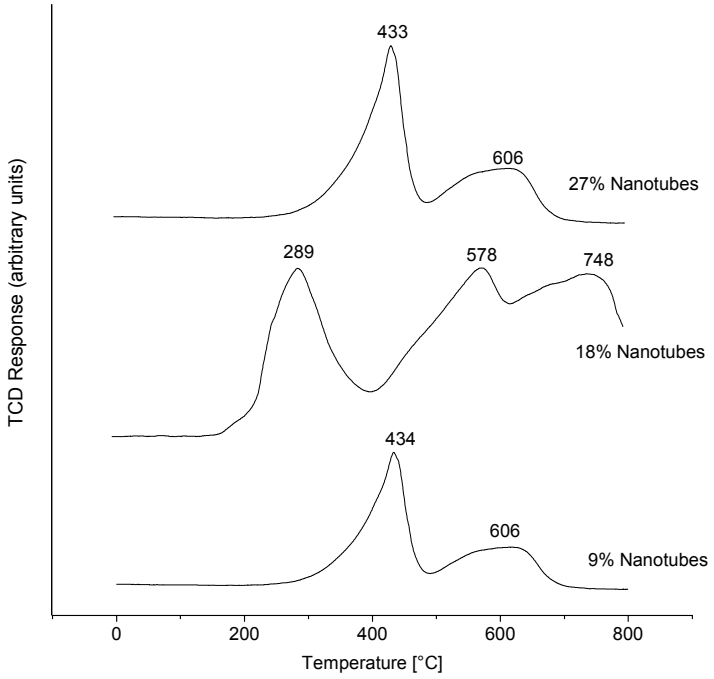
433
606
27% Nanotubes
289
578
748
18% Nanotubes
434
606
9% Nanotubes
TCD Response (arbitrary units)
0
200
400
600
800
Temperature [°C]

c)

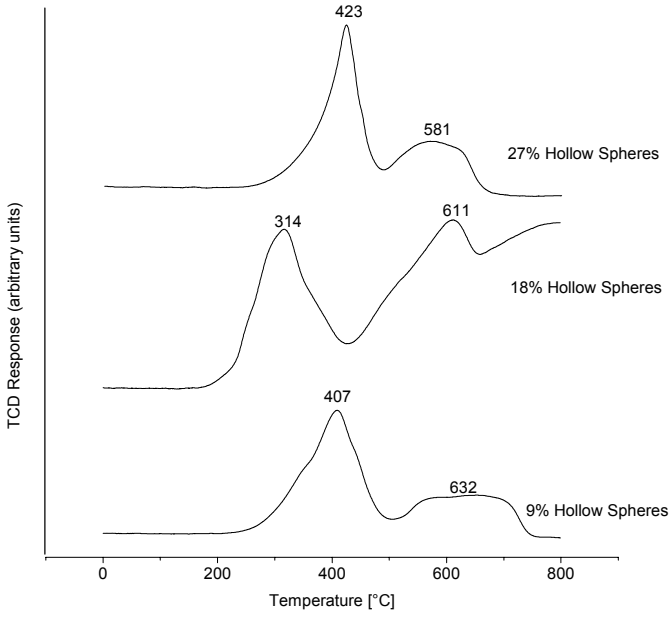
423
581
27% Hollow Spheres
314
611
18% Hollow Spheres
407
632
9% Hollow Spheres
TCD Response (arbitrary units)
0
200
400
600
800
Temperature [°C]

d)

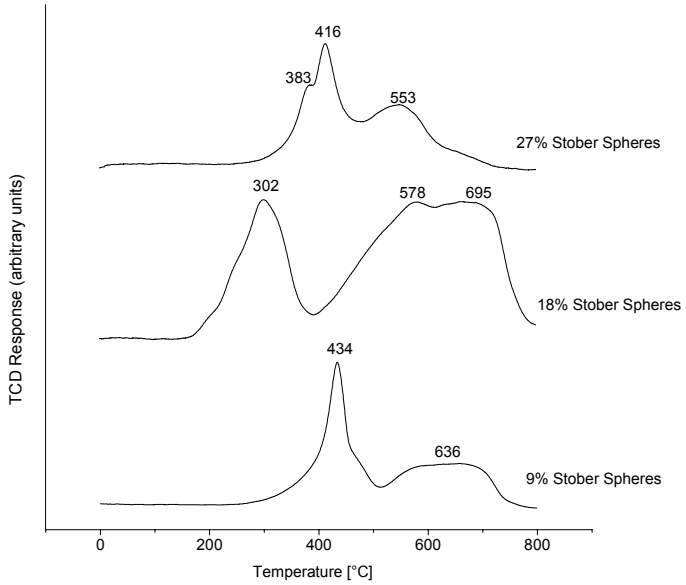

Figure 7.2. TPR profiles of catalysts a) Ruhrchemies, b) Nanotubes, c) Hollow spheres, d) Stöber spheres

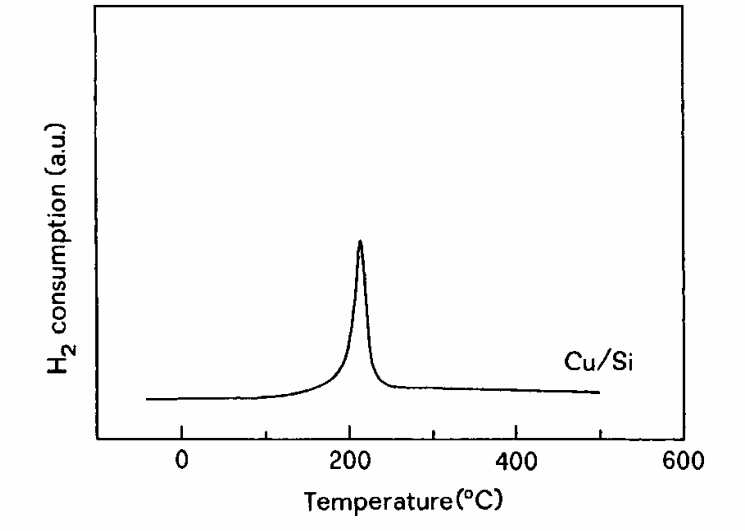

Figure 7.3. TPR profile of copper supported on silica*.

* In this case Stöber spheres were used. It was found that the reduction of copper is relatively unaffected by the amount and type of support used. Carniti and co-workers[30] also observed this.

7.3.3 Transmission Electron Microscopy (TEM) Study

TEM images of catalysts after calcination (prior to the FT synthesis) are shown in Figures 7.4 – 7.11. The images are mostly of the 18% SiO_2 catalysts because the BET surface area measurements and TPR study showed that their surface areas were higher than that of other catalysts (which implies better dispersion of iron onto the supports) and also they reduced much easier (T_{onset} lower by 130 °C) compared to other catalysts (except the 18Ruhr catalyst). The images of 9Ruhr, 9Nano, 9Stob and 9Holo are included for comparison purposes.

The images in Figure 7.4 and Figure 7.8 show that in both the 9% and 18% Ruhrchemie catalysts, the iron phase is well mixed with the support. [The darker regions in the images are where the iron species are located.[2] In the TPR study the reduction profiles of the catalysts showed that the copper is intimately mixed with the iron, it is therefore very difficult to see it in a TEM image unless an EDX is done]

In the nanotube supported catalysts (both 9% and 18%) some of the iron is outside the tubes while much of it is inside the tubes (Figures 7.5 and 7.9). (A XPS study was done to confirm this). The iron that is inside the tubes is well dispersed while that which is outside the tubes is in the form of clusters that are not well dispersed.

The Stöber sphere supported catalysts are different because the images (Figures 7.7 and 7.11) show that the iron is not well mixed with the support. In

the 9Stob catalyst iron islands (not in contact with the support) are seen all over the sample while the iron clusters in the 18Stob catalyst are slightly dispersed onto the support.

The hollow sphere supported catalysts are the most interesting because the iron phase is well dispersed in the 18Holo catalyst (Figure 7.6), but not well mixed with the support in the 9Holo catalyst (Figure 7.10). Furthermore the images in Figures 7.6 a and c show that some hollow spheres have broken up. Figure 7.6c shows that in some regions of the catalyst the hollow sphere structure has collapsed completely. This means that some hollow sphere structures collapsed during the calcination process which was not expected.

In the first part of the thesis it was found that the synthesized silicas (i.e. nanotubes, hollow spheres, etc) are thermally stable up to 900 °C. It could be that even though the silica material itself is stable, some hollow sphere structure collapses during the heat treatment because the walls of the structures are not thick enough (this was observed in Figures 7.6 and 7.10). This was not the case with the nanotubes because the TEM images show that their tube walls are very thick.

The hollow sphere supported catalysts are therefore not expected to be good catalysts because when some of the support structure has collapsed, it becomes very easy for the iron to sinter and therefore become ineffective. However the Ruhrchemie and nanotube supported catalysts are expected to

show some reasonable F-T activity because the iron is well dispersed onto the support, therefore more iron will be exposed to the reaction.

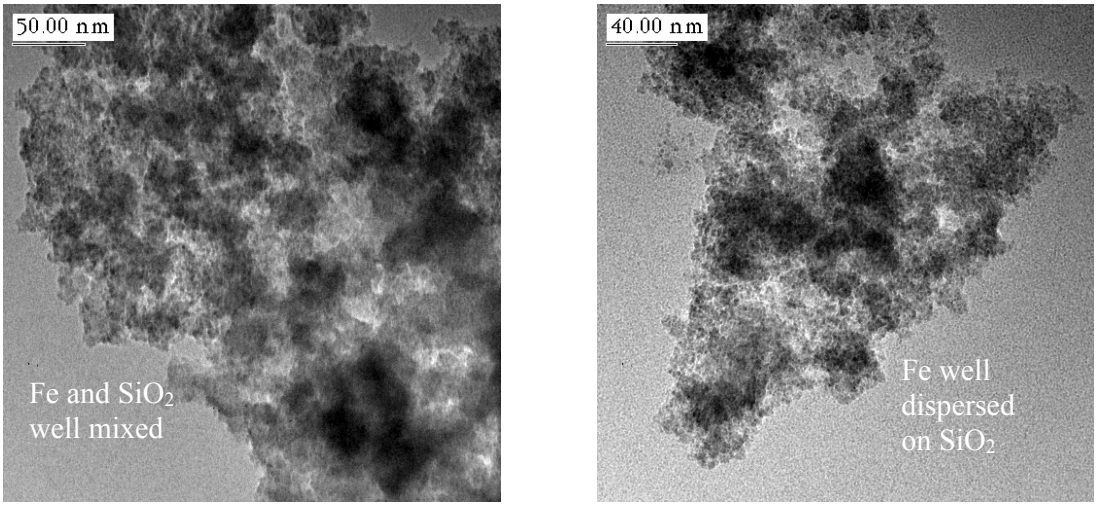

Figure 7.4. TEM images of the 18Ruhr catalyst.

a)

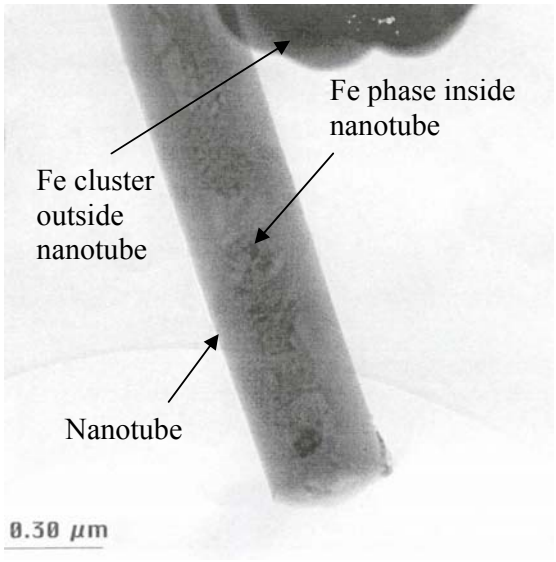

b)

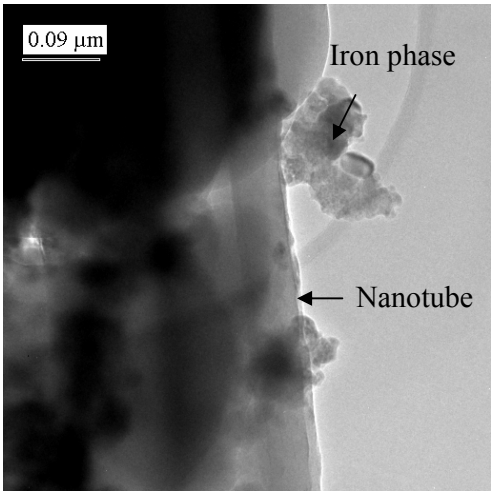

c)

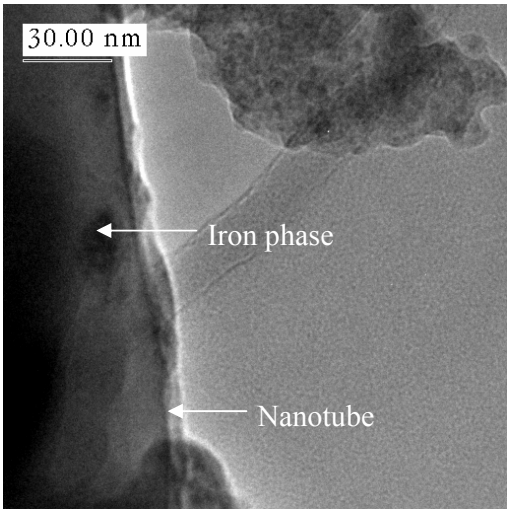

Figure 7.5 (a, b and c). Low and high magnification TEM images of the 18Nano catalyst

a)

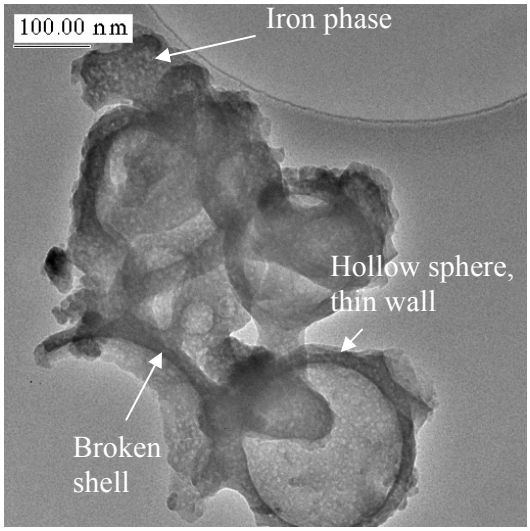

b)

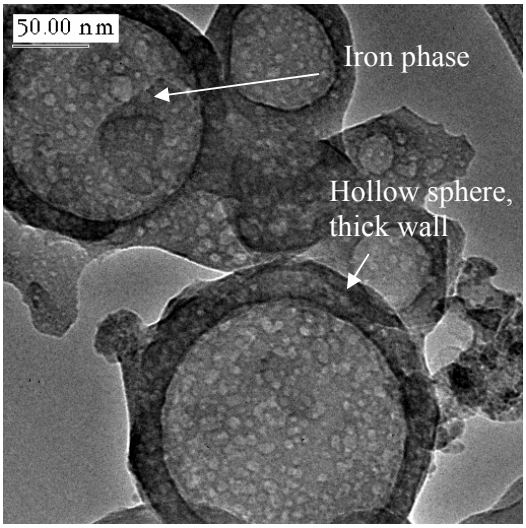

c)

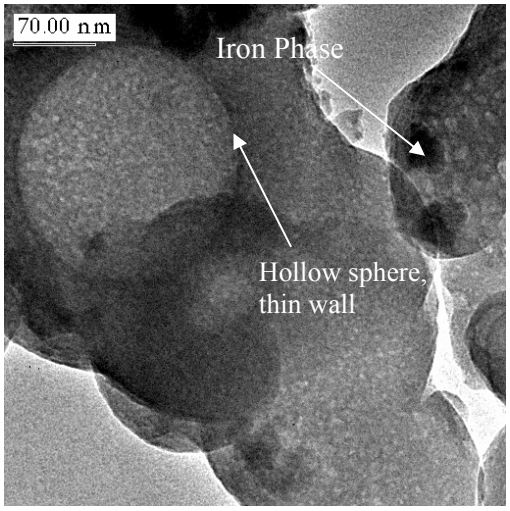

Figure 7.6 (a, b and c). TEM images of the 18Holo catalyst.

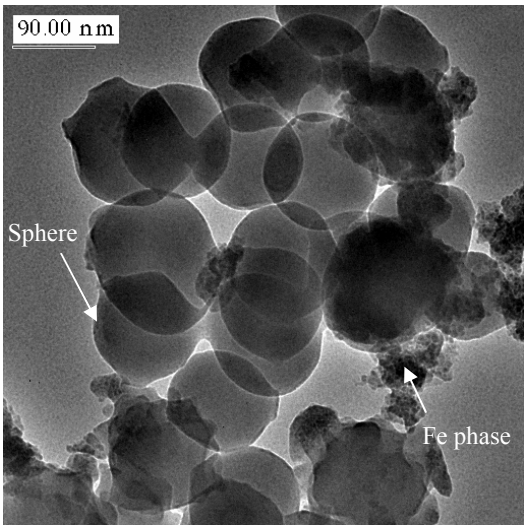

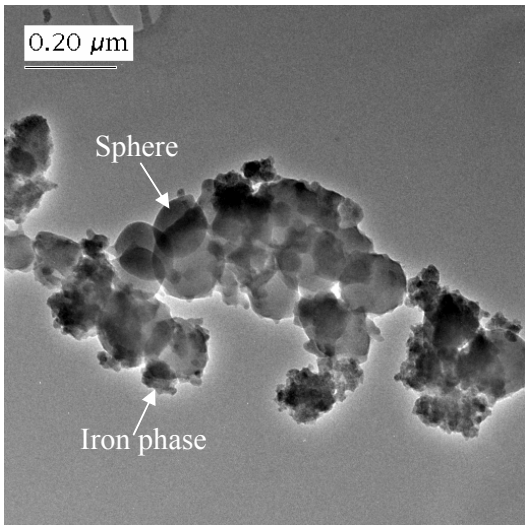

Figure 7.7. TEM images of the 18Stob catalyst.

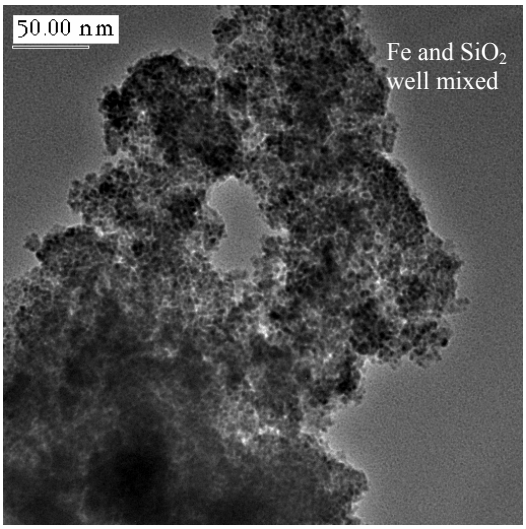

Figure 7.8. TEM image of 9Ruhr catalyst.

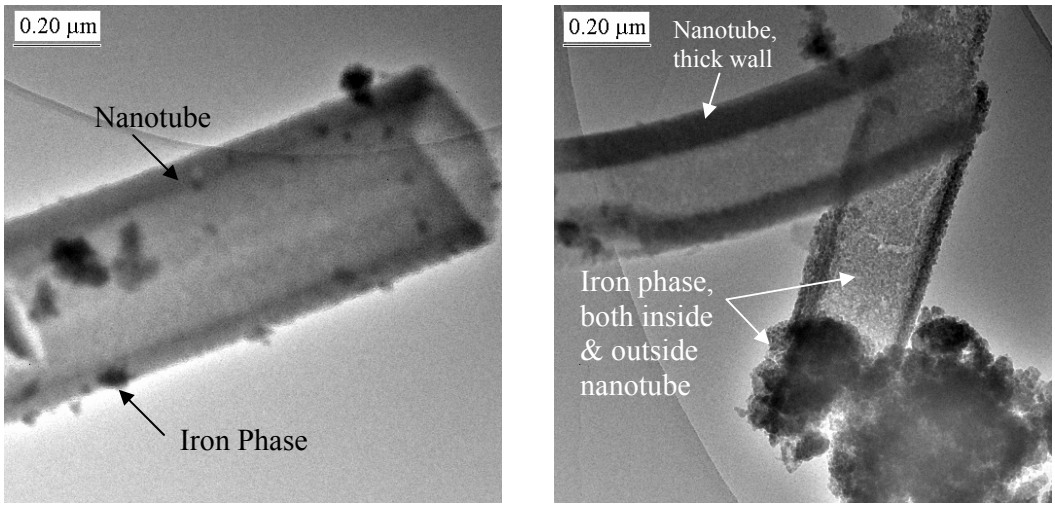

Figure 7.9. TEM images of the 9Nano catalyst.

a) b)

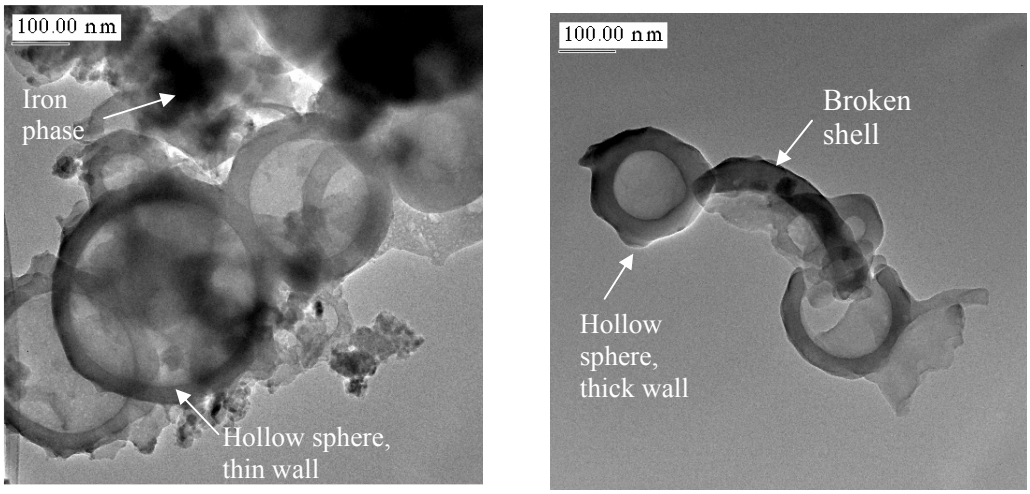

Figure 7.10. a) TEM image of 9Holo catalyst, b) TEM image showing some broken hollow spheres.

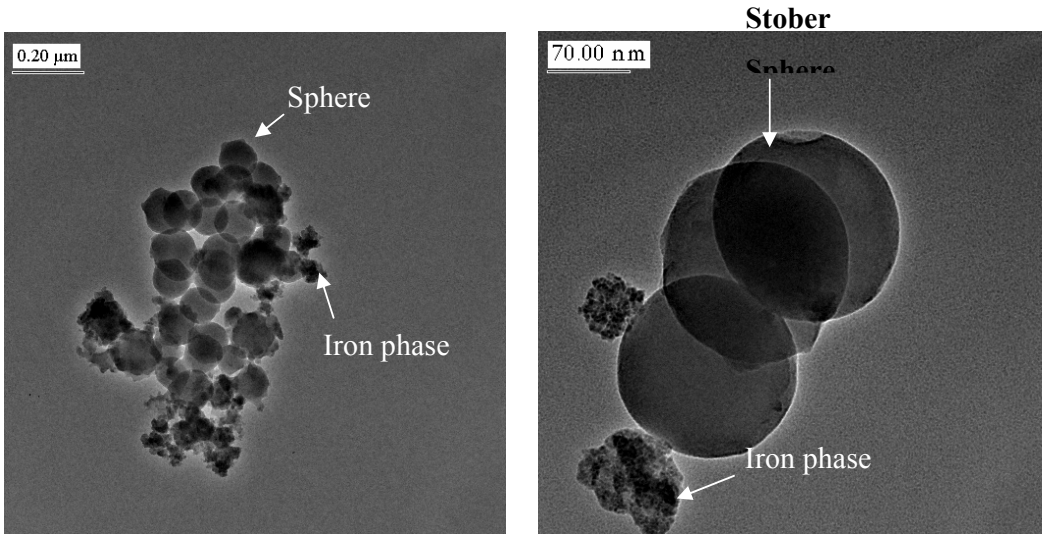

Figure 7.11. Low and high magnification TEM images of the 9Stob catalyst.

7.3.4 Reactor Study

Catalyst activity and stability, measured by CO conversion as a function of time on stream, are shown in Figure 7.12. It is well known from the literature that at a fixed set of process conditions, the CO conversion can be used to evaluate FTS activity i.e. higher conversion implies higher catalyst activity.[5] The results in Figure 7.12 show that the Ruhrchemie catalyst was the most active catalyst, followed by the catalyst supported on nanotubes, Stöber spheres and hollow spheres respectively. Catalysts containing 18% silica showed the best activity compared to the 9% and 27% silica catalysts. Indeed the characterisation studies that were carried out prior to FTS showed that
1) the TPR profiles of the 18% silicas were different from the others i.e. T_{onset} was lower which meant that they reduced easier and/or their extents of reduction were higher, 2) their surface areas were slightly higher which implied that the iron was better dispersed on the supports compared to the other catalysts.

The 18Ruhr and 18Nano catalysts had high activities (which were almost similar) because in both catalysts the iron was well dispersed onto the supports which resulted in more metal being exposed to the surface and also more metal being reduced. The Ruhrchemie catalysts had higher activities in all catalyst categories used (i.e. 9%, 18% and 27%) because the iron was well mixed onto the support. Whereas with the nanotube supported catalysts only the 18Nano catalyst had a high metal dispersion (TEM studies showed this). The observed increase in activity with increasing dispersion and degree of

reduction in our study is in agreement with what was observed in other iron FT studies.[13,31,32].

The 9% silica catalysts had more iron but showed lower activities, this could be due to the fact that they were not reduced to a larger extent or that their metal dispersions were lower compared to the 18% catalysts.

The catalyst activity normally decreases with increasing amounts of silica because of high support to metal ratios.[7] This could explain why the catalysts with a composition of 27% SiO_2 with the exception of 27Ruhr showed very low activities. Possible explanations for the decrease in catalyst activity with the increasing support content are 1) a lower degree of reduction and 2) a reduction in the effective potassium content of the catalyst. The latter is due to a reaction between potassium and silica,[12,33] to form less basic silicate, or to decreased Fe/K contact on the matrix with more silica.

The 27% silica catalysts are very stable even though the 27Nano, 27Stob and 27Holo had very low activities. The increase in stability with addition of silica support may be the result of stabilization of iron crystallites during synthesis and/ or interaction between the potassium and silica. The latter decreases the surface basicity of the catalyst and thus reduces the rate of carbon deposition. Bukur and co-workers[7] also found that the FTS activity decreased with increasing amount of SiO_2, however Egiebor and Cooper[11] found that the activity changed only slightly as the support concentration increased. The differences in trends (activity versus support concentration) in Egiebor and

Cooper's study and the present study together with Burkur's one may be due to the differences in methods of catalyst preparation, activation procedures and process conditions employed in the different studies.

a)

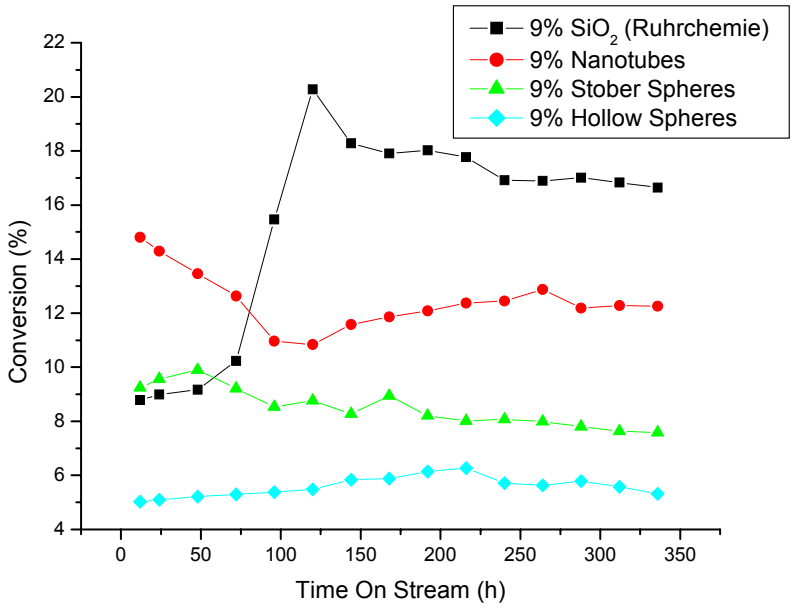

b)

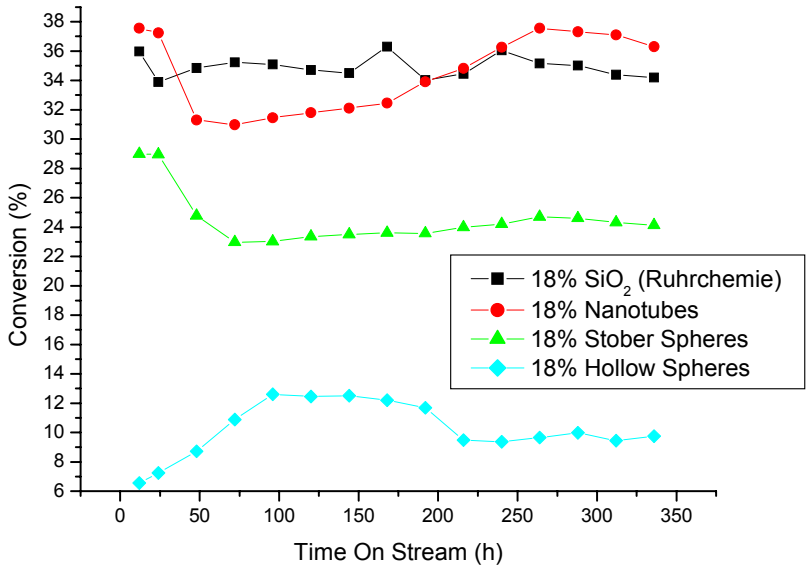

c)

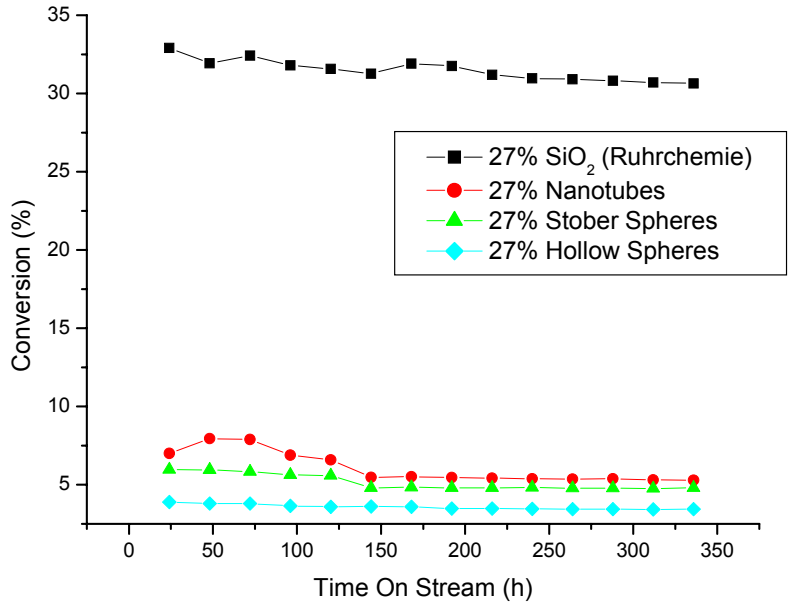

Figure 7.12. Effect of support type and content on catalyst activity and stability: a) 9% SiO_2, b) 18% SiO_2, c) 27% SiO_2

A summary of the activity and selectivity data is shown in Table 7.2. It appears that the support type did not have a marked effect on the product selectivities (hydrocarbon product distribution, olefin selectivities and CO conversion to CO_2), as no trend could be derived from the results. The graph with all the hydrocarbon selectivities is shown in Figure 7.13. Lack of observable differences in methane (except 18Nano catalyst) and higher hydrocarbon selectivities indicated that the increased activity in the 18Ruhr and 18Nano catalysts was not due to an electronic iron-support effect. It was more likely a result of increased iron dispersion.

Figure 7.14 shows a plot of the olefin to paraffin ratios of catalysts. The 18Nano and 18Ruhr catalysts formed more C4 and C5 olefins than other catalysts. Previous studies[4,5,9] have shown that olefins are produced as primary products of Fischer-Tropsch synthesis over iron catalysts. Paraffins are also formed directly but to a lesser extent. It is then conceivable that the high percentage of paraffinic hydrocarbons observed with the other catalysts (other than 18Nano and 18Ruhr) arises from the hydrogenation of olefins

The α values for all the catalysts were high which relate to the observation that mostly high molecular weight products were formed. This is because in low temperature F-T (250 °C was used in the study) higher hydrocarbon products are predominantly formed. Also the potassium that was added to the catalysts increases the chain length of the hydrocarbon products. The effect of potassium on hydrocarbon selectivities observed in the present study is in

agreement with the results obtained in several earlier studies with a variety of iron catalysts.[4,7,8,9]

The ratio of CO_2 production to total CO consumption represents a measure of the water-gas shift (WGS) activity, and is listed in Table 7.2. The use of different supports did not have a marked effect on the WGS activity, as no trends could be derived for the catalysts, although the 18Nano catalyst showed the lowest WGS activity. This may be attributed to potassium that is present in the catalysts. Potassium is known to promote the rate of WGS reaction.[7-10] Thus the catalyst behaviour, with respect to the WGS activity, was largely determined by the potassium content rather than differences arising from the use of different supports.

Table 7.2. Summary of reactor study data

Sample	9Ruhr	9Nano	9Holo	9Stob	18Ruhr	18Nano	18Holo	18Stob	27Ruhr	27Nano	27Holo	27Stob
Time on stream (h)	336	336	336	336	336	336	336	336	336	336	336	336
CO Conversion (%)	18.8	11.3	5.2	10.2	35.1	36.3	11.8	24.1	30.4	5.4	3.7	4.4
r_{co}* (Specific activity)	1.73	0.88	0.47	0.61	8.75	5.34	0.85	1.92	0.76	0.45	0.33	0.41
Extent of WGS	0.63	0.86	0.81	0.68	0.75	0.31	0.38	0.65	0.82	0.45	0.69	0.64
Hydrocarbon selectivity (%)												
C_1	3.8	4.2	2.4	3.8	4.8	10.4	4.5	4.0	4.2	5.1	6.2	3.9
C_2 - C_5	9.4	9.5	12.2	10.1	8.9	15.1	9.4	9.5	8.6	14.5	16.3	10.8
C_6 – C_{10}	11.8	27.0	21.4	24.3	15.4	16.2	11.8	11.5	12.0	16.7	19.3	18.4
C_{11} – C_{15}	11.9	24.8	23.4	25.9	34.4	28.5	28.2	12.3	50.0	29.3	25.7	30.2
C_{16}+	63.1	35.2	40.6	35.9	36.5	29.9	46.1	62.6	24.4	34.4	32.5	36.7
Olefin / paraffin ratio												
C3=/C3	0.46	0.26	0.44	0.21	0.71	-	-	0.30	-	0.21	0.19	0.25
C4=/C4	0.16	0.34	0.51	0.35	0.63	0.85	0.26	0.22	0.63	0.53	0.24	0.33
C5=/C5	0.17	0.29	0.24	0.32	0.70	0.74	0.39	0.23	0.60	0.65	0.28	0.31
C6=/C6	0.54	0.48	0.23	0.51	0.19	0.16	0.52	0.55	0.18	0.39	0.31	0.52
C7=/C7	0.59	0.31	0.39	0.40	-	0.21	0.37	0.57	-	0.30	-	0.44
α value	0.88	0.79	0.82	0.72	0.88	0.70	0.84	0.89	0.81	0.80	0.75	0.84

* r_{co} = mmol CO reacted / g/ s

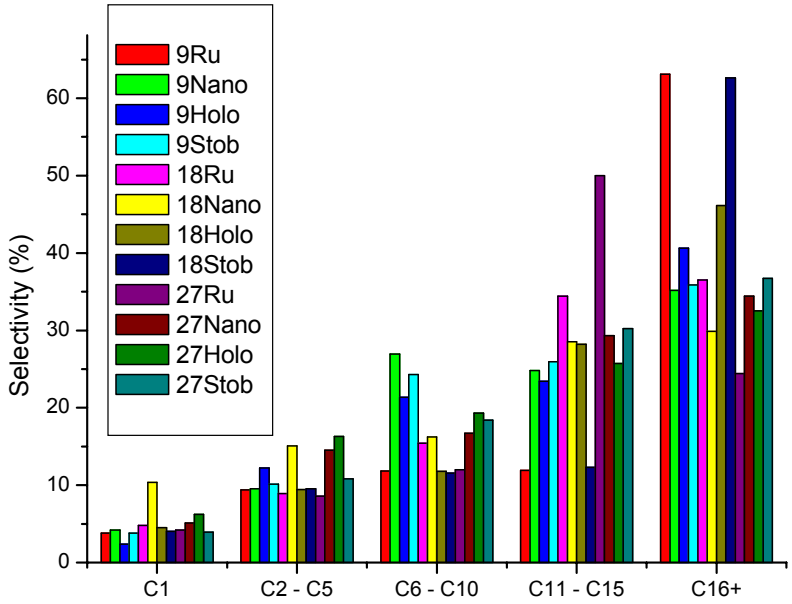

Figure 7.13. Selectivities of catalysts

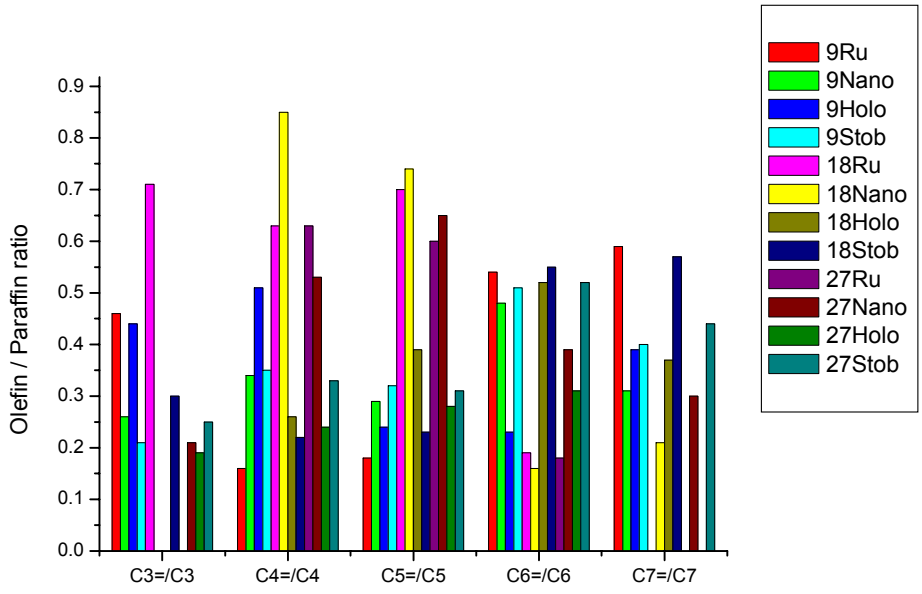

Figure 7.14. Olefin to paraffin ratios of catalysts

7.3.5 Mössbauer Spectroscopy

After 336 hours on stream when the catalysts were still fairly stable and active, they were taken out of the reactor in order to do Mössbauer spectroscopy analyses. Mössbauer spectroscopy was used as a bulk characterisation technique to identify the phases that are present in the 'working' catalysts, so as to relate the nature of the working catalyst with the active phase(s) responsible for F-T synthesis.[6,10,34]

Currently there is disagreement or confusion on this relationship caused by the fact that the reduction of the iron catalyst in hydrogen may lead to a zero-valent iron state, but upon exposure to a synthesis gas the metallic iron is rapidly converted to a carbide phase or a mixture of carbides.[4,10,35-37] Further at high syngas conversions, the reaction mixture becomes oxidizing and magnetite is also formed.[4,10,38-40] Therefore during FT synthesis the bulk iron may be distributed among several phases: e.g. carbides, oxides and metallic iron.

Numerous studies have been published concerning correlations between phases present in the iron catalyst and its reaction behaviour, as summarised, for example by Satterfield *et al*[40] and Dweyer and Hardenbergh.[41] However there is no clear consensus as to which of the phases is responsible for catalyst activity. Several models have been proposed and the two which are most frequently cited are the carbide model[35,36,42] and the competition model.[43] In the carbide model iron is not considered to be active for the F-T synthesis, but the surface carbides with their underlying iron carbide bulk

structure are, whereas in the competition model iron atoms at the surface are considered as the active sites. In the latter model both bulk carbidation and F-T synthesis (hydrocarbon formation) have a common surface carbidic precursor. In addition to these two postulates concerning the nature of the active phase, Teichner and co-workers[44,45] proposed that magnetite (Fe_3O_4) is the active phase in F-T synthesis. Validity of the latter proposal was questioned,[31] but some evidence in its support has also been presented.[46-48]

The hyperfine interaction parameters of selected catalysts* are listed in Table 7.3. The results showed that the two most active catalysts i.e. the 18Ruhr and 18Nano catalysts had different phase compositions. The 18Ruhr catalyst had an iron phase composition of χ' – $Fe_{2.5}C$ and superparamagnetic iron oxides or carbides. [Superparamagnetic behaviour is normally observed for crystallites that are less than 7 nm in size.[49] Low-temperature measurements are however needed in order to determine the nature of the iron phases in the small particles exhibiting superparamagnetic behaviour]. The 18Nano catalyst consisted of χ' – $Fe_{2.5}C$, α – Fe, Fe_3O_4 and superparamagnetic iron oxides or carbides. The 18Stob catalysts also consisted of χ' – $Fe_{2.5}C$, α – Fe, Fe_3O_4 and superparamagnetic iron oxides or carbides.

*The 18% SiO_2 catalysts were studied by Mössbauer spectroscopy because they showed better conversions and activity. 9Ruhr and 9Holo were also studied for comparison with the same support/binder type as they have a different Si/Fe ratio.

This finding supports the hypothesis that carbide formation is a requirement for active F-T catalysts. It also suggests that metallic iron is necessary for carbiding to occur, hence the need for a reduction pretreatment. The presence of Fe_3O_4 in used catalysts has been reported previously.[4,39,49,50] It has been suggested that the water vapour formed during FTS is responsible for the oxidation of metallic iron and/or carbides to Fe_3O_4.[4,39]

The 18Holo catalyst which was the least active catalyst in the 18% SiO_2 category was the only one found to have the ε' – $Fe_{2.2}C$ phase together with the χ' – $Fe_{2.5}C$ and some superparamagnetic iron oxides or carbides. The 9Holo catalyst which was even less active than the 18Holo catalyst did not have the ε' – $Fe_{2.2}C$ in its composition (it is also interesting to note that both the 18Ruhr and 9Ruhr catalysts did not have any α – Fe or Fe_3O_4). The absence of the ε' – $Fe_{2.2}C$ in the 9Holo catalyst and some presence of unidentified superparamagnetic iron species in the catalysts make it very difficult to conclude which iron carbide or phase contributes to the high activity of the catalysts. It could be that the ε' – $Fe_{2.2}C$ is formed first and then converted to χ' – $Fe_{2.5}C$ during the F-T reaction via the reaction $2.5Fe_{2.2}C \rightarrow 2.2Fe_{2.5}C + 0.3C$ (in agreement with what Jung[51] suggested), and that in the 18Holo catalyst the transformation was not yet complete after 336 hours on line.

Therefore, in order for a conclusive argument to be reached low temperature Mössbauer must in future studies be done so that all the iron species are identified.

Table 7.3. Hyperfine interaction parameters of the Fe based catalysts

Sample Id	IS (mms^{-1})$_{Fe}$	QS (mms^{-1})	B_{HF} (T)	% Fe	Phase
18Ruhr	0.20	0.02	21.1	48.6	χ' – $Fe_{2.5}C$
	0.19	0.11	17.5		
	0.30	0.02	9.4		
	0.87	2.38	-	5.2	Fe^{2+}
	0.35	0.88	-	46.2	Fe^{3+}
18Nano	0.23	0.09	21.2	51.9	χ' – $Fe_{2.5}C$
	0.19	0.14	17.7		
	0.26	0.02	10.2		
	0.0	0.05	33.5	3.8	α – Fe
	0.64	-0.04	45.5	29.3	Fe_3O_4
	0.29	0.03	48.7		
	0.87	2.37	-	2.6	Fe^{2+}
	0.32	0.86	-	12.4	Fe^{3+}
18Stob	0.22	0.07	21.2	62.2	χ' – $Fe_{2.5}C$
	0.19	0.10	17.8		
	0.11	0.02	10.8		
	0.03	-0.14	33.7	3.8	α – Fe
	0.73	0.02	45.6	12.6	Fe_3O_4
	0.22	0.0	47.6		
	0.87	2.40	-	3.7	Fe^{2+}
	0.33	0.84	-	17.7	Fe^{3+}
18Holo	0.27	0.04	21.7	57.0	χ' – $Fe_{2.5}C$
	0.23	0.04	17.4		
	0.26	0.02	10.9		
	0.17	0.02	18.9	12.7	ε’ – $Fe_{2.2}C$
	0.72	2.13	-	2.6	Fe^{2+}
	0.33	0.94	-	15.4	Fe^{3+}
9Ruhr	0.25	0.04	21.4	40.2	χ' – $Fe_{2.5}C$
	0.19	0.13	17.6		
	0.32	0.02	10.7		
	0.87	2.25	-	6.1	Fe^{2+}
	0.34	0.88	-	53.7	Fe^{3+}
9Holo	0.27	0.04	21.6	53.0	χ' – $Fe_{2.5}C$
	0.16	0.12	18.2		
	0.29	0.02	9.8		
	0.0	0.05	33.0	2.4	α – Fe
	0.85	-0.08	45.5	4.1	Fe_3O_4
	0.15	0.20	47.8		
	0.87	2.34	-	8.4	Fe^{2+}
	0.35	0.74	-	31.2	Fe^{3+}

7.4 Conclusions

Characterisation studies together with F-T reactivity data showed that the use of silica with various morphologies as supports/binders for the iron catalysts does not have an effect on the catalyst selectivity and that the activity of the metal is largely influenced by the metal dispersion and degree of reduction of the catalysts. From the new supports/binders that were used, silica nanotubes seem to have a big potential in being used as supports because the metal becomes well enclosed and dispersed inside the nanotubes. The WGS activity was largely influenced by the potassium that is present in the samples and not the support type.

Mössbauer spectroscopy showed that some active catalysts contained χ' – $Fe_{2.5}C$ and some unidentified superparamagnetic iron species while other catalysts also contained α – Fe and Fe_3O_4 in addition to χ' – $Fe_{2.5}C$ and some unidentified superparamagnetic iron species. Therefore low temperature Mössbauer must be done so that all the iron species are identified and a conclusive argument is reached on the exact composition of an active catalyst.

7.5 References

1. A.K. Datye, Y. Jin, L. Mansker, R.T. Motjope, T. Dlamini and N.J. Coville, *Stud. Surf. Catal*., **130**, 306, (2000).
2. Y. Jin and A.K. Datye, *J. Catal.*, **196**, 8-17, (2000).
3. M.D. Mehul, D.S. Kalakkad, K.E. Coulter, S.D. Köhler, M.S. Harrington, N.B. Jackson, A.G. Sault and A.K. Datye, *J. Catal.*, **156**, 185-207, (1995).
4. M.E. Dry, The Fischer-Tropsch Synthesis in *Catalysis Science and Technology 1*, J.R. Anderson, M. Boudart, Eds., Spring and Verlag: New York, 159-255, (1981).
5. D.G. Burkur, X. Lang, D. Mukesh, W.H. Zimmermann, M.P. Rosynek and C. Li, *Ind., Eng., Chem., Res.*, **29**, 1588-1599, (1990).
6. D.G. Burkur, K. Okabe, M.P. Rosynek, C. Li, D. Wang, K.R.P.M. Rao and G.P. Huffman, *J. Catal*., **155**, 355, (1995).
7. D.G. Burkur, D. Mukesh and S.A. Patel, *Ind. Eng. Chem. Res*., **29**, 194 – 204, (1990).
8. R.B. Anderson, B. Seligman, J.F. Schultz and M.A. Elliot, *Ind. Eng. Chem*., **44**, 391 – 397, (1952).
9. H. Arakawa and A.T. Bell, *Ind, Eng, Chem, Process Des, Dev*., **22**, 97 – 103, (1983).
10. D.G. Burkur, M. Koranne, X. Lang, K.R.P.M. Rao and G.P. Huffman, *Appl. Catal.*, **126**, 85 – 113, (1995).
11. N.O. Egiebor and W.C. Cooper, *Can. J. Chem. Eng*., **63**, 81 – 85, (1985).
12. G.B. McVicker and M.A. Vannice, *J. Catal*., **63**, 25 – 34, (1980).

13. F.J. Berry, L. Liwu, L. Dongbai, W. Chengyu, T. Renyuan and Z. Su, *Appl. Catal.*, **27**, 195 – 205, (1986).
14. A.Y. Khodakov, A. Griboval-Constant, R. Bechara and V.L. Zholobenko, *J. Catal.*, **206**, 230, (2002).
15. R.B. Anderson, W.K. Hall, A. Krieg and B.J. Seligman, *J. Am. Chem. Soc.*, **71**, 183, (1949).
16. J.A. Lapszewics, H.J. Loeh and J.R. Chipperfield, *J. Chem. Soc., Chem. Commun.*, **913**, (1993).
17. D. Vanhove, Z. Zhang, L. Makambo and M. Blanchard, *Appl. Catal.*, **9**, 327, (1984).
18. B. Ernst, S. Libs, P. Chaumette and A. Kiennemann, *Appl. Catal. A*, **186**, 145, (1999).
19. (a) F. Miyaji, S.A. Davis, J.P.H. Charmant and S. Mann, *Chem. Mater.*, **11**, 3021, (1999). (b) M. Trau, N. Yao, E. Kim, Y. Xia, G.M. Whitesides and I.A. Aksay, *Nature*, **390**, 674, (1997). (c) H. Yang, N. Coombs and G.A. Ozin, *Adv. Mater.*, **9**, 811, (1997).
20. J. Haber, *Pure Appl. Chem.*, **63**, 1227, (1991).
21. D.A.M. Monti and A. Baiker, *J. Catal.*, **83**, 323, (1983).
22. A.J.H.M. Kock, H.M. Fortuin and J.W. Geus, *J. Catal.*, **96**, 261, (1985).
23. X. Gao, J. Shen, Y. Hsia and Y. Chen, *J. Chem. Soc. Faraday Trans.*, **89 (7)**, 1079, (1993).
24. M.V. Cagnoli, S.G. Marchetti, N.G. Gallegos, A.M. Alvarez, R.C. Mercader and A.A. Yeramian, *J. Catal.*, **123**, 21, (1989).
25. A.F.H. Wielers, A.H.J.M. Kock, C.E.C.A. Hop, J.W. Geus and A.M. van der Kraan, *J. Catal.*, **117**, 1, (1989).

26. Y.Y. Huang and J.R. Anderson, *J. Catal.*, **40**, 143, (1975).
27. M.C. Hobson Jr and H.M. Gager, *J. Colloid Interface Sci*., **34 (3)**, 357, (1970).
28. S. Yuen, Y. Chen, J.E. Kubsh, J.A. Dumesic, N. Topsoe and H. Topsoe, *J. Phys. Chem*., **86**, 3022, (1982).
29. R.J. Madon and W.F. Taylor, *J. Catal*., **69**, 32, (1981).
30. P. Carniti, A. Gervasini, V.H. Modica and N. Ravasio, *Appl. Catal. B*, **28**, 179, (2000).
31. R.A. Dictor and A. Bell, *J. Catal*., **97**, 121, (1986).
32. R. Snel, *J. Mol. Catal*., **53**, 129 – 141, (1989).
33. M.E. Dry and G.J. Oosthuizen, *J. Catal*., **11**, 18 – 24, (1968).
34. L.D. Mansker, Y. Jin, D.B. Burkur and A.K. Datye, *Appl. Catal*., **186**, 277 – 296, (1999).
35. J.A. Amelse, J.B. Butt and L.J. Schwartz, *J. Phys. Chem*., **82**, 558, (1978).
36. G.B. Raupp and W.N. Delgass, *J. Catal*., **58**, 348, (1979).
37. H. Jung and W.J. Thomson, *J. Catal*., **134**, 654, (1992).
38. R.B. Anderson, in P.H. Emmett (Ed.), Catalysis, Vol. 4, Van Nostrand-Reinhold, New York, 29, (1956).
39. R.B. Anderson, The Fischer-Tropsch Synthesis, Academic Press, Orlando, FL, (1984).
40. C.N. Satterfield, R.T. Hanlon, S.E. Tung, Z. Zou and G.C. Papaefthymiou, *Ind. Eng. Chem. Prod. Dev*., **25**, 407, (1986).
41. D.J. Dweyer and J.H. Hardenbergh, *J. Catal*., **87**, 66, (1984).
42. G.B. Raupp and W.N. Delgass, *J. Catal*., **58**, 361, (1979).

43. J.W. Niemantsverdriet and A.M. van der Kraan, *J. Catal*., **72**, 385, (1981).
44. J.P. Reymond, P. Meriadeau and S.J. Teichner, *J. Catal*., **75**, 39, (1982).
45. F. Blanchard, J.P. Reymond, B. Pommier and S.J. Teichner, *J. Mol. Catal*., **17**, 171, (1982).
46. J.B. Butt, *Catal. Lett.*, **7**, 61, (1990).
47. S. Soled, E. Iglesia and R.A. Fiato, *Catal. Lett*., **7**, 271, (1990).
48. C.S. Kuivila, P.C. Stair and J.B. Butt, *J. Catal*., **118**, 299, (1989).
49. T.R. Motjope, *Effect of preparation variables on precipitated catalysts for Fischer-Tropsch synthesis using Mössbauer spectroscopy*, MSc Dissertation, University of the Witwatersrand, Johannesburg, (2000).
50. E.S. Lox, G.B. Marin, E. de Grave and P. Bussiere, *Appl. Catal*., **40**, 197 – 218, (1988).
51. H. Jung and W.J. Thomson, *J. Catal*., **139**, 375, (1993).

CHAPTER EIGHT

CONCLUSIONS

PART I

The sol-gel method is a method for preparing inorganic materials from molecular precursors. It not only allows the preparation of known materials in a novel way but also of materials with unusual compositions and properties. In particular, the template directed sol-gel synthesis of organized inorganic matter offers a new and wide-ranging approach to the synthesis of useful materials with controlled architecture and porosity across a range of length scales.

The studies that were carried out in this thesis evaluated the effect of templates and synthesis conditions on the properties and structures (nano- and micro) of silica materials that are obtained by the templated sol-gel method.

Five types of morphologies were found in the silica materials obtained with different templates and they were categorised as hollow tubes, filled tubes, hollow spheres, solid spheres and amorphous material. The studies that were carried out with various templates revealed that the self-assembly of the template is highly influenced by synthesis conditions. Sphere formation was

found to be a competitive reaction to tube formation. Sphere shaped templates are formed under certain synthesis conditions (e.g. at 75 °C) while rod-like templates are favoured under certain synthesis conditions (e.g. low temperatures). The formation of rod-like crystals leads to the formation of tubular silica materials while sphere shaped templates lead to the formation of spheres.

The studies with DL-tartaric acid as a template revealed that synthesis conditions (temperature, NH_4OH concentration, water/ethanol concentration, time before NH_4OH addition, static versus stirred conditions, stirring rate and solvent) all have an effect on the microstructure of the silica and influence the formation of particular silica morphologies. Indeed, the effects observed are those expected from diffusion and kinetic/thermodynamic considerations.

Of all the synthesis conditions investigated, temperature, stirring and reaction time had the largest effect on the silica structure. These factors have a direct bearing on template formation. The formation of silica tubes is enhanced at lower temperatures rather than at elevated ones and this can be due to the fact that at a lower temperature molecules (reagents, template) diffuse more slowly and thus have enough time to self-assemble.

Studies with citric acid also revealed that synthesis conditions (i.e. temperature, NH_4OH concentration, water/ethanol concentration, time before NH_4OH addition, static versus stirred conditions, stirring rate and solvent) influence the formation of particular silica morphologies. It is thus important to

carefully control these synthesis conditions. Temperature, water/ethanol dilution and stirring rate played a large role in structure formation. The formation of tubes was enhanced at lower temperatures (< 50 °C). This effect can be related to diffusion and stability of the template. Only hollow spheres were obtained at 75 °C. This could arise from the fact that at that temperature some evaporation of ammonia occurs leading to the presence of less ammonium citrate template crystals for tube formation.

For both DL-tartaric acid and citric acid the formation of tubes appeared to be sensitive to the amount of water (water/ethanol dilution) present in the reaction mixture. More tubes were formed under stirred conditions and the tubes were also longer than the ones formed under non-stirred conditions.

DL-tartaric acid influenced the formation of longer and more uniform tubes compared to citric acid. Tubes that are formed in DL-tartaric acid are hollow and open ended; however the ones formed in citric acid are a mixture of filled and hollow but closed tubes. Hollow spheres are exclusively formed when citric acid is used at 75 °C while only filled spheres are formed when DL-tartaric acid is used. The surface areas for the silica formed from DL-tartaric acid are lower than the areas obtained from citric acid. Hence it appears that the template also plays a role in the formation of various silica morphologies. This can be attributed to the fact that crystals formed for each template are slightly different. (The size of the molecule, orientation of the hydroxyl groups and inter-molecular H-bonding etc. contribute to this).

The nitrogen adsorption-desorption isotherms of silica materials obtained from both templates showed that the materials were mesoporous with some microporosity present in them. The formation of fragmented tubes is believed to be caused by the fact that the reactions are carried out in basic media and formed silica tubes can react with excess OH^- ions thereby causing the tubes to lose their smooth shape as the silica is dissolved away from the tube surface. Furthermore, the dissolved silica can re-precipitate on the tubes and spheres to generate the amorphous materials observed by TEM and SEM.

The studies with mucic and tartronic acid also showed that the template together with synthesis conditions (such as solvent, temperature and stirring) affect the resulting silica morphology. Mucic acid influenced the formation of silica materials with high surface areas, mesopores and a morphology that reveals fragmented tubes. Tartronic acid influenced the formation of hollow tube materials with low surface areas and a combination of micro- and mesopores. The yield of the tubes was higher at lower temperatures for both templates.

When sugars were used only spherical particles were obtained and some sugars gave SiO_2 particle sizes that are smaller than the ones that are normally obtained by the sol-gel method. Therefore it appears that a combination of both COOH and OH groups are needed in a template in order to obtain tubular structures.

TEM and SEM have shown that by using different templates, the particle size and structure of the silica are altered at the nanoscale level. Other properties that are highly influenced by variation of templates and conditions are texture, surface area and the material's thermal decomposition. Hence it is possible to 'design' silica materials with specific properties, Table 8.1 gives a summary of how this can be achieved.

Table 8.1 Summary of types of silicas and properties that can be obtained by using different templates and synthesis conditions.*

Template	Synthesis condition	Structure	Particle size[a] [µm]	Surface area [m^2/g]	Types of pores
DL-tartaric acid	0°C, ethanol	Hollow tubes	L: 100 – 250 D: 0.2 – 0.6	25	Meso + micropores
Citric acid	75°C, ethanol	Hollow spheres	S: 0.17 – 0.20	47	Meso + micropores
Glucose	25°C, ethanol	Solid spheres	S: 0.3 – 0.5	17	Meso + micropores
Mucic acid	75°C, diethyl ether	Fragments	-	188	Mesopores
Mucic acid	25°C, diethyl ether	Fragmented tubes + spheres	L: 1.13 – 3.51 D: 0.22 – 0.41 S: 0.11 – 0.33	263	Mesopores
Gluconic acid	25°C, ethanol	Solid spheres	S:0.003 – 0.01	5	Meso + micropores

[a]L = length of tube, D = outer diameter of tube, S = diameter of sphere
* Only selected cases were chosen from the thesis chapters

PART II

The inherent preparative advantages offered by the sol-gel method have prompted its use for the synthesis of many oxidic catalytic supports notably silica and alumina.

The use of silica with various morphologies as supports/binders for an iron Fischer-Tropsch catalyst was evaluated. The various silica morphologies were found to affect the physico-chemical properties and activities of the catalysts but not the catalyst selectivities .

The Ruhrchemie catalysts had a much higher surface area than the other catalysts. (i.e. catalysts supported on nanotubes, Stöber spheres and hollow spheres). The 18% SiO_2 catalysts had higher surface areas than the 9% SiO_2 and 27% SiO_2 catalysts. This can be due to the fact that the metal was better dispersed onto the support/binder in 18% SiO_2 and Ruhrchemie catalysts.

The Ruhrchemie catalyst was the most active catalyst followed by the catalyst supported on silica nanotubes, Stöber spheres and hollow spheres respectively. Catalysts containing 18% silica showed the best activity compared to the 9% and 27% silica catalysts. Possible explanations of this are: 1) the TPR profiles of the 18% silicas were different from the others i.e. T_{onset} was lower which meant that they reduced easier and/or their extents of reduction were higher, 2) their surface areas were slightly higher.

The activity was found to be high in the catalysts that had high metal dispersions such as the Ruhrchemie catalysts and the 18% nanotube catalyst. The lack of observable differences in the selectivities of the catalysts indicated that that the Fe-silica interaction was not the dominant factor in determining the selectivity.

The product distribution and WGS activity were largely influenced by the potassium that is present in the samples and not the support type.

Mössbauer spectroscopy was used as a bulk characterisation technique to identify the phases that are present in the 'working' catalysts, so as to relate the nature of the working catalyst with the active phase(s) responsible for F-T synthesis. Mössbauer spectroscopy showed that some active catalysts contained χ' – $Fe_{2.5}C$ and some unidentified superparamagnetic iron species while other catalysts also contained α – Fe and Fe_3O_4 in addition to χ' – $Fe_{2.5}C$ and some unidentified superparamagnetic iron species. Therefore, in order for a conclusive argument to be reached, low temperature Mössbauer studies must be done so that all the iron species are identified and the exact compositions of the active catalysts are known. The findings support the hypothesis that carbide formation is a requirement for active F-T catalysts. It also suggests that metallic iron is necessary for carbiding to occur, hence the need for a reduction pre-treatment.

The studies that were carried out in the thesis showed that from the list of new supports/binders that were used, silica nanotubes seem to have a remarkable

potential for use as supports. It appears that as the metal becomes enclosed and dispersed inside the nanotubes the activity of the nanotube supported catalyst becomes comparable to that of a standard Ruhrchemie catalyst.

APPENDIX 1

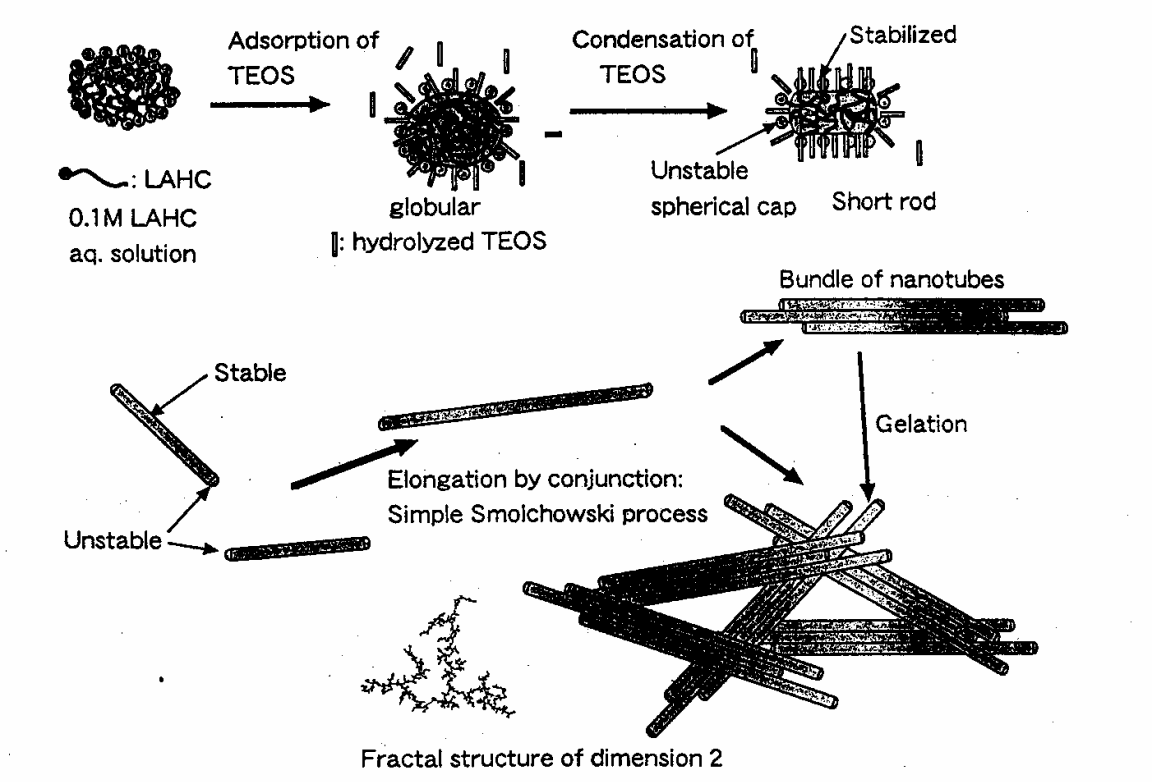

Mechanism for the formation of silica nanotubes in the presence of laurylamine hydrochloride as a template. This has been proposed by Adachi and co-workers (Ref. 19 in chapter 2).

APPENDIX 2

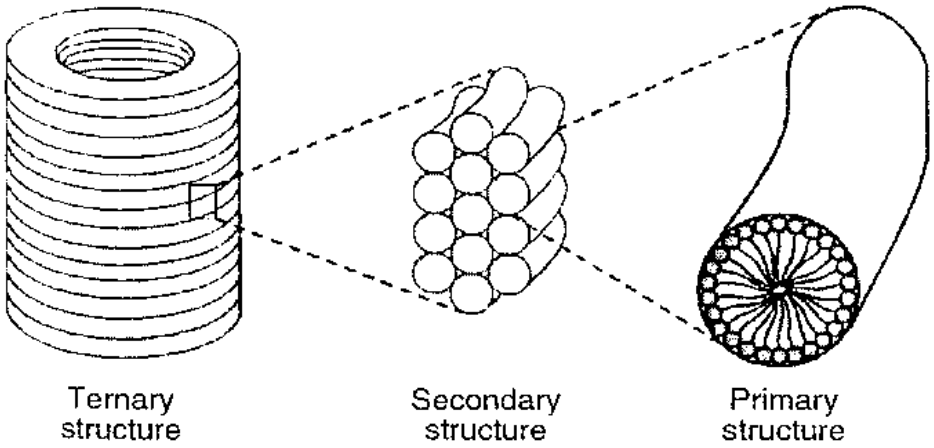

Schematic representation of the different hierarchy levels in hollow ordered mesostructured silica fibers. This has been proposed by Kleitz and co-workers (Ref. 29 in chapter 2)